SYSTEM STUDY OF TWO DIMENSIONAL MAGNETIC RECORDING SYSTEM

A DISSERTATION
SUBMITTED TO THE FACULTY OF THE GRADUATE SCHOOL

OF THE UNIVERSITY OF MINNESOTA

BY

YAO WANG

IN PARTIAL FULFILLMENT OF THE REQUIREMENTS

FOR THE DEGREE OF

DOCTOR OF PHILOSOPHY

PROFESSOR RANDALL H. VICTORA, ADVIOSR

August 2014

Acknowledgements

It is my fortune and pleasure to have a great professor - Randall Victora - to be my advisor of PhD program in UMN. I appreciate his encouragement and patience in my scientific pursuit. I enjoyed the great benefits of his unique insight and profound knowledge of magnetic recording and micromagnetic theory during the research, especially his prudent research attitude will guide me in the future work.

I would also like to acknowledge the great advice from Dr. Fatih Erden in Seagate Technology during my work.

I am thankful to all my committee members Prof. Jian-ping Wang, Prof. Keshab Parhi and Prof. William Cooper for their time, kindness and efforts of serving in my committee.

It has been a memorable experience with members of Professor Victora's group and other students in MINT center. I would like to thank Yan Dong for her knowledge and experience I've inherited. I express the deepest appreciation to Sean Morgan for his encouragement and support during my most difficult time. I would like to express my special thanks to Chuan Zhang, Bo Yuan, Te-lung Kong for their help in my first year. I also would like to thank all the colleagues including Yisong Zhang, Stephanie Hernandez, Xiaohui Chao, Sumei Wang, Mazin Maqableh, Eliot Estrine, Xi Chen, Tao Qu, Xiaowei Zhang, Todd Klein, Eunkyung Cho, Andrew Block, Anirudh Sharma , Madhukar Reddy, Pin-wei Huang, Yipeng Jiao and many other friends for their friendship and help.

I am deeply grateful to my parents and sister. Without their love, support, tolerance and advice, I would have never gone so far.

Dedication

With gratitude to my parents.

Abstract

In order to increase areal density above 1 Tbit/in^2 for magnetic recording system, a two dimensional magnetic recording (TDMR) system has been proposed as a possible candidate to solve the trilemma of writability, signal-to-noise ratio and thermal stability. Usually a shingled writer and two dimensional signal processing are implemented during the writing and reading process for TDMR system, respectively. However, reaching the user density as high as possible with a micromagnetic writer and reader, combined with read channel is still a challenge for the study of TDMR. In this dissertation, a novel reader design is proposed to readback above 1 Tbit/in^2 density from granular media in a TDMR system, which can even exceed 10 Tbits/in^2 user areal densities when combined with oversampling signal processing. Such a reader design is also extended to readback of bit patterned media with 10 Tbits/in^2 densities. A proposed shingled micromagnetic writer combined with the new reader is able to reach user density above 4 Tbits/in^2 and near 6 Tbits/in^2 for 8nm and 6nm Voronoi grains, respectively.

Readback at ultra-high density from a granular media with a realistic reader, such as that envisioned for two-dimensional magnetic recording, is quite challenging due to the increased inter-track interference, inter-symbol interference, increased writing errors and an extremely low signal-to-noise ratio (SNR) environment. A novel reader design is proposed to address the difficult problems for readback, which avoids the necessity for a complex 2-D detector and head array, or latency issues if a single head was employed in the normal orientation. The key idea is a rotated sense head, so that the shields are aligned down-track, combined with oversampled signal processing to regain the lost down-track resolution. Based on a random Voronoi grain model with perfect writing,

simulation indicates that the new design can decrease the BER by a factor of five compared to a normally positioned head array, and greatly increase user areal density above 10 Tbits/in^2 for a single-rotated singled head with sampling period of 2nm, a minimum mean squared error equalizer, and pattern-dependent noise prediction detector. If a quasi-cyclic low-density parity-check (QC-LDPC) code is implemented for error correction, the performance of a normally oriented head array is about 8.5 dB worse than the rotated head array (RHA).

The study indicates that the significant improvement in performance in the rotated head compared to the normally oriented head can be attributed to the larger amplitude of its dibit response and the reduced overlap between conditional probability density functions. This new design is also examined for densities of 2-7 Tbits/in^2 for TDMR system; simulation shows that the new design achieves a density gain of 1.7X (single head) and 2.1X (head array) over a normally oriented single head at a target bit error rate (BER) of 10^{-3} with oversampling signal processing.

If the rotated reader is used to readback bit patterned media recording at 10 Tb/in^2 density, it offers more than 20 dB gain compared with a normally oriented head array for a target BER of 10^{-3}. The tradeoff between oversampling and increased target length is examined. Island jitters are found to be non-Gaussian distributed. The performance of the new design is also investigated for various bit patterns, island jitter and head noise.

Micromagnetic writing on 8nm grains and readback with various readers has also been studied. For a conventional writer recording a pseudo-random binary sequence with 2 Tbits/in^2 channel bit density, user densities of 1.52 Tbits/in^2 and 1.09 Tbits/in^2 can be achieved with a rotated single sense head (RSH) and a normally oriented single head

(NSH) respectively, using oversampling signal processing. Simulation indicates that a RSH with multiple scans and 2D equalization provides better resistance to a skew angle of 15° than NSH. An optimized shingled writer is proposed; simulation indicates that a RSH and RHA can reach a user areal density of 3.76 and 4.52 Tbits/in^2 for 2 grains per channel bit, which is close to the predicted maximum user areal density (4.66 Tbits/in^2) for this grain size obtained with an ideal writer and reader.

Table of Contents

List of Tables

List of Figures

Chapter 1 Introduction

In this chapter, the background information combined with the motivation and outline of the thesis is presented. A brief history of data storage technology is first introduced. The magnetic components for recording are reviewed. Then the challenges and physically fundamental limits are discussed, and possible candidates for density above 1Tbits/in^2 are explained with their own advantages and disadvantages. Additionally the signal processing technique for the read channel is briefly described. Finally, the scope of the thesis is presented.

1.1 Development of data storage technology

The hard disk drive has undergone both evolutionary and revolutionary changes at a tremendous pace since its invention. Fig.1.1 indicates how the areal density of magnetic recording increased since the first commercial product [1.1]. The first commercial hard disk drive was introduced by IBM in 1956, which was called the random access method of accounting and control (RAMAC). It can store about 5MB data with the areal density of 2Kb/in^2 and provide a data transfer rate of 8.8 KB/s [1.2]. By the end of 1990s, the longitudinal magnetic recording (LMR) has been the dominant technology for hard disk drive, where the magnetization lies in the plane of a thin film media [1.3]. However, the difficulty of striking a balance among thermal stability, signal-to-noise ratio and writability make LMR slow down and remain below 130 Gbits/in^2 [1.4]. Around 2005, perpendicular magnetic recording (PMR), where the magnetic anisotropy aligns perpendicular to the media planes, has taken the place of LMR in HDD product as it can achieve the areal density of above 500 Gbits/in^2 [1.5] [1.6] [1.7]. It is believed the limitation of the achievable areal density by PMR is around 1 Tbits/in^2 [1.8]. In order to

further increase the density above 1 Tbits/in^2, some novel magnetic recording architectures have been proposed, such as heat-assisted magnetic recording (HAMR) [1.9], [1.10], bit patterned magnetic recording (BPMR) [1.5] and two dimensional magnetic recording (TDMR) [1.7], [1.11] . In 2013, Seagate demonstrated the milestone storage density of 1 Terabits per square inch with HAMR [1.12]. It is further believed that achieving toward or above 10 Tbits/in^2 is possible by using the HMAR technology to write on the bit patterned media [1.13].

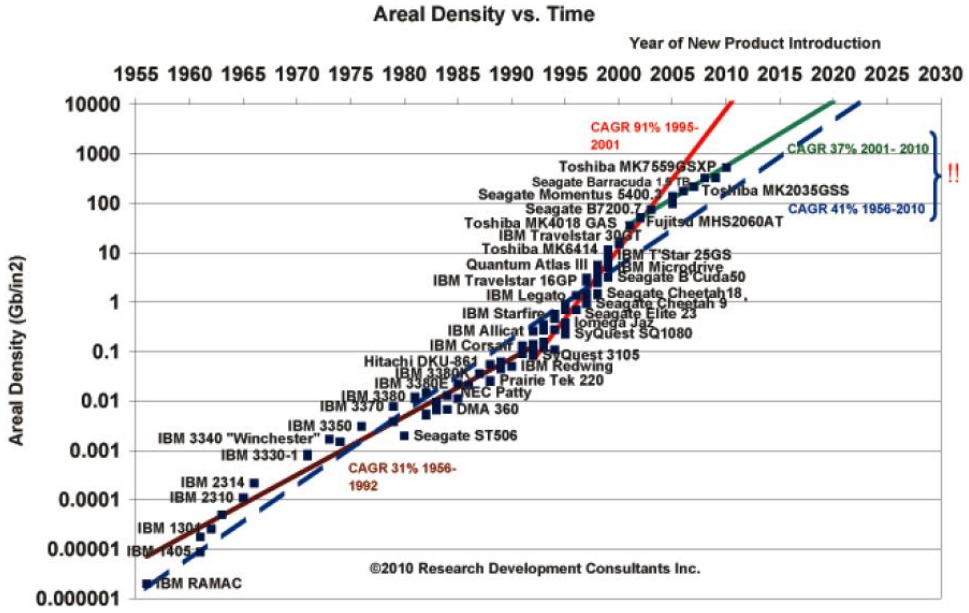

Figure 1.1 The areal density history in magnetic hard disk drive industry [1.1].

1.2 Basic magnetic component for perpendicular magnetic recording

1.2.1 Basic components of hard disk drive

The basic components of hard disk drive are shown as Fig.1.2 [1.14]. For a typical hard disk drive (HDD) design, those flat circular disk named platters are utilized to keep the recorded data, which are held by a spindle. The platters are made from a nonmagnetic material, coated with a thin layer of magnetic material of thickness 10~20nm, then coated

with a carbon layer as protection. The information is written and read by the write/read head, which is located at the tailing edge of slider. Usually there are multiple platters for each HDD, and one write/read head for each platter. The rotation of the platter is controlled by a spindle motor, while during the writing and reading process, the read/write head assembly is moved radially across the spinning platters with an actuator arm controlled by a voice coil actuator. The fly height between the slider and the spinning disk is controlled with a self-pressurized air bearing mechanism. When the head assembly and slider are positioned along the radical direction, different data tracks are written on the disk.

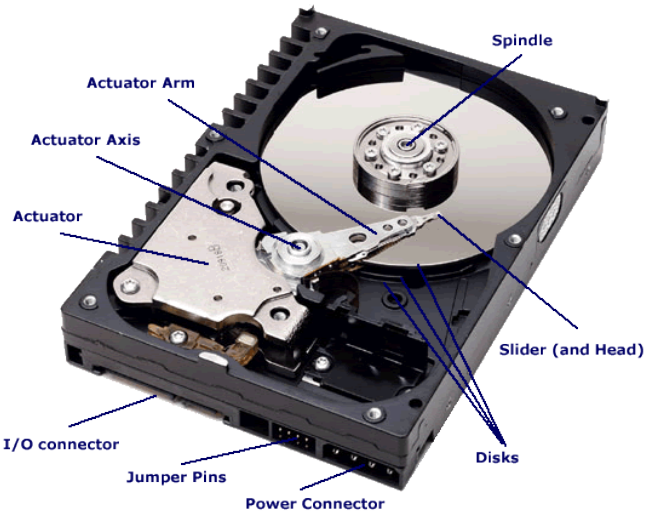

Figure1.2 Basic components of hard disk drive [1.14].

A hard disk drive usually consists of four major parts: a head-disk assembly (i.e. magnetic read/write heads and magnetic disk), data detection electronics and write circuit, mechanical servo and control system and interface to microprocessor. Here we will focus on the head-disk assembly, the data detection scheme and writing current control due to their closeness to the research.

1.2.2 Basics of magnetic recording

A nonvolatile information storage device is constructed from a physical system accommodating two distinctive states. Such two states can be altered back and forth by a transducer, and produce distinguishable signal detected by the other transducer. For magnetic recording, the two distinctive states are formed by magnetic hysteresis, and altered by the different magnetic field produced by the magnetic writer and sensed by the magnetic reader. There are two important magnetic recording systems during the development of magnetic recording technology, i.e. the longitudinal and perpendicular magnetic recording system, illustrated by Fig.1.3 [1.15], [1.16]. For longitudinal magnetic recording, the anisotropy of the medium grains is longitudinal, which aligns the magnetization within the plane of thin recording layer. The bits are written with the stray field in the medium near the head gap, which is produced with the ring head driven by a writing current [1.17]. For perpendicular magnetic recording, the anisotropy of the medium grains is perpendicular to the plane of recording layer. The bits are written with a monopole writer, whose field can be ideally doubled due to the magnetic image offered by the soft underlayer under the recording layer. Currently the LMR has been replaced by PMR due to the great advantage offered by PMR with respect to achievable density. In longitudinal recording, the space charged domain walls formed between the bits produce large magnetostatic fields, which destabilize the recorded magnetization and broaden the transition. Correspondingly, severe transition jitter and nonlinear transition shift are produced. On the contrary, the magnetostatic fields produced by the grains in PMR stabilize the magnetization and favors sharp transitions due to the perpendicular anisotropy of the medium grains. Also the thicker media guarantees more thermal

stability and the greater field produced by the monopole writer and SUL make larger medium coercivity possible.

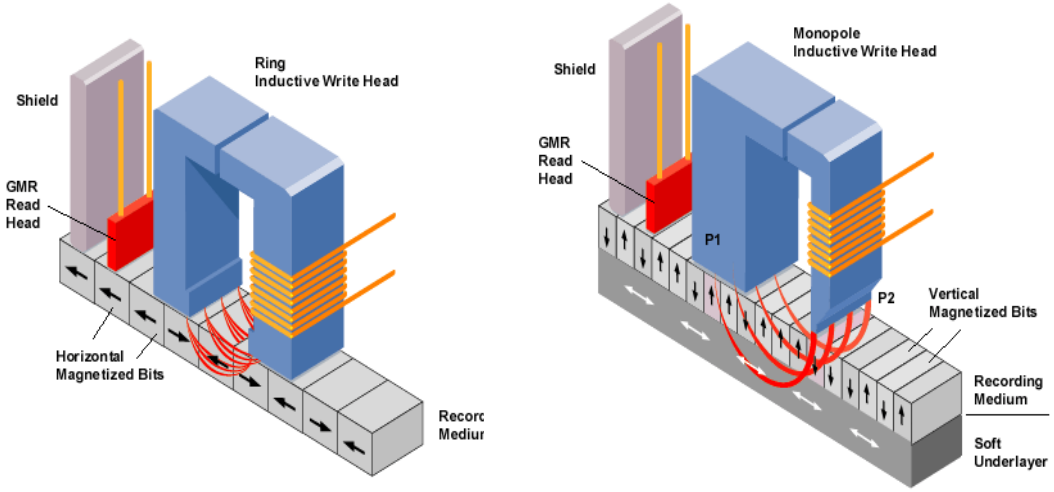

Figure 1.3 Longitudinal recording system (left) and perpendicular recording system (right) [1.15], [1.16].

1.2.3 Magnetic write head

Usually, a perpendicular writer is made from soft magnetic material with high permeability and electrical resistivity. The high flux density, high field gradient, low adjacent track erasure field and low remnant field are desirable for a good writer design. For perpendicular recording, due to the imaging effect and closed flux loop offered by the SUL, the perpendicular write field produced by the monopole is much stronger compared to that of the ring head in LMR. However, the maximum field produced by the main pole is limited by its magnetization. Since the highest magnetization typically reported for magnetic materials is about 1980 emu/cm^3, the maximum magnetic field produced by the writer can only reach $4\pi M_s \approx 2.4T$. Due to the requirement of a tiny main pole in the

writing process of magnetic storage owing to the required gradient and avoid any of adjacent neighbor erasure, the actual recording field is much smaller than 2.4T [1.18].

In order to decrease the erasure of adjacent bits caused by the writing with the mono pole, a trailing shield is placed in the proximity of the trailing edge to increase the field gradient without decreasing the field substantially. Correspondingly, a sharper transition is written at the trailing edge of the writer when the head moves, and an improved bit error rate performance can be achieved. As the density keeps increasing, the track width is compressed to increase the total areal density. Under such a condition, it is important to obtain a low adjacent track erasure field while keeping the high field gradient along the down-track direction. Correspondingly a smaller main pole and wrap around shield (WAS) is needed to guarantee high field gradients on both down-track and cross-track directions and keeps the lower adjacent track erasure field, shown in Fig.1.4 [1.19]. When the areal density increases higher, the main pole size is needed to be further decreased in order to decrease the erasure of adjacent bits and tracks; however, too small main pole cannot produce strong enough field to write the high coercivity grains. This dilemma can be solved with a new writing scheme called shingled writing [1.6], [1.11]. The shingled writer uses its corner to write a wide track, and then trims the previous track width into a narrower track utilizing the track overlap when it moves across one track away, shown in Fig.1.4. Correspondingly, a wider writer can be used to write a narrower track. Besides only the field gradients along the two sides of the writer corner are concerned, the constraints on the design of the writer are loosened compared to the writer design for conventional magnetic recording. If the user density near 10 Tbits/in^2 is desired, a laser and a waveguide combined with near field transducer are positioned near the

conventional perpendicular writer to write the bits on the medium above Curie temperature, and store it when it cools down; such a technology is called HAMR [1.9], [1.10].

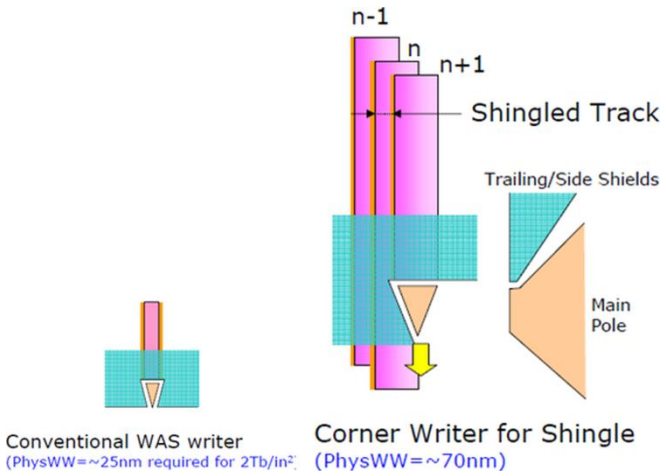

Figure 1.4 The air bearing surfacre (ABS) view of conventional writer (left) and shingled writer (right) [1.19].

1.2.4 Magnetic recording media

In order to reach the stable and satisfying writing performance for perpendicular recording, the recording media needs satisfy several requirements such as high coercivity, perfect squareness, uniform grain size and well isolated granular structure. At the beginning of magnetic recording, particulate media was fabricated. With the development of vacuum technology, thin film media can be fabricated, which can offer a smooth surface and higher packing density compared to particulate media. With the increase of recording density, smaller grains with higher anisotropy are needed to keep the thermal stability of the grains and enough SNR; however the field produced by the writer is limited by the magnetization of the material. Correspondingly, some new media designs are needed to solve this dilemma. Victora and Shen [1.20] proposed an exchanged coupled composite media for perpendicular magnetic recording, which consists of

magnetically hard and soft region. The high anisotropy of the hard region keeps the thermal stability of the grain, while the easier switching of the magnetization in the soft region facilitates the rotation of the magnetization in the hard region, decreasing the switching field. Another multilayer exchange spring media was designed by Suess [1.21] for magnetic recording, where domain walls nucleated in the bottom softest region is propagated along the column of grains. Such a media can decrease coercivity more than a factor of two while keeping the same energy barrier as a single phase media.

1.2.5 Magnetic read head

Prior to 1990, a inductive head was used as a magnetic read head for all hard disk drives, whose readback signal magnitude is proportional to the magnetic flux from the recorded bit, the number of turns of coils wrapped around the head and the relatively velocity between the head and disk. However, the magnetic flux produced by a smaller bit decreased when the recording density increases and the number of turns of coils and the disk velocity (limited by engineering techniques) make the readback signal from an inductive head too small to provide adequate signal-to-noise ratio, which require the invention of more powerful detectors. However, magnetoresistive (MR) heads were the successful answer, which become a landmark in magnetic recording history and boost the achievable density greatly. Compared to the inductive head, the magnetoresistive heads read back based on a totally different principle. The resistance of the head changes when the magnetic flux from the disk changes, which is independent of the disk velocity. Correspondingly, the readback signal is the same for any speed. Besides, the resultant signal from the magnetoresistive head is directly proportional to the MR ratio, which

produces a larger signal than that of inductive head. Hence the SNR of readback signal is improved greatly.

In 1988, the first observation of giant magnetoresistance (GMR) by Grünberg and Fert were made on Fe/Cr/Fe trilayers and multilayers [1.22], [1.23]. Such a structure exhibits a low and high resistance state when the ferromagnetic layers are parallel or antiparallel to each other, respectively. The principle for GMR can be briefly explained with a two channel model, shown in Fig.1.5 [1.24]. It is known that the travelling electrons interact with the ferromagnetic superlattice differently when their spin directions are opposite to the magnetization of the lattice compared with the parallel case. Hence one spin direction scatters less as it passes through both layers in the parallel case, while both spin directions scatter equally at the antiparallel case.

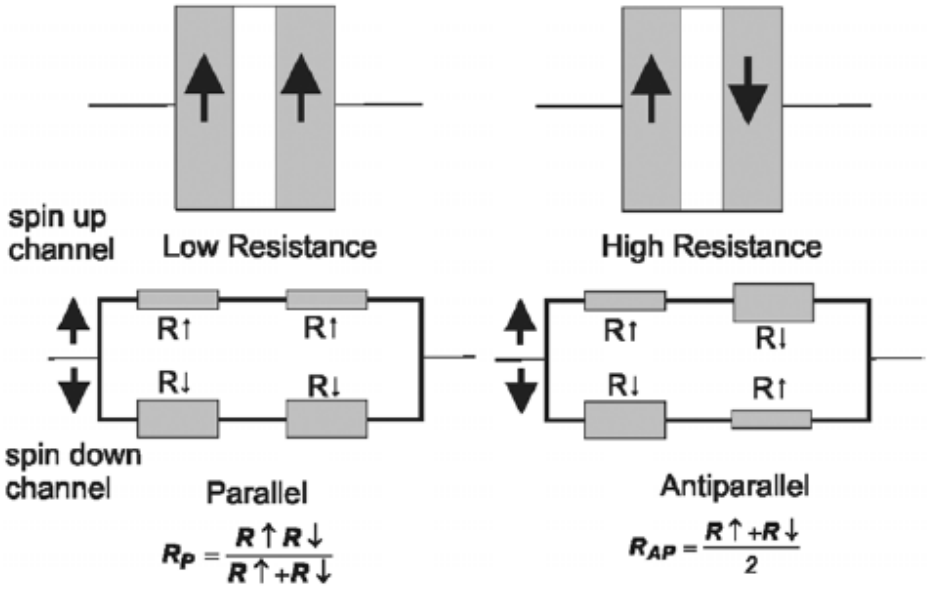

Figure 1.5 Spin valve based on the GMR effect [1.25].

When the MR device is used as a magnetic read head, the magnetostatic field produced by the recorded patterned on the media causes the switching of local magnetic moment in the free layer, correspondingly the magnetoresistance of the head varies depending on the

relative direction of the magnetizations in the multiple layers. In order to enhance the SNR of the readback signal for MR head, usually the sensing structures are positioned between two soft magnetic layers named shields to prevent the sense of magnetic flux from adjacent bits. Additionally a longitudinal bias scheme is utilized with two permanent magnets abutting the MR element along the longitudinal direction in order to maintain the single-domain state of the element, but without sacrificing its sensitivity.

There are two types of GMR head depending on the relative direction of current and the layer plane, which are current-in-plane (CIP) GMR and current perpendicular to plane (CPP) GMR heads [1.25], [1.26]. The CIP GMR head is first adopted as the read head in hard disk drive in early 1990s, it shows great performance improvement compared to the anisotropic magnetoresistive (AMR) head and inductive head. However it seems to be reaching its limit due to the decrease of head efficiency with the decreasing read gap length or read track width and a rising temperature caused by a large sense current density. And thus for the recording density over 100-200 Gbpsi, the CPP GMR seems to be the next generation of read head due to its larger intrinsic MR ratio, lower heating issue by the current and increased ΔRA (the resistance change and element area product), illustrated as Fig.1.6 [1.26]. If the recording density further increases, the ΔRA of CPP-GMR needs to be further increased with some new material and structure, such as choosing material with large spin asymmetry coefficients [1.27], utilizing a half-metallic magnet [1.28] or some confined-current-path structures [1.29]. Another magnetic tunnel junction (MTJ) device is widely used as the read head, which shows much larger MR ratio than that of GMR device. For example, CoFeB/MgO/CoFeB MTJs shows the giant TMR effect, and the MR ratios can reach 200-500% at room temperature (RT). However,

the low RA products and much higher MR ratios are needed for high recording density. For example, a RA product below 1Ω um^2 and a MR ratio of above 50% are required for areal recording densities above 500 Gbit/inch^2 [1.30]. Hence a low RA product and a high MR ratio with MTJs are needed for high recording density.

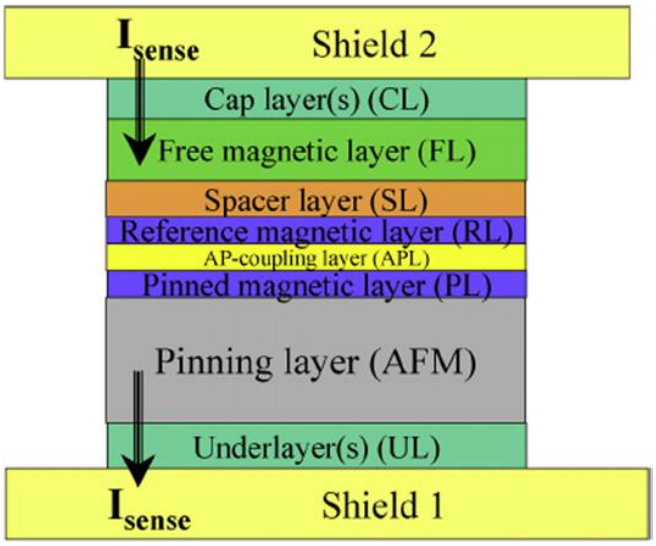

Figure.1.6 The ABS view for optimizing CPP read-head structure [1.27].

1.3 Challenges for magnetic recording above 1Tb/in^2

In order to increase the storage density, the bit size needs to be decreased during the recording process. However, the signal-to-noise ratio (SNR) is proportional to the number of magnetic grains per bit (N), namely SNR (dB) ~ log (N) [1.31]. It is necessary to scale the size of magnetic grains when scaling the bit size so as to keep good enough SNR. By scaling all the relevant physical dimensions (such as bit size, grain size, writer and reader geometry, magnetic fly height, media thickness), the magnetic hard disk drive industry successfully increased the recording density by around 30% per annum for perpendicular magnetic recording technologies over the past ten years. However, thermal stability will prevent the continuing scaling of the magnetic grains for ultra-high density

recording, in other words, grain size smaller than the physical limit is likely to allow the magnetization to switch within a shorter time than the required time-scale (e.g. 10 years) for magnetic recording technology due to thermal fluctuation [1.32].

Superparamagnetism is a form of magnetism, in which small ferromagnetic or ferromagnetic nanoparticles may exhibit a behavior (such as the random flip of the magnetization under the influence of temperature) even at temperature below the Curie temperature. For the change of magnetization, usually irreversible switching needs to overcome an energy barrier ΔE in some part of the particle configuration, and thermal energy can greatly aid the crossing of the energy barrier. Assuming a uniaxial and single domain particle and the magnetic field applied along the easy axis, then the energy barrier needed to overcome to switch from one direction to the other direction is $\Delta E = K_u V[1 - \frac{H}{H_k}]^2$, where K_u is the anisotropy constant of the material, V is the volume of the particle and $H_k = {}^{2K_u}/_{M_s}$. If $K_u V$ is too small when the grain size shrinks, then thermal energy can overcome the anisotropy energy to randomly switch the magnetization from one easy axis direction to the other even without the applied field. Usually the anisotropy energy $K_u V$ for the granular grain in data storage is within the range of $40k_BT$ and $70k_BT$ to make it thermal stable around 10 years, where k_B is the Boltzmann constant.

Correspondingly, the superparamagnetic limit imposes a well-known trilemma of SNR, thermal stability and writability for magnetic recording, shown as Fig.1.7. First, as mentioned before, when the number of grains per bit is decreased, the SNR becomes inferior. Additionally, the transition noise take the dominant role since the reduction of bit size reduces the area of low noise region. Correspondingly the grain size needed to be

decreased to keep enough grains per bit for enough SNR. It seems increasing K_u is inevitable for the thermal stability, which also means higher magnetic field produced by the writer is necessary to switch the magnetization of the grain. However, the maximum field produced by the main pole is decided by its magnetization. Since the highest magnetization for all reported magnetic materials is about 1980 emu/cm^3, the maximum magnetic field produced by the write can only reach $4\pi M_s \approx 2.4T$. Due to the requirement of a tiny main pole in the writing process of magnetic storage considering the gradient and avoid of adjacent neighbor erasure, the actual recording field is much smaller than 2.4T [1.18].

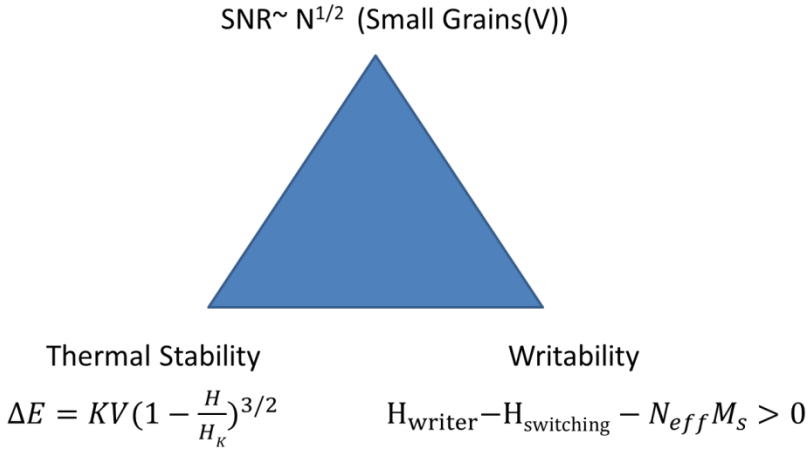

Figure 1.7 The trilemma for increasing magnetic recording densities.

1.4 Possible candidates for density above 1 Tbits/in^2

It seems the trilemma for magnetic recording has produced a dead end; fortunately, several new recording architectures are being explored to increase the areal density beyond these limits. Such new options include bit patterned magnetic recording (BPMR) [1.5],[1.33], heat assisted magnetic recording (HAMR)[1.9],[1.10] and shingled write

recording (SWR) [1.11] combined with 2-D readback and signal processing, namely two-dimensional magnetic recording (TDMR) [1.7].

1.4.1 Bit-patterned magnetic recording

For conventional granular media, the irregularity of grains and the strong magnetic interaction among grains cause severe modulation noise and transition noise, and the SNR is degraded at ultra-high areal density. For BPMR [1.5], [1.33], the information is stored at a uniform, well-defined and separated magnetic island with lithographical technology, which reduces the transition noise and non-linear bit shift. It also provides a solution for superparamagnetic problems as the thermal stability is decided by the anisotropy and whole volume of a single island instead of a single grain, shown in Fig.1.8. With micromagnetic simulation, the recording performance of BPMR for areal density of $4Tbit/in^2$ is studied [1.33].

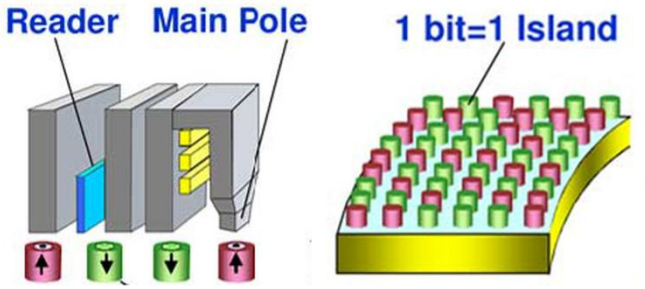

Figure1.8 Schematic of BPMR system [1.13].

Traditional lithography techniques seem inadequate to fabricate BPM with feature size less than 20nm, although electron beam lithography, limited by its low throughput, can be applied for such a small feature [1.13]. Also, lithography jitter can cause variations in islands size and position. In addition, the variation in writing synchronization and fluctuation in switching field leads to writing error. When the areal density is increased, inter-symbol interference (ISI) and inter-track interference (ITI) will be prominent due to

the close arrangements of islands on both down and cross track directions. Correspondingly, this thesis involves the readback and explores the optimum performance of such an environment with severe ITI, ISI, and island jitters for the BPMR system.

1.4.2 Heat –assisted magnetic recording

HAMR is proposed to address the writing issue for granular media with extremely high anisotropy, such as FePt whose switching field is around 50 kOe [1.10]. In heat-assisted recording, the temperature of a high-anisotropy medium is locally elevated above the Curie temperature to facilitate the writing process by significantly reducing the magnetization switching field, and then quickly dropped below Curie temperature to store recorded information [1.9]. The heating and cooling process is implemented on the same time scale of about 1ns to achieve the necessary data rate and large thermal gradient for a sharp transition. An example of an HAMR system is shown in Fig.1.9 [1.10]. A free-space laser beam is coupled into a waveguide on the trailing edge of the slider using a grating coupler. The previous technology of slider's fabrication, air bearing and magnetoresistive reader used in current perpendicular magnetic recording are still implemented here. In order to form a diffraction limited focal spot, the waveguide is shaped to form a planar solid immersion mirror (PSIM) [1.34]. A near field transducer (such as a beaked metallic plate antenna) would further concentrate the focused optical spot. With such high temperatures required for HAMR, the lubricant and the carbon overcoat for the medium should be carefully designed to avoid poor tribological performance caused by the high temperature.

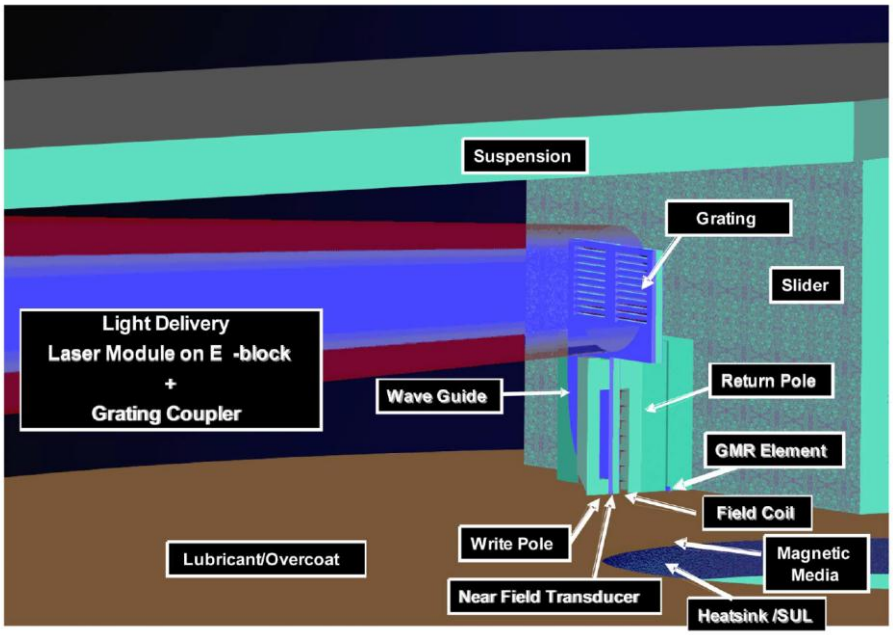

Figure 1.9 A schematic diagram of an HAMR recording system [1.10].

There are three challenges for HAMR technology as follows: (1) Development of small grain recording medium with good thermal and magnetic properties; (2) Development of integrated optical and magnetic write head; (3) avoid any of the failure mechanisms caused by the elevated temperatures in the head, medium, and at the head-disk interface.

1.4.3 Two-dimensional magnetic recording

TDMR combines two important techniques: shingled write recording (SWR) and 2-D read back and signal processing. Shingled writer uses a much wider writer to write data by heavily overlapping tracks; correspondingly the resulting tracks are much narrower than the original written width, shown as Fig.1.10 [1.7]. For a shingled writer, since the corner of the head is used to write the magnetization patterns, the design of such a head is thus much relaxed compared to a conventional head. As the track pitch is independent of head magnetic write width, the singled writer can provide much stronger write field

brought by the larger main pole. Also the sharp corner-edge field brings narrower erase band, which enables us to increase track density.

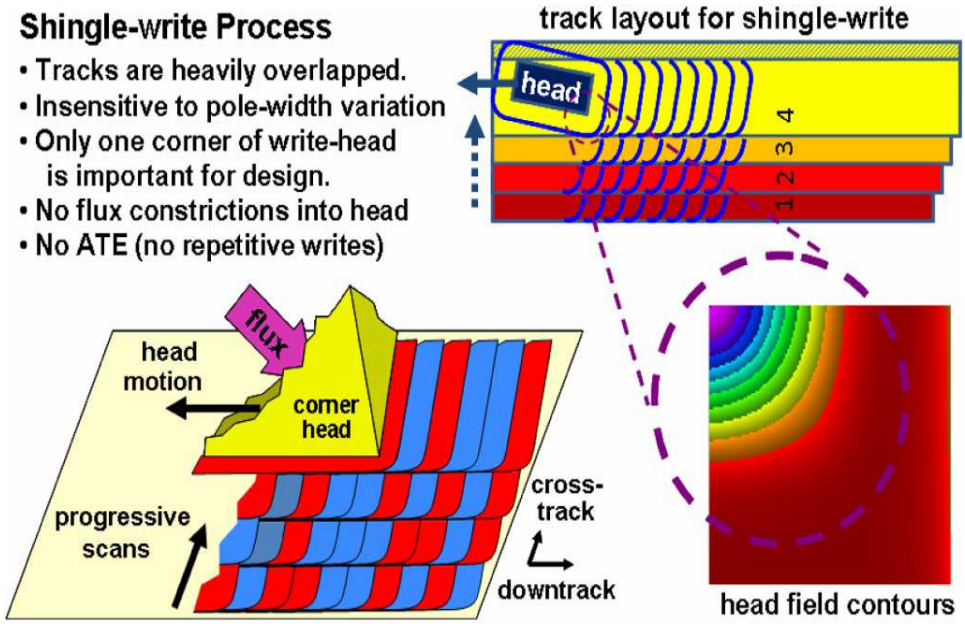

Figure 1.10 Illustration of shingled-writing [1.7].

For readback, previous researchers usually assumed that 2-D signal processing which utilizes the adjacent tracks' information is needed for TDMR due to the similar high level of inter-symbol interference (ISI) and inter-track interference (ITI). The information about the current or adjacent track might be obtained with a head array or several passes of a single head. Prototypes of conventional 1-D channels are now being built with iterative detectors; similar techniques should be developed for 2-D detection, although there is no practical 2D version of a Viterbi detector or its soft-detection derivatives. Reference [1.35] has utilized 2-D maximum a posteriori (MAP) detectors in a TDMR system and compared the performances of various detectors such as inversion, 1-D and 2-D MAP detectors in a TDMR system. Reference [1.36] placed a special emphasis on the suitability of the Voronoi model for the purpose of designing detectors for a TDMR system, and proposed several detection schemes, such as three-track Viterbi algorithm

and the decision feedback Viterbi algorithm. Reference [1.37] used a linear minimum mean-squared error (MMSE) equalizer and a low-density parity-check code to study the detection in TDMR system. In this thesis, considering the asymmetric sensitivity head response causing the asymmetric level of ITI and ISI, we proposed a rotated reader design for sensing very high density magnetic recording data, such as that envisioned for two-dimensional magnetic recording. The simulation indicates that the user density can reach above 10 Tbits/in^2 with the new design, which also avoids a much more complex 2-D detector.

1.5 Overview of signal processing techniques

From the perspective of signal processing and coding techniques, the data storage system can be treated as a communication system. A block diagram of the magnetic recording system is shown as Fig.1.11. Before the writing process, the information is encoded. The actual bits of information which have to be stored on the magnetic medium are referred as "user bits". The stream of user bits is encoded with an error correction code (ECC) and then a modulation code prior to recording them in the form of changing magnetization pattern. The purpose of the ECC encoder is to introduce extra bits to the input stream to detect and correct some of the errors in the detected data. The modulation encoder is necessary due to different system requirements such as the channel synchronization, data detection and recording density consideration. Then the writing precompensation is used by adjusting the writing current to reduce the effect of nonlinear transition shift. In the read channel, usually a finite impulse response (FIR) equalizer is used to shape the channel response to a desired and shorter partial-response target to allow the practical implementation of maximum-likelihood sequence detection (MLSD).

Here sampling rate of the sampler before the equalizer can vary. If the signal is oversampled before the equalization, then it's called a fractional spaced equalizer. If a softer decision decoding is performed, the soft-output Viterbi algorithm (SOVA) detector or the Bahl-Cocke-Jelinek-Raviv (BCJR) detector will take the place of Viterbi detector (VD). The partial-response target combined with the maximum likelihood detector is known as the partial-response maximum likelihood (PRML) receiver. In the receiver end, the modulation code and the error correcting code are decoded to recover the user data. For the next paragraphs, we will introduce some basic signal processing and coding techniques used in magnetic recording systems.

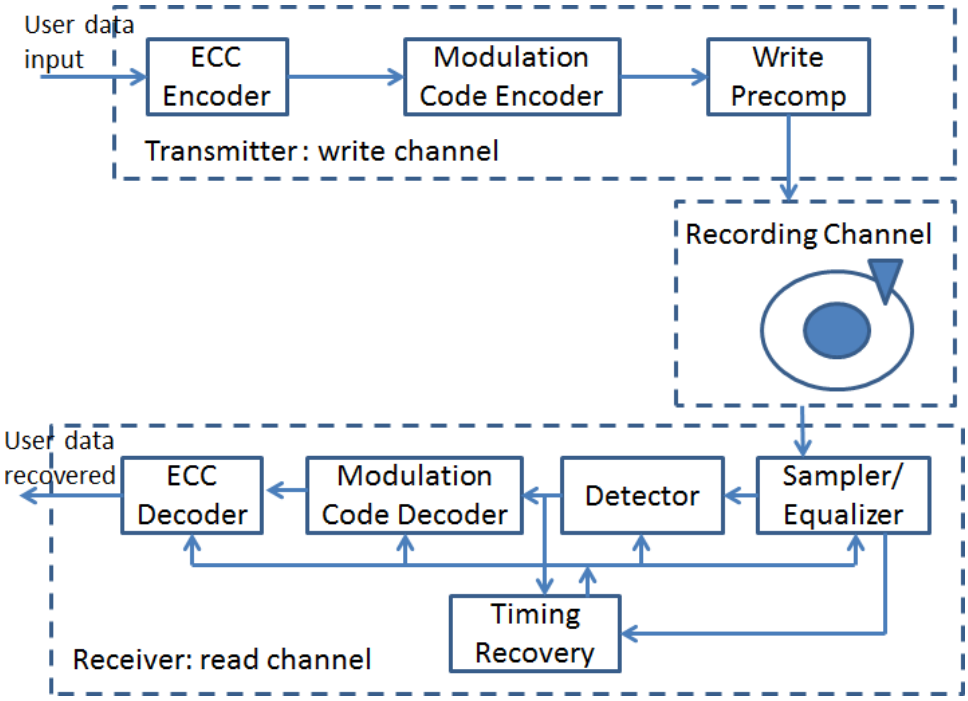

Figure 1.11 System diagram of the perpendicular recording system.

1.5.1 Modulation code

The purpose of a modulation code (constrained code) is for the channel synchronization, data detection and recording density consideration. On one hand, the code has to ensure the magnetization changes at least once within a certain number of channel bits, as long

segments of uniformly magnetized pattern will cause serious problems in channel synchronization and detection [1.38], [1.39]. For synchronization, the phase-locked loops circuit adjusts the phase of oscillator by comparing the signal from the current transition with the prior values of the PLL clock. Correspondingly a long stream of zeros makes the generation of phase update signals impossible and result in phase shifts. On the other hand, the modulation code can constrain the minimum distance between adjacent transitions during the recording process to avoid inter-symbol interference (ISI) and nonlinear distortion.

For a peak detection system, run length-limited (RLL) code (namely (d, k) code) is used as a modulation code to enhance the performance. Such a code constrain the symbols "1" to be separated by at least d and at most k symbols "0" during an encoded sequence. Analogous to the (d, k) code, a class of constrained codes denoted as (0, G/I) code is implemented in the PRML channel to aid the recovery and simplify the design of the Viterbi detector for the channel [1.40]. G means a global constraint which limits the maximum run length of "0" symbols in any code string. I means an interleaved constraint, which limits the maximum lengths of 0 symbols in each of the interleaves of a coded sequence. For the need of a high channel capacity, a constrained code with a very high code rates is used in real systems.

1.5.2 Partial response equalization

When the recording densities are low, intersymbol interference can be ignored due to the adjacent transition being written sufficiently far away to result in a relatively isolated voltage peak; thus peak detection technologies are utilized. When the recording density is further increased, the intersymbol interference shifts peaks of readback signal and

decreases the signal amplitude, which causes poor performances for a peak detector. Correspondingly, a new channel called a partial-response maximum likelihood (PRML) channel was proposed to overcome the channel ISI [1.41], [1.42]. The basic idea for partial response is to introduce several controlled amount of ISI into the recording data pattern instead of trying to eliminate it. It usually assumes that the superposition of readback signal from the adjacent track is linear and the shape of readback signal from an isolated transition is exactly known. In order to decrease the state in the ML detector, usually a finite impulse response (FIR) filter is utilized to shape the channel response to some desired, shorter partial-response target. A classic type of partial-response channel, class IV partial response (PR4) channel is widely used since the PR channel is proposed. And the PR4 channel and its extended family of channels can be expressed with the following polynomials,

$$y(D)=(1-D)(1+D)^N \tag{1.1}$$

where $N\geq 1$. For N=1,2 and 3, the channels that use y(D) as the channel transfer function are called PR4, EPR4 and E^2PR4 channels, respectively. The higher N is, the longer bit periods that a target pulse extends over.

Later, the general partial response (GPR) target was proposed, which uses arbitrary real numbers instead of integer value in the PR target. The equalizer using GPR target reduces the noise enhancement and meanwhile whitens the noise compared to integer-value PR equalizer [1.43], [1.44]. Reference [1.43] indicates the monic constraint on the equalizer target response tends to whiten the noise samples at the equalizer output compared to the fixed-energy constraint. Also the noise-predictive maximum likelihood (NPML) detector is proposed based on the GPR target [1.45].

When the recording density keeps increasing, the track width is compressed to increase the recording areal density; correspondingly the inter-track interference becomes more and more severe and even comparable to ISI. Lots of novel equalization schemes have been proposed to address the ITI issue in higher recording density. The performance of a read channel in the presence of both ITI and additive white Gaussian noise (AWGN) were analyzed with maximum-likelihood (ML) sequence detection [1.46], however such an ML detector is quite complex when there is ITI. Then the suboptimal joint-track equalization was first proposed in [1.46] and subsequently optimized and utilized in perpendicular recording and BPMR [1.47], [1.48]. The core idea for joint-track equalization is a one-dimensional equalizer with a 2D GPR target to match the channel response of the main track with ITI. For detection, a Viterbi algorithm with a modified trellis is utilized, where the modified trellis was obtained by adding branches considering the ITI from immediately adjacent tracks. Further, a two-dimensional (2-D) equalizer with a 2-D GPR target based on the minimum mean square error (MMSE) is proposed for the read channel with ITI [1.49], which forces the ITI to be zeros and keeps only the controlled ISI to avoid the complex 2-D Viterbi detector. Under severe ITI and ISI, the use of iterative decision feedback detection (IDFD) [1.50] can provide superior performances compared to the conventional 1-D equalization. Furthermore, multi-track detection is proposed in [1.51] combined with joint-track equalizer and 2D equalizer , where the core idea is that a posteriori probabilities (APPs) obtained from the detection of two adjacent-tracks is used as a priori information for the detection on the center track.

1.5.3 Detection

Before the invention of the PRML channel, peak detection was utilized in the longitudinal magnetic recording. For perpendicular magnetic recording, combined with a partial response target, the Viterbi or other trellis based detector is used to detect the data sequence, which avoids the computational unfeasibility for pure maximum likelihood sequence estimation.

The conventional Viterbi detector is an optimum sequence detector for a read channel with ISI and AWGN. Its basic principle is to maximize the conditional probability$\Pr(\bar{y}|\bar{s})$, where $\bar{y}$ and $\bar{s}$ are the received and input sequence, respectively. The Viterbi detector is a trellis based detector, where the number of states are decided by the modulation method and finite memory determined by the PR target length for PRML channel. It selects the sequence that minimizes the accumulated branch metric as a surviving sequence and discards the other merged sequences to the same state.

When soft decision decoding is needed, the soft-output Viterbi algorithm (SOVA) or the Bahl-Cocke-Jelinek-Raviv (BCJR) detector will be used instead of the VD with hard decision. SOVA considers a prior probability of the input symbol, and produces a soft output measuring the reliability of the hard bit decision of the Viterbi algorithm by considering the difference between the chosen branch metrics and the discarded branch [1.52]. The BCJR algorithm is based on a trellis running two Viterbi-like algorithms. It recursively calculate the forward state metrics and the backward state metrics, which are associated with the branch metrics to estimate the a posteriori probability of each bit.

As the media noise in perpendicular magnetic recording channel is nonstationary, correlated and data-dependent, the conventional Viterbi detector is no longer the optimal detector since the noise is not AWGN. Correspondingly, modifications to the

conventional Viterbi detector are needed. A pattern-dependent noise predictive Viterbi detector[1.53],[1.54],[1.55], which embedded a branch-dependent prediction of the noises for each branch metric to better characterize the data-dependent nature of the transition noises, shows a superior performance over the convention Viterbi detector. Pattern-dependent noise predictive detector (PDNPD) is a near maximum likelihood sequence estimation scheme for zero-mean, data-dependent, finite-memory Gauss-Markov noise. Reference [1.56] proposed a mean-adjusted pattern-dependent noise prediction for the channel consisting of both jitter noise and NLTS.

When the recording density keeps increasing, the track width is compressed and ITI becomes a major detriment to detection, especially in TDMR systems. Correspondingly, some multi-track detector, even 2-D detectors are proposed and utilized in ultra-high recording density. Reference [1.57] views the off-track interference as the response of the channel to an independent data sequence, simultaneously estimates the two data sequences by joint PRML detection, and then simply discards the adjacent track data at the end. Different from usually 1D detectors which suppress ITI with equalization, a 2-D maximum a posteriori probability (MAP) detector [1.58], which treats ITI as useful information to help the decision, is utilized in TDMR system, and it's proved to obtain a great density gain compared to 1-D MAP detector. However it is still prohibitively complex even for modest sector sizes. The separable 2-D MAP detector [1.59] treats 2-D ISI matrix as a product of a column and a row vector, and then a 2-D channel can be treated to be a concatenation of two 1-D channels. Hence a relatively low-complexity detector can be developed.

1.5.4 Error correction codes

The noises, nonlinear distortions and interference may cause errors for detection in magnetic recording systems. Losing the information in a hard disk drive should be kept as an extremely low-probability event, and the ultimate probability of error should be around 10^{-14}. Correspondingly, error correction codes (ECC) is used after the detection to correct errors during the writing and reading process, and it greatly boosted the reliability of data recovery.

Usually, there are two types of error-correcting codes: codes of block type and codes of convolutional type. Among the block typed code, a Reed-Solomon (RS) code and the low-density parity-check (LDPC) codes are the two most important ECCs in magnetic recording. RS codes are maximum distance separable (MDS) codes among the (n, k) cyclic codes, namely it can achieve the maximum minimum Hamming distance: $d_{min}=n-k+1$, and it can correct any burst of errors with a length of (n-k)/2. Meanwhile the hard decoding of RS codes makes it easy to be implemented. The LDPC code could replace the RS code in the future magnetic recording systems due to its near-capacity performance. Additionally the adaptation of a parallelizable decoder, lower error-rate floor and the superior performance in burst errors makes LDPC codes superior to turbo codes.

1.5.5 Writing precompensation

Nonlinear transition shift (NLTS) is a phenomenon in which the transition location is shifted due to the magnetostatic field produced by previous written transitions. The complex nature of the nonlinear effects for NLTS means that very few theoretical studies on the optimal precompensation of NLTS have been carried out. Usually the amount of precompensation needed for NLTS is measured using several different approaches.

Pseudorandom sequences are used to measure the NLTS, which involves the recording of a binary pseudorandom sequence and the capture and processing of the playback waveform [1.60]. Harmonic elimination technique is also used to measure the nonlinear bit shift, which is useful for designing, tuning and testing PRML precompensation schemes [1.61]. In order to precompensate NLTS, besides the classic dibit precompensation, other theoretical studies are carried out to obtain the optimal amount of precompensation. Lim and Kavčić [1.62] showed how to compute these optimal precompensations for partial erasure and nonlinear transition shift in a longitudinal channel with dynamic programming, whose objective was to minimize the mean-squared error between the output signal of a noisy, nonlinear channel and that of a linear channel without noise. Wu [1.63] proposed a multilevel precompensation scheme which precompensates different amounts for different dominant NLTS cases beyond the dibit transition in order to minimize the BER of the read channel.

1.6 The scope of this thesis

As mentioned previously, TDMR is a promising candidate to reach density above 1 Tbits/in^2. Usually a shingled writer is used to write data, and two dimensional signal processing and powerful error correcting codes is used for recovering the readback signal and reaching ultra-high storage density. However, on one hand, most signal processing researchers utilized some simplified and unrealistic models (such as perfect writing, 2-D symmetric Gaussian reader, extremely sharp resolution) and too complex advanced signal processing techniques (such as 2-D detector) to study the detection in TDMR systems, which makes the results far from the realistic system and such signal processing algorithms are not likely to be utilized in the hard disk drive due to the high complexity

and latency. On the other hand, the researchers, who use micromagnetic simulation to design the shingled writer and reader, most focus on the magnetic specification of the head and media without really optimizing and analyzing the performance as a whole system combined with a read channel, which makes such a design less accurate for a complex recording system such as TDMR.

In this thesis, we combined both micromagnetic simulation and signal processing to study the specifications and performance of TDMR system. First, a novel system design for sensing very high magnetic recording data, such as that envisioned for TDMR, is proposed. The key idea is a rotated sense head, so that the shields are aligned down-track, combined with oversampled signal processing to regain the lost down-track resolution. Based on a random Voronoi grain model, the bit error rate reached by both a rotated sense head and normally positioned head array are compared with sampling period of 2 nm, a minimum mean squared error equalizer, and pattern-dependent noise prediction detector. The user density reached by the new design is greatly increased above 10 Tbits/in^2. The performances of both heads are further studied by using the quasi-cyclic low-density parity-check (QC-LDPC) code in a TDMR system. The significant improvement in performance of the rotated head compared to the normally oriented head is studied and explained from a signal processing perspective. The decoded performances of both heads are studied. The performance of a rotated sense head is also examined for densities of 2-7 Tbits/in^2 recorded on granular media for a TDMR system. The density gain achieved by the new design is compared to the normally oriented head. Detection for bit patterned media recording at 10 Tbits/in^2 densities is studied with various readers and bits arrangements; the performances of various systems are compared. The tradeoff

between oversampling and increased target length is examined. Island jitter distribution is also studied. The performance of the new design is also investigated for various bit patterns, island jitter and head noise. The TDMR system performance is also studied with micromagnetic writing on 8nm grains and readback with various readers, including both skewed and no skew cases. Also a 3D shingled write head including main pole, side shields and trailing shields are designed and optimized to obtain large field and gradient. After the magnetization patterns are written with such a writer, they are readback with a rotated reader and the achievable density is examined with the PRML channel. The performance reached by the proposed shingled writer and reader is compared to that of perfect writer and reader.

The organization of the thesis is as follows: In Chapter 2, the basic theoretical principle of micromagnetic models is presented. In Chapter 3, a new reader design is proposed for TDMR system to reach 10 Tbits/in^2 densities. The BER and achievable user density reached by various heads are studied in the read channel with both signal processing and LDPC codes. The reason for the superior performance of the new design is explained from signal processing perspective. In Chapter 4, the performance of a rotated sense head is examined for densities of 2-7 Tbits/in^2 recorded on granular media for TDMR system. And the density gain reached by the designed reader compared to conventional reader design is studied for a target BER of 10^{-3}. In Chapter 5, the detection in BPMR system at 10 Tb/in^2 is studied with various readers for both the AWGN channel and more realistic read channel with jitter noises. Jitter distributions are studied. In Chapter 6, we show how to reach above 4 Tbits/in^2 and 6 Tbits/in^2 user density with an optimized micromagnetic shingled writer and the propose reader. The performances of a TDMR

system written with conventional writer and readback with various readers are also compared.

Chapter 2 Micromagnetic Modeling

Micormagnetics was first proposed by Landau and Lifshitz in 1935, and then developed by William Fuller Brown, Jr. "Micromagentics is a field of physics related with the prediction of magnetic behavior at sub-micrometer length scales, which are large enough for the atomic structure of the material to be ignored while small enough to reveal details of the transition region between domains"[2.1].

2.1 Landau-Lifshitz –Gilbert equation

The dynamic motion of the magnetization for a single domain particle can be described by the Laudau-Lifshitz-Gilbert equation:

$$\frac{d\vec{M}}{dt} = \frac{\gamma}{1+\alpha^2}\vec{M} \times \vec{H}_{eff} - \frac{\alpha\gamma}{(1+\alpha^2)M_s}\vec{M} \times (\vec{M} \times \vec{H}_{eff}) \quad (2.1)$$

Where γ=1.76×10^7 Oe^{-1}s^{-1} is the gyromagnetic ratio of the free electron spin, α is the damping constant, $\vec{M}$ is the magnetization moment of the particle, $\vec{H}_{eff}$ is the total effective field acting on the magnetization. Strictly speaking α is not constant, and depends nonlinearly on the magnetization. It has a strong correlation with the microstructure of the material. In numerical simulations, α for hard magnetic materials (such as magnetic medium) is usually taken to be 0.1 or larger, while α for the soft magnetic material (such as magnetic write head and soft under layer) is taken less than 0.05. Usually the effective field $\vec{H}_{eff}$ consists of an applied field, anisotropy field, magnetostatic field, exchange field and thermal agitation field during the simulation of magnetic recording.

The first term on the right hand side of the equation (2.1) is responsible for the gyromagnetic procession of the magnetic moment $\vec{M}$ caused by the toque term $\vec{M} \times$

$\vec{H}_{eff}$, whose angular frequency ω is $|\frac{\gamma}{1+\alpha^2}\vec{H}_{eff}|$. It is called Larmor precession with angular frequency $\omega = r\vec{H}_{eff}$ when α is zero. The second term on the right hand is a damping term added by Gilbert in 1955 in order to describe the dissipation of magnetic energy. Such a torque term $\vec{M} \times (\vec{M} \times \vec{H}_{eff})$ force the magnetization towards the effective field direction. The mechanics of equation (2.1) can be better understood with Fig.2.1.

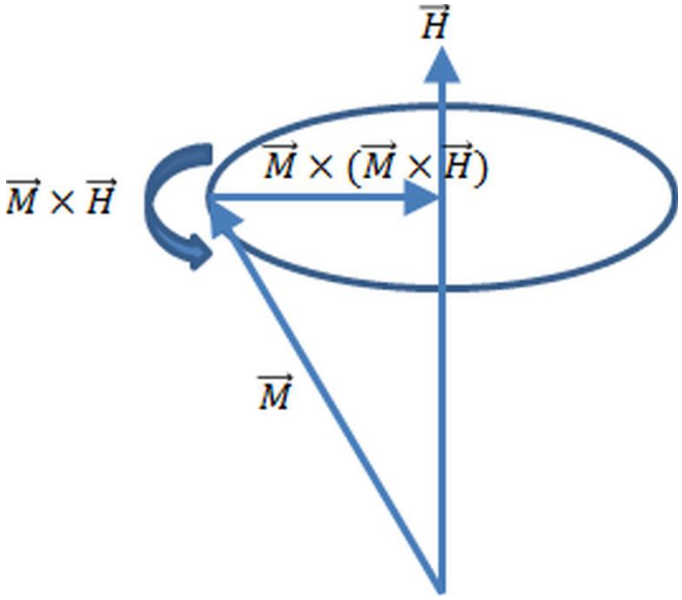

Figure 2.1 Damped gyromagnetic precession of the magnetization moment $\vec{M}$.

During simulation, the LLG equation can be solved with such numerical methods as the Runge-Kutta method or the predictor-corrector method. The latter method can reach four times faster than the Range-Kutta method due to the fewer numbers of steps after the initial conditions are established.

2.2 Discretization of magnetic recording system

Classic Micromagnetics allows for a continuous distribution of magnetization, however, such a continuum system is replaced with a discrete system for the convenience

of numerical simulation. Usually the soft magnetic material (such as write head and soft under layer) is divided into uniform cubic or cells due the continuity of material [2.2]. However the hard magnetic material (such as the recording medium) is divided into the irregular Voronoi cells considering the non-uniform material property and the similarity to actual size distribution. The discretization of the magnetic recording system is illustrated as Fig.2.2. In this simulation, the Voronoi construction which consists of randomly distributed polygons on a plane is used for the grain morphology. The average Voronoi grain diameter, standard deviation of diameter, nonmagnetic boundary spacing and medium thickness can be adjusted for the simulation of the recording medium.

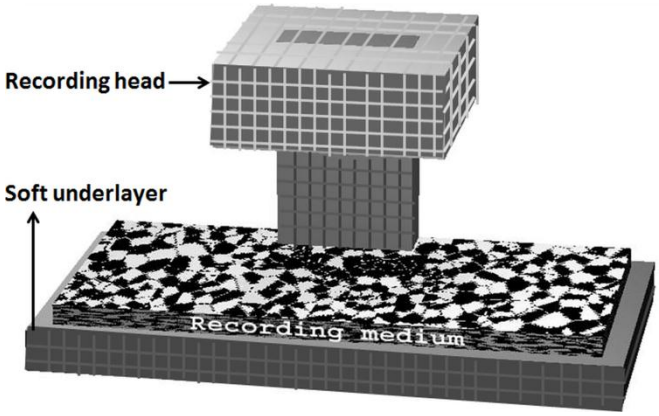

Figure 2.2 Discretization of a perpendicular magnetic recording system using a monopole and Voronoi grains with soft underlayer [2.3].

2.3 Energy term and associated field

During the simulation, the total effective magnetic field in the LLG equation $\vec{H}_{eff}$ consists of the anisotropic field $\vec{H}_{ani}$, magnetostatic field $\vec{H}_{mag}$, exchange field $\vec{H}_{exch}$ and the external applied field $\vec{H}_{app}$. With them, the exchange field is short-range field, while the magnetostatic field is the long-range dipole-dipole interaction requiring lots of computation time. Without considering the magnetoelastic and surface anisotropy effects,

the total magnetic energy of a single domain grain when an external field is applied can be shown in Eqn.(2.2),

$$E_{total} = E_{ani} + E_{mag} + E_{exch} + E_z \tag{2.2}$$

where E_{ani} , E_{mag} , E_{exch} and E_z are the magnetocrytalline anisotropy energy, magnetostatic interaction energy, intergranular exchange coupling energy and Zeeman energy.

Correspondingly, the effective field can be obtain by taking derivative of total energy E_{total} with respect to the magnetization $\vec{M}$, expressed as Eqn.(2.3),

$$\vec{H}_{eff} = -\frac{\partial E_{total}}{\partial \vec{M}} = -\left(\frac{\partial E_{ani}}{\partial \vec{M}} + \frac{\partial E_{mag}}{\partial \vec{M}} + \frac{\partial E_{exch}}{\partial \vec{M}} + \frac{\partial E_z}{\partial \vec{M}}\right) \equiv \vec{H}_{ani} + \vec{H}_{mag} + \vec{H}_{exch} + \vec{H}_{app} \tag{2.3}$$

Then every energy term and the associated field will be introduced in the next sections.

2.3.1 Magnetostatic energy

The magnetostatic potential is similar to the electrostatic potential: it can be derived from $\nabla \times \vec{H} = 0$ as

$$\vec{H} = -\nabla \emptyset_m \tag{2.4}$$

Inside the material, $\nabla \cdot \vec{B} = \mu_0 \nabla \cdot (\vec{H} + 4\pi \vec{M})$=0, $\emptyset_m$ satisfies Poisson's equation as:

$$\nabla^2 \emptyset_m = 4\pi \nabla \cdot \vec{M} \tag{2.5}$$

Then outside the material, the potential satisfies the Laplace's equation as

$$\nabla^2 \emptyset_m = 0 \tag{2.6}$$

The two boundary conditions for the potential with flux continuity are,

$$\emptyset_{in} = \emptyset_{out} \tag{2.7}$$

$$\frac{\partial \emptyset_{in}}{\partial n} - \frac{\partial \emptyset_{out}}{\partial n} = 4\pi \vec{M} \cdot \vec{n} \tag{2.8}$$

Then the solution for the potential is

$$\emptyset_m = -\iiint \frac{\nabla\cdot\vec{M}(\vec{r}')}{|\vec{r}-\vec{r}'|} d^3\vec{r}' + \iint \frac{\vec{M}(\vec{r}')\cdot\vec{n}}{|\vec{r}-\vec{r}'|} d^2\vec{r}' \quad (2.9)$$

where $\nabla\cdot\vec{M}$ and $\vec{M}\cdot\vec{n}$ are the volume magnetic charge density and surface magnetic charge density, respectively. $\overrightarrow{r'}$ and $\vec{r}$ are the source and observation coordinates, respectively.

Then by combining Eqn.(2.4) and (2.9), we can obtain the magnetostatic field as Eqn.(2.10),

$$\vec{H}(\vec{r}) = -\iiint \frac{\nabla\cdot\vec{M}(\vec{r}')}{|\vec{r}-\vec{r}'|^3}\ d^3r'(\vec{r}-\vec{r}') + \iint \frac{\vec{M}(\vec{r}')\cdot\vec{n}}{|\vec{r}-\vec{r}'|} d^2\vec{r}'(\vec{r}-\vec{r}') \quad (2.10)$$

In the simulation, the magnetization is uniform within the volume of the grain, i.e. $\nabla\cdot\vec{M}(\vec{r}') = 0$. Then the Eqn.(2.10) becomes as follows,

$$\vec{H}(\vec{r}_i) = \iint \frac{\vec{M}(\vec{r}_j')\cdot\vec{n}}{|\vec{r}_i-\vec{r}_j'|} d^2\overrightarrow{r_j}(\vec{r}_i-\vec{r}_j') = \sum_{j=1}^{NG} T_{i,j}\vec{M}(r_j) \quad (2.11)$$

where $\vec{H}(\vec{r}_i)$ is the magnetostatic field felt by the *i*th grain, $\vec{M}(r_j)$ is the magnetization of the *j*th grain , NG is the number of grains and $T_{i,j}$ is an interaction tensor from the jth grain to ith grain, which can be expressed as Eqn.(2.12)

$$T_{ij} = \begin{bmatrix} T_{ij}^{xx} & T_{ij}^{xy} & T_{ij}^{xz} \\ T_{ij}^{yx} & T_{ij}^{yy} & T_{ij}^{yz} \\ T_{ij}^{zx} & T_{ij}^{zy} & T_{ij}^{zz} \end{bmatrix} \quad (2.12)$$

When the magnetostatic field between the regular cubic discretization within the soft magnetic material is calculated, the method proposed by Schabes Aharoni [2.4] can be used. The method presented an exact analytic formula for the magnetostatic interaction energy of a three-dimensional array of ferromagnetic cubes, and then exact formulas for the effective magnetostatic interaction field can be derived based on the energy equation.

It is a quite convenient tool for three-dimensional micromagnetic calculation. When magnetostatic field calculation is carried on for the hard magnetic material (such as Voronoi shaped grains), there are two types of magnetostatic interaction due to the side surfaces (rectangular shape) and the top and bottom surfaces (Voronoi shape), shown in Fig.2.3. For the side surface, these rectangular sides are meshed into smaller rectangles, and then the surface interaction is calculated. For the top and bottom surfaces, the Jacobian integral technique [2.5] is used to map the irregular shape into a square for surface integration calculation.

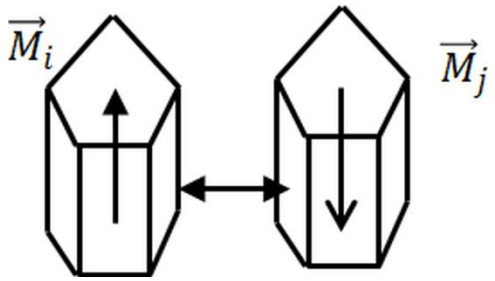

Figure 2.3 Magnetostatic interaction between two Voronoi grains.

2.3.2 Exchange coupling energy

Ferromagnetic materials have the characteristic of the strong interaction between spins, which makes each spin tend to align or anti-parallel to the other surrounding spins. Such an interaction was the origin of the "molecular field" hypothesized by Weiss, long before the discovery of spin and quantum physics. Actually the spin-spin interaction energy called the exchange interaction energy originates from the Pauli Exclusion Principle in quantum physics and Coulomb electrostatic energy. The exchange interaction of M atoms can be expressed with the Heisenberg Hamiltonian format as Eqn.(2.13).

$$E_{ex} = -\sum_{i,j=1}^{M} J_{i,j}\vec{s}_i \cdot \vec{s}_j \qquad (2.13)$$

where $J_{i,j}$ is the exchange integral, which is most significant for the nearest neighbor electrons and decreases rapidly with increasing distance. $J_{i,j} > 0$ for ferromagnetic material, while $J_{i,j} < 0$ for antiferromagnetic material, correspondingly the spins tend to orient parallel and antiparallel for the ferromagnetic and antiferromagnetic material for the minimum energy requirement, respectively.

In the micromagnetic simulation for the recording medium, the exchange coupling energy between the nearest neighbor grains in the medium is calculated based on Eqn.(2.13), and the expression is as Eqn.(2.14), where J is the exchange coupling constant.

$$E_{ex} = -J \sum \vec{M}_i \cdot \vec{M}_j \qquad (2.14)$$

For Voronoi shaped grains in recording media, the interfacial area between grains varies due to the varying grain boundaries between every grain and its nearest neighbors. Considering such an effect, the exchange energy between two grains is assumed to be proportional to their interfacial area as the number of pairs of spins between the grains' boundary is proportional to the interfacial area. Then the total exchange energy calculated with Eqn.(2.14) should be modified as Eqn.（2.15）,

$$E_{ex} = -J \sum \vec{M}_i \cdot \vec{M}_j \frac{S_{ij}}{S_{ave}} \qquad (2.15)$$

Where S_{ij} is the interfacial area between the *i*th grain and the *j*th grain, and S_{ave} is the average side area if grains were hexagons. Then the corresponding exchange field at the *i*th grain can be calculated as,

$$H_{ex} = -2J \sum \vec{M}_j \frac{S_{ij}}{S_{ave}} \qquad (2.16)$$

Besides the energy expression in Eqn.（2.15）used for the hard magnetic material (such as Voronoi grains), there is another exchange energy expression for continuous magnetization which can be derived from discrete system using Eqn.(2.14) , and the final exchange energy density is given as [2.6],

$$E_{ex} = \frac{1}{2} C[(\nabla m_x)^2 + (\nabla m_y)^2 + (\nabla m_z)^2] \tag{2.17}$$

where $C = \frac{2JS^2}{a} c$, a is the edge of unit cell, c=1,2 and 4 for a simple cubic, bcc and fcc crystal structure respectively.

2.3.3 Magnetocrystalline anisotropy energy

It is found that the magnetization usually has a certain favorable direction (called the easy axes) and an unfavorable direction (called the hard axes), which is called magnetic anisotropy. Magnetocrystalline anisotropy is one of the magnetic anisotropies, which will be discussed as follows. The reason for magnetocrystalline anisotropy is that in the presence of a weak spin-orbit coupling, the magnetization will be coupled to electron orbitals and thus have a lowest or highest energy along certain symmetry axes. For magnetic recording, the magnetic material with uniaxial crystalline anisotropy (i.e. the hexagonal close-packed structure) is used as the perpendicular magnetic recording media. The uniaxial anisotropy energy density can be expressed as a power series of the form as Eqn.(2.18),

$$E_{ani} = \sum_n K_{un} \sin^{2n}\theta \tag{2.18}$$

To the first order, the uniaxial anisotropy energy density can be approximated as

$$E_{ani} = K_u \sin^2\theta = K_u(1 - \cos^2\theta) = K_u(1 - \left|\vec{k} \cdot \vec{m}\right|^2) \tag{2.19}$$

, where K_u is the anisotropy energy constant (removing the constant term K_{u0} and combing the effect of K_{u1} and K_{u2} into K_u), $\vec{k}$ and $\vec{m}$ are the easy axis direction and magnetization direction, respectively. The effective anisotropy field can be obtained by taking the derivative of the energy density with respect to the magnetization vector as Eqn.(2.20),

$$\vec{H}_{ani} = -\frac{\partial E_{ani}}{\partial \vec{M}} = H_k(\vec{k} \cdot \vec{m})\vec{k} \tag{2.20}$$

Where $H_k = \frac{2K_U}{M_s}$ is called the anisotropy field.

2.3.4 Zeeman energy

The Zeeman energy is the magnetic energy of a grain under an applied field $\vec{H}_{app}$, which can be expressed as

$$E_z = -\vec{M} \cdot \vec{H}_{app} \tag{2.21}$$

Then the effective field can be derived as

$$\vec{H}_Z = -\frac{\partial E_Z}{\partial \vec{M}} = \vec{H}_{app} \tag{2.22}$$

2.3.5 Thermal fluctuation

The thermal disordering effect to magnetization can be described with a random fluctuation field $\vec{H}_{thermal}$ [2.7]. The basic assumption is that the thermal agitation effect by a random process is that the random thermal forces have much shorter correlation time (about 10^{-13} sec) than the response time (10^{-10} sec) of the magnetic system. Correspondingly the Brownian motion can be used to describe the magnetization. And the thermal agitation process can be expressed as Eqn. (2.23),

$$\langle H^i_{thermal}(t) H^j_{thermal}(t+\tau)\rangle = \sigma^2 \delta_{ij} \delta(\tau) \tag{2.23}$$

Where i,j=1,2,3, and $\sigma^2 = \frac{2k_B T\alpha}{\gamma M_s V \Delta t}$, V is the grain volume, symbol k_B and T are the Boltzmann constant and the temperature, respectively. The Dirac δ means the autocorrelation time of the fluctuation field is much shorter than the response time of a single-domain particle.

Chapter 3 Novel Reader Design for 10 Tbits/in^2 User Areal Density in Two Dimensional Magnetic System

3.1 Introduction

Various schemes for magnetic recording at user bit densities of 10 Tbits/in^2 have been proposed including two-dimensional magnetic recording (TDMR) [3.1], shingled Bit Patterned Magnetic Recording (BPMR), and Heat Assisted Magnetic Recording (HAMR), possibly in combination with BPMR. Individual bit dimensions at 10 Tbits/in^2 are, at most, 8 x 8 nm, with substantially smaller values for those systems writing on conventional media where raw error rates are likely to be very high. In particular, TDMR attempts to store a channel bit in very few grains of a conventional magnetic medium in order to achieve 1-1.5 data bits/grain [3.2],[3.3]. The irregular grain boundaries and random distribution of grains produce extremely low signal-to-noise ratio (SNR). Bit patterned media, by virtue of its regularity, is expected to alleviate some of these issues, but is difficult to fabricate. All of these techniques will require read heads capable of sensing this data, preferably with a single pass.

In a TDMR system, various 1-D and 2-D sub-optimal detectors have been used. An inversion detector has been studied [3.4], and reasonable error rate performance was reported. The maximum-likelihood (ML) and maximum a posteriori (MAP) detectors based on the trellis or graph of the TDMR channels have been studied [3.5]. Huang and Kumar [3.6] used a linear minimum mean squared error equalizer and a low density parity check code to study the detection in a TDMR system.

In this chapter, a novel system design is proposed for reading two-dimensional magnetic recording (TDMR) systems. The concept is also appropriate for other very high density media such as BPMR. Based on a random Voronoi grain model, the simulation indicates that for bits with dimension of 8nm×6nm, grains of 5.5nm diameter and reader width of 18nm, the BER drops from 20.9% for a normally oriented head array to 4.2% for a single rotated conventional head. A minimum mean squared error (MMSE) equalizer and pattern-dependent noise prediction detector (PDNPD) with increased sampling rate are used. The density is greatly increased to 10.1Tbits/in^2. Furthermore, density can be increased to 10.9 Tbits/Inch^2 if the free layer width can be further reduced by a factor 2.

3.2 The design of the reader

3.2.1 Previous read head array

Readback at high density requires exceptional resolution that, to date, has not seemed possible using a single read head without multiple passes. Previously, we [3.3] employed an array of read heads as shown in Fig.3.1. A threshold detector, combined with a two-dimensional generalized partial response (GPR) equalizer using the MMSE criterion [3.7], was designed for signals from the head array. This detection scheme was demonstrated to work well. As it is known that the Viterbi detector based on ML sequence detection outperforms the threshold detector with the symbol detection, a 1D Viterbi algorithm (VA) was also used with a redesigned 2D partial response (PR) target. Here, a constraint on the 2D GPR target that forces inter-track interference (ITI) to zero and keeps only the controlled inter-symbol interference (ISI) was imposed in order to avoid the need for a 2D Viterbi algorithm.

However the simulation indicated that there is almost no gain for the Viterbi detector compared to the threshold detector, shown in Table 3.1.

Head type	Detector type	Bit 16nm×16nm	Bit 12nm×12nm	Bit 10×10nm	Bit 8nm×8nm
Single head	Threshold	4.84%	11.09%	14.20%	19.97%
Normal oriented head array (sampled per bit)	Threshold	0.93%	4.43%	8.24%	14.73%
	Viterbi	0.91%	4.39%	8.24%	14.61%
Normal oriented head array (sampled per 1nm)	Threshold	0.18%	3.24%	6.62%	13.58%
	Viterbi	0.16%	3.20%	6.58%	13.47%

Table 3.1 BER for detection with normally oriented single head and head array with threshold and Viterbi detector

Analysis shows that this unexpected result is caused by the geometry and arrangement of the reader relative to the bit size. For example, using a free layer width and thickness of 18nm (cross-track direction) and 4nm (down track direction) and a shield to shield spacing of 11 nm implies that each head reads 3 tracks (for 7X7 nm bits) simultaneously. Under this circumstance, the ITI is only addressed by 3 poorly resolved signals, while the down-track ISI can be corrected by, in principle, a continuum of much better resolved signals. Therefore, the superior attributes of the Viterbi detector are wasted solving the less significant problem, with the result that it shows essentially no improvement relative to the normally inferior threshold detector. This suggests that a rearrangement of our system is needed to make sure that a powerful detection mechanism addresses the most important problem.

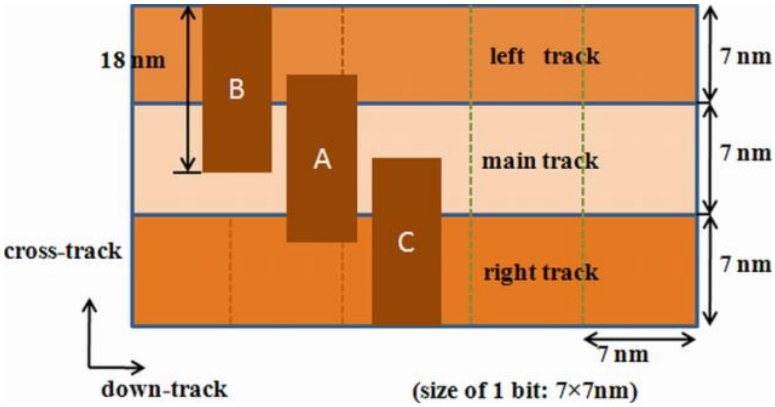

Figure 3.1 Schematic of an array of three conventional MR heads on continuous media.

3.2.2 Rotated head design

The above discussion suggests that rotation of the read head, together with oversampling in the down-track direction will greatly improve performance. The idea is that resolution in the cross-track direction will be provided by tightly placed shields and the resolution in the down-track direction (where large amounts of information can be provided) will be given by signal processing. Here, we tried the new design with both a single head, shown in Fig.3.2 (b), and a head array.

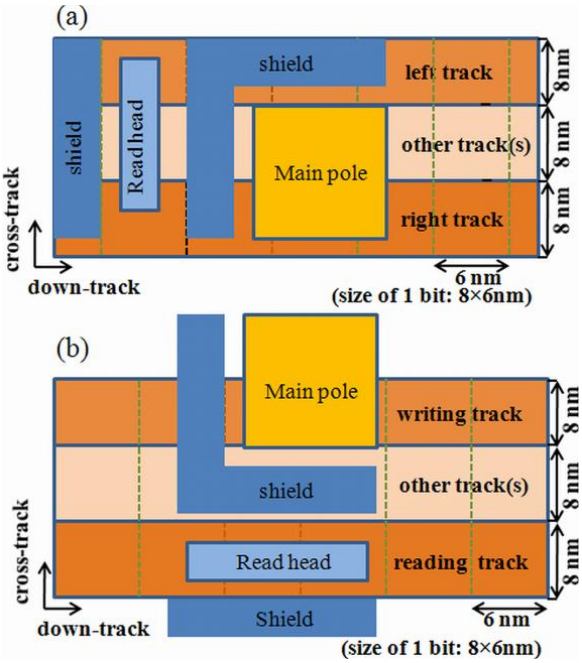

Figure 3.2 (a) Normal single head design; (b) Rotated single head design

In our new design, the conventional GMR-based read head has a shield to shield spacing (SSS) of 11nm.The length of each head is taken to be 18nm, which is larger than a bit length of 7nm.This permits easier fabrication and more thermal stability of the free layer. The height of the head is 18nm. Here, we assume a magnetic fly height of 3nm, a recording layer thickness of 10nm and a seed layer thickness between the SUL and recording layer of 2nm.

We show that this approach combining a 90° rotation of the head, so that the inherently narrow shield-shield spacing (usually used to gain downtrack resolution) blocks side read, combined with oversampling in the down track direction to regain the lost resolution, yields the required densities. Usually, it is assumed that the sampling rate is once per bit; however there is no reason why the sampling rate cannot be increased if the cost is not that high. Especially in a TDMR system, the extremely low SNR makes the increase of sampling rate necessary to obtain more useful information about the signals from the head. In this study, a sampling period of 2nm (f≈10GHz) or 3nm (f≈6.67GHz) is reasonable when the average rotation speed for the hard drive is assumed as 20m/s.

Besides the severe media noise, we also included the Johnson noise and magnetization noise as head noise. The magnetization noise of the GMR reader can be estimated by eq.(7) in [3.8]. We assume $P=I_b^2R$, MR ratio $\Delta R/R$ = 15%, free layer stiffness H_{stiff} = 10Oe, damping constant α =0.01, gyromagnetic ratio γ = 17.6 Mrad/(s Oe), free layer magnetization M_{sf} =1600 emu/cm^3, resistivity ρ equals 20 uΩ·cm, and biasing current I_b=5mA. The Johnson noise can be estimated as Eqn.(3.1), [3.9]

$$SNR_j = \frac{\varepsilon^2 P_{bias}(\frac{1}{2}\frac{\Delta R}{R})^2}{(4k_B T f_B)} \tag{3.1}$$

The "efficiency" ϵ is around 0.2, f_B is the bandwidth of signal. The calculated SNR for various sampling periods is shown in Table 3.2.

Sampling period	6 nm	3nm	2nm
Bandwidth of Signal (GHZ)	3.33	6.67	10
Magnetization noise (SNR/dB)	30.7	27.7	26.0
Johnson noise(SNR/dB)	23.1	20.1	18.3
Total noise(SNR/dB)	22.4	19.4	17.6

Table 3.2 Noises for various sampling periods.

3.3 Detection schemes with the new head design

3.3.1 Detection system architecture

During the writing process, a perfect writer has been used based on a Voronoi grain model [3.10], where a Voronoi grain is magnetized by the channel bit containing the centroid of the grain cell. Playback signals for the conventional MR head are numerically evaluated using the reciprocity principle applied to a potential acquired from a finite difference code [3.10], [3.11]. The reciprocity principle states that the playback signal is equal to the convolution of the head magnetic potential and the written magnetization pattern on the recording media, expressed as Eqn.(3.2).

$$V_{bits} = \int_{media} \Phi_{head}(\mathrm{x}' + \mathrm{x}, \mathrm{y}', \mathrm{z}') \nabla \cdot M(x', y', z') dx' dy' dz' \tag{3.2}$$

We assume composite media whose hard layer includes a synthetic antiferromagnet [3.12]. Thus the voltage can be obtained by subtracting the head potential at the hard/soft interface from the potential at the top of the recording media.

The design of our detection system is shown in Fig. 3.3. Although the system is similar to common channel models, there are a few obvious differences. First, most previous research on detection has not included the head design and the relationship

among the head, equalizer and detector: however, we have proposed a new head design and tried to exploit the relationship between these factors. Additionally, unlike most previous work, we obtain the playback signals using the reciprocity principle instead of a channel model with read sensitivity function. Furthermore, it's usually assumed [3.7] that the channel samples each bit once: we find the BER will drop significantly if sampling rate is increased during the scan of this proposed head. Last but not least, previous research has usually assumed the media and reader noises as Gaussian and varied the SNR without physical basis: however, in our model, the media noise is controlled by varying the number of grains per bit in the Voronoi model, and reader noise is taken to be flat band-limited noise with SNR dependent on data rate and free layer volume, according to accepted physical models [3.8],[3.9].

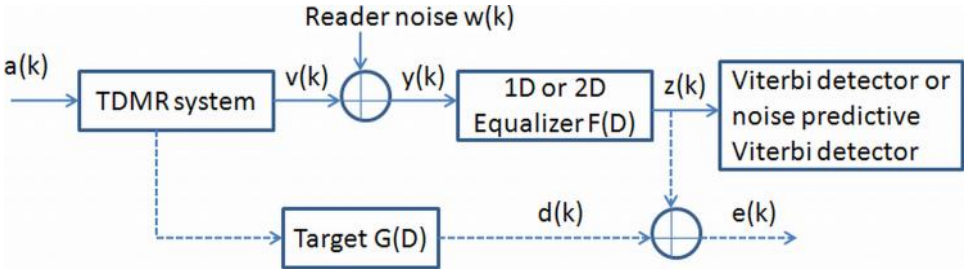

Figure 3.3 Schematic of the detection system architecture.

3.3.2 Detection with rotated single head

For a rotated head, the ISI is more severe than ITI. We combat the ISI with a 1D equalizer and an improved Viterbi detector; In the cross-track direction, the shields are utilized to combat the ITI. For the design of the 1D MMSE equalizer [3.13], we make the target of size 1×3, namely the length of ISI is 3. This constraint can be shown as

$$g = [1, g_1, g_2] \tag{3.3}$$

The constraint can be expressed as eq.(3.4),where c=1 and $E=[1,0,0]^T$.

$$E^T g = c \tag{3.4}$$

Here the monic constraint (g_0=1) is adopted for its optimal target shape. Then the optimized target and equalizer coefficient vector can be obtained with Eq. (3.5), (3.6) and (3.7).

$$\lambda = (E^T (A - T^T R^{-1} T)^{-1} E)^{-1} c \tag{3.5}$$

$$g = (A - T^T R^{-1} T)^{-1} E\lambda \tag{3.6}$$

$$f = R^{-1} T g \tag{3.7}$$

We choose a target of size 1×3 and equalizer of size 1×15×(bit length/2) or 1×15×(bit length/3) for a sampling period of 2 or 3nm. The playback signals calculated using the reciprocity principle are considered to be the channel output signals y, the channel input data is a. Hence, the auto-correlation matrix of the channel output R, the cross-correlation of the input data and the channel output data T, and the auto-correlation of the input data A can be expressed as R=E{$y_k y_k^T$}, T={$y_k a_k^T$} and A={ $a_k a_k^T$ }.

The Viterbi detector in the partial response maximum likelihood (PRML) system is optimal in the presence of additive white Gaussian noise (AWGN). Media noise, which is nonstationary, correlated, and data-dependent, can cause serious performance degradation in a TDMR system when compared to a system operating with the same amount of AWGN. Correspondingly, a data-dependent full local feedback noise prediction schemes [3.14] has been adopted for the rotated single head in our TDMR system. In this scheme, the Viterbi detector recursively updates the cumulative metrics for each state using the update equations (3.8),

$$\mu_k(s') = \min_{(s,s')} \mu_{k-1}(s) + [y_k - h_0 \widetilde{a_k}(s,s') - \sum_{j=1}^{v} h_j \, \tilde{a}_{k-j}(s) - \Delta_k(s,s')] \tag{3.8}$$

where $\mu_{k-1}(s)$ is the cumulative metric associated with state s at time k-1, h_0, h_j are the coefficients of the finite impulse response polynomial for the partial response channel,

$\tilde{a}_{k-j}$ are the data bits on the surviving path leading to s, $\Delta_k(s,s')$ is the branch-dependent prediction of the noise, and

$$\Delta_k(s,s') = \sum_{i=1}^{L} w_i[\bar{a}(s,s')]\,\tilde{n}_{k-j}(s). \quad (3.9)$$

Here, $\bar{a}(s,s') = \tilde{a}_k(s,s')\tilde{a}_{k-1}(s) \ldots \tilde{a}_{k-(K-1)}(s)$ are the K data bits on the surviving path leading to s together with the data bits associated with the branch(s,s'). The taps of the noise prediction filter $w_i[\bar{a}(s,s')]$ depend on $\bar{a}(s,s')$ and are the solution of the Yule-Walker equations, similar to Eq.(8) in Ref. [3.14]. Here, we choose data dependent length K within the range of 5 and 7 depending on bit size, the noise predictor length L=8.

In our rotated head array design, ISI and ITI can both be addressed using 2-D equalization and detection as originally envisioned for TDMR. By imposing a constraint on the 2D target that forces ITI to zero and keeps only the controlled ISI, the conventional VA can handle ISI well. If we make a target of size 3 ×3, namely the length of ISI and ITI are 3, these constraints are similar to Eq.(15) to (19) in Reference [3.7]. Then the optimized target and equalizer coefficient vectors can still be obtained with Eq. (5), (6) and (7). Here we choose the target of size 3×3 and equalizer of size 3×15×(bit length/2) or 3×15×(bit length/3) when sampling period is 2 or 3nm.

3.4 Numerical evaluation

Results for a rotated single head (RSH) are shown in Table II for a center-to-center grain size (grain pitch) of 5.5 nm with standard deviation of 20%. Here every result is the average of 25 trials with each trial having a different 10500 bits PRBS. Error bar are 0.1%. The results indicate that BER is reduced with a PDNPD compared to a Viterbi detector owing to the embedding of the data dependent prediction of the noise into the branch metrics. For bits of dimension 9nm x 10nm and 8nm grains, the BER can drop

from 15.73% for a normal head array (NHA) to 1.67% for RSH for 2nm sampling. It can also be seen that oversampling is crucial: sampling once per bit increases BER by about a factor 2 despite the decrease in head noise owing to the decreased bandwidth. (This oversampling could be replaced by long channel target length, but at considerable detector expense.) The data densities can be calculated using the Shannon Capacity limit [3.15] by assuming the magnetic channel as Binary Symmetric Channel (BSC) and allowing a very long codeword, expressed as Eqn.(3.10) and (3.11).

$$C_{BSC} = \left(1 + BER \cdot log_2(BER) + (1 - BER) \cdot log_2(1 - BER)\right) \quad (3.10)$$

$$\text{User Density} = C_{BSC} \cdot \text{Channel Density} \quad (3.11)$$

For 8 nm grains, the user data density reaches around 6.3 Tbits/inch^2. The user density increases to 10.1Tbits/in^2 for the same head when the grain size is decreased to 5.5nm, as shown in Table 3.3. We believe this to be the highest simulated density ever demonstrated. We find that, when the bit size is comparable to the shield to shield spacing, the ITI is insignificant compared to the media noise.

We have also examined the tradeoff between head noise and sense head dimensions. Results for several head widths are shown in table 3.4, where a bit size of 8×6nm is used. It can be seen that smaller dimensions, if they can be fabricated, will increase user density despite the increase in noise from thermal fluctuations.

Bit size	5×10nm	6×8nm	7×7nm	8×6nm	9×6nm	8×7nm
BER(NHA,VA)	23.7%	22.7%	21.5%	20.9%	17.8%	20.1%
BER (RSH,VA) –bit sampling	15.2%	11.5%	8.7%	8.4%	6.8%	5.9%
BER(RSH,VA)-3nm sampling	9.8%	6.3%	5.9%	5.7%	5.2%	4.1%
BER(RSH,VA) -2nm sampling	9.7%	5.9%	5.0%	4.7%	3.7%	2.9%
BER(RSH,PDNDP)	9.6%	5.7%	4.6%	4.2%	3.3%	2.4%
Density(NHA,VA)Tbits/in^2	2.7	3.1	3.3	3.5	3.9	3.2
Density(RSH,VA)Tbits/in^2	7.0	9.1	9.4	9.8	9.2	9.3
Density(RSH,PDNDP) Tbits/in^2	7.0	9.2	9.6	10.1	9.4	9.6

Table 3.3 BER for both single head with Viterbi Detector and PDNPD for 5.5nm grain

Head width	24nm	18nm	12nm	9nm
BER(RSH,PDNDP)	5.6%	4.2%	3.3%	2.9%
Density(RSH,PDNDP) Tbits/in^2	9.3	10.1	10.7	10.9

Table 3.4 BER for various head widths

We have extended our simulation to include an array of rotated heads (RHA) with oversampled signals. Tables 3.5 and 3.6 show that this approach greatly reduces BER compared with a normal head array, but there is only a small overall improvement of user density compared to a single rotated head.

Bit size	8×10nm	9×9nm	10×8nm	9×10nm
BER(RHA,VA)	4.2%	3.8%	6.5%	1.5%
BER(NHA,VA)	19.7%	16.6%	11.8%	15.7%
Density(RHA,VA) Tbits/in^2	6.0	6.1	5.3	6.4
Density(NHA,VA) Tbits/in^2	2.3	2.8	3.8	2.7

Table 3.5 BER for both head arrays for 8nm grain.

Bit size	5×10nm	6×8nm	7×7nm	9×6nm	6×9nm
BER(RHA,VA)	3.8%	3.8%	4.7%	3.4%	1.5%
BER(NHA,VA)	23.7%	22.7%	21.5%	17.8%	22.4%
Density(RHA,VA) Tbits/in^2	9.9	10.3	9.6	9.4	10.6
Density(NHA,VA) Tbits/in^2	2.7	3.1	3.3	3.9	2.8

Table 3.6 BER for both head arrays for 5.5nm grain.

In the previous section, a novel system design for sensing very high density magnetic recording data is investigated. The rotated single head with oversampled signals, MMSE equalizers and PDNPD has been proposed, and the BER can be decreased compared with a normally positioned head array, increasing density to 10 Tbits/inch^2. Also a rotated head array reaches slightly better performance compared to a single rotated single head. While demonstrated for conventional media, this system design should also be very

useful for BPMR.

3.5 Study on response of various reader designs

In the previous section, we proposed a novel system design for readback at ultra-high density from granular media [3.16] with perfect writing: the key idea involves use of a rotated sense head, so that the shields are aligned down-track, and oversampled signal processing is used to regain the lost down-track resolution. However, our previous studies have focused on the detector, and did not consider any coding scheme. Additionally, the previous research [3.16] only tried to explain improvements brought by the new design from a geometric viewpoint, but understanding from the signal processing perspective is still needed.

In this study, we present and explain the performance of rotated and normally oriented heads from a signal processing perspective, and examine the performance of various coded designs by varying the bit-aspect ratio (BAR) using the quasi-cyclic low-density parity-check (QC-LDPC) code [3.17] with codeword length of 4096 bits. First, the linear responses for TDMR system readback with both normally and rotated heads are studied. The read head sensitivity (RHS) response of the realistic reader calculated using the physically accurate reciprocity principle is also analyzed. Based on the channel model, a linear minimum mean square error (LMMSE) equalizer is employed for equalization and a QC-LDPC decoder is used for error corrections. Meanwhile the possible channel capacities reached by various readers are studied, and the performance discrepancies among various decoded systems are compared. The simulation indicates that with an oversampled signal, 2D LMMSE equalizer and LDPC codes, a user bit density near 10 Tbit/in^2 is feasible for a rotated head array.

3.5.1 Linear responses of various readers

Previously, a rotated reader design shown in Fig.3.2 (b) combined with oversampling signal processing was proposed for readback at ultra-high density from both granular media [3.16] with perfect writing. Here, a conventional giant magnetoresistance (GMR)-based head is used, and the dimension of the free layer is 18nm × 18nm ×4nm, shield-to-shield spacing is 11nm and magnetic fly height is 3nm. Perfect writing is used to write a pseudo-random binary sequence (PRBS) on 10nm thick exchanged coupled composite (ECC) media with 5.5 nm Voronoi grains, where a Voronoi grain is magnetized by the channel bit containing the centroid of the grain cell. For readback, the physically accurate reciprocity principle [3.11] is used by convolving a head potential from a finite difference code [3.10] with the divergence of media magnetization to obtain the playback signals for the GMR head, shown as Eq.(3.2). Then the readback signal is considered as the channel output, and a 1-D LMMSE equalizer is employed for equalization.

In order to characterize the system's linear response that shows the spatial resolution along the down track direction, the dibit extraction technique [3.18] is utilized, which uses the cross-correlation of a PRBS and the playback waveforms, expressed with Eqn.(3.12). The benefit of such a method is that it does not require any timing information about the signal other than the period of the PRBS. Here the x^7+x^3+1 PRBS sequences are used to write 8nm ×8nm bits during the writing process.

$$h[m] = \frac{r_{sa}[m]}{1+1/N} + \frac{\sum_m r_{sa}[m]}{1+N} \tag{3.12}$$

where N=127 is the length of PRBS, r_{sa} is the cross correlation of readback signal and PRBS.

We compared the dibit responses for a given PRBS of a normally oriented singled

head (NSH) without adjacent track interference (ATI), and a NSH and a rotated singled head (RSH) with ATI, shown as Fig.3.4. All the geometric and physical parameters are the same for both NSH and RSH.

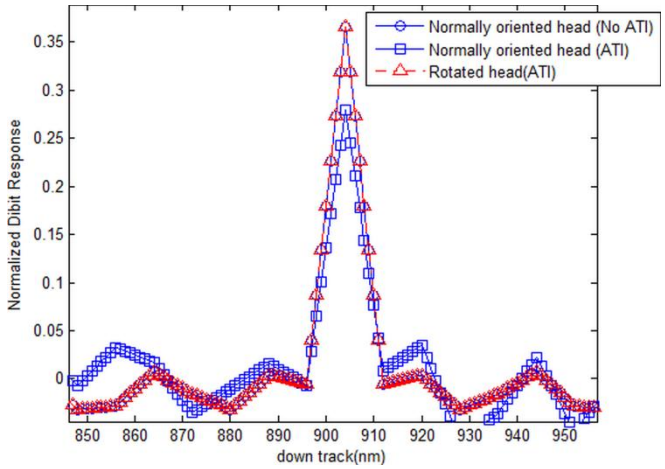

Figure 3.4 Normalized dibit responses along the down-track direction for the normally-oriented head with and without ATI and rotated single head with ATI (Normally oriented head with no ATI closely overlaps rotated head with ATI).

Fig.3.4 indicates that the amplitude of the dibit response of the normally oriented single head (NSH) decreases due to the adjacent track interference (ATI) compared to the case without ATI. However, the rotated single head yields a normalized dibit response that is equal to that of the ATI free signal from the normally oriented head. It means that the RSH can successfully resolve an 8nm track with ATI, even though the free layer length (18nm) is much wider than the current track (8nm).

3.5.2 Read head sensitivity response

Previous research [3.5], [3.19] assumed a 2-D Gaussian profile for the head response with a symmetric T_{50} (defined as the time for the step response to go from 25% to 75% of its maximum) along both down track and cross track directions. Correspondingly, the 2-D MAP detector outperformed the 1-D MAP detector, since the former one treats ITI as useful information to help the decision while the latter one treats ITI as noise. However,

the actual situation is different owing to the read head sensitivity (RHS) response obtained with the physically accurate reciprocity principle for the rotated single head, shown as Fig.3.5. The RHS response is obtained with the reader design in Fig.3.2 (b) for readback of 8nm×8nm bits.

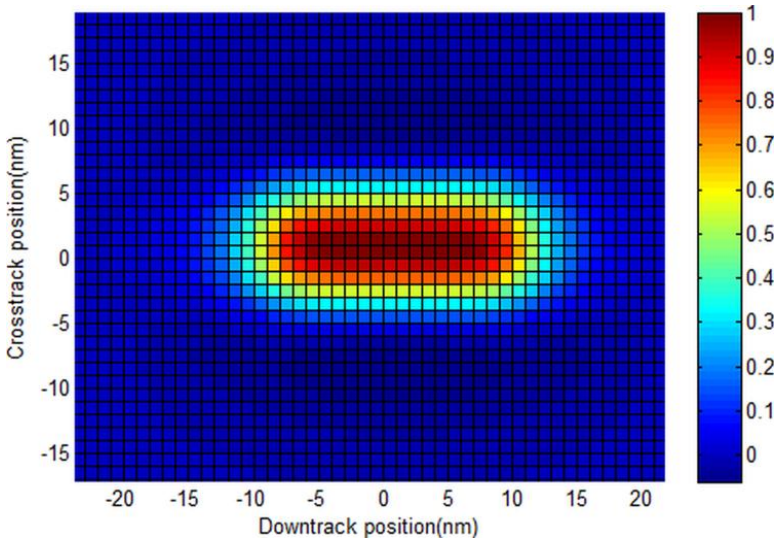

Figure 3.5 Read head sensitivity response for rotated head in the simulation.

It is easy to show that the T_{50} along the down track direction is much larger than that along the cross track direction based on Fig.3.5. The calculation for the step responses along both directions indicate that $T_{50\text{down-track}} \approx 2.6 T_{50\text{cross-track}}$, which also means the ISI is much more severe than ITI for the low bit aspect ratio (BAR) case. Reference [3.5] indicates that the performance of a 1-D detector is comparable to the much more computationally-intensive 2-D detector when ITI turns out to be significantly smaller than ISI. Correspondingly, the ITI and ISI can be treated differently in the channel. If the ITI is negligible for the rotated head when the track width is large, then the narrow shield to shield spacing along the down track direction is sufficient to guarantee the resolution along the cross track direction. If the track width is further decreased, e.g., 8nm, the rotated head array combined with 2-D equalization which forces the ITI to be zero can

still lead to satisfactory results [3.16] because the ITI is still much smaller than ISI as suggested by Fig.3.5. Hence the fundamental reasons for the rotated head design are: (1) the geometry of the normally oriented head makes ITI much worse than ISI for low BAR cases, which are inevitable for extremely high channel density; (2) the inability of a normally oriented head array to adequately sample in the cross-track direction to compensate for the poor resolution makes the performance inferior.

3.6 Signal processing and performances comparisons for various readers

3.6.1 The channel capacities for various readers

Previous research [3.5] indicates that the performance of an inversion detector is close to the superior 2-D MAP detector at high densities due to the predominant role of media noise compared to the insignificant additive electronic noises. In this study, considering the convenience of obtaining the log likelihood ratio (LLR) for LDPC codes, a LMMSE equalizer is used to take into account the random distribution of grains within the bit cells. The LMMSE equalizer can be derived as Eq.(3.13).

$$f^{LMMSE} = \arg\min_{f} E[(x_{i,j} - (y * f)_{i,j})^2] \tag{3.13}$$

Correspondingly the mean squared error between channel input, $\{x_{i,j}\}$, and the equalized output, $\{(y*f)_{i,j}\}$ is minimized. Here y is the output of the channel, f are equalizer coefficients, and E [•] denotes the expectation. For a normally oriented single head, a 1-D equalizer of size 1 × [15 × bit length/2nm] is adopted for a sampling period of 2nm, where the target size is 1×3. For both normally oriented and rotated head array, a 2-D equalizer of size 3× [15 × bit length/2nm] is used when the sampling period is 2nm, where the target size is 3×3.The block diagram of the TDMR channel architecture is shown as Fig.3.6. Perfect writing is used to shingle write a channel density of about 12

Tbits/in^2.There is a 1D to 2D converter in the TDMR architecture that simply wraps a 1D codeword into a 2D block to prepare for the shingled writing process.

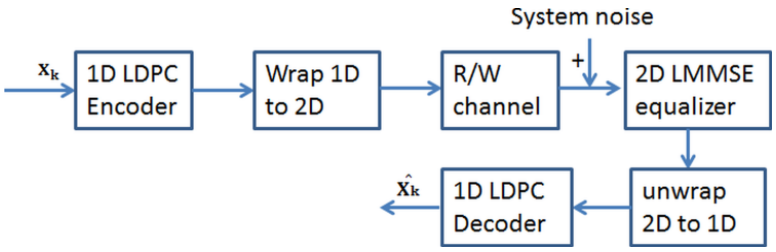

Figure 3.6 Block diagram for LDPC-coded TDMR system.

The reader noise is taken to be flat-band-limited noise with SNR dependent on the data rate and free layer volume, according to the accepted physical models. The magnetization noise and Johnson noise are both included in the head noise. The reader SNR for sampling per 2nm is about 18 dB. Varying the BAR varies the amount of ITI and ISI introduced by the readers and it also affects the writing performance of the writer. Correspondingly, during simulation, the BAR is varied to obtain the optimum performance for each system. The bit error rate (BER) is obtained for various readers from the simulation and is shown in Fig.3.7. Simulation indicates that the BER for the rotated head array (RHA), normally oriented head array (NHA) and NSH are about 2.7%, 9.3% and 12.0% for their optimum BARs of 0.67, 3.5 and 3.5, respectively. Clearly avoiding the effect of interference along both down and cross track directions are major concerns for both RHA and NHA: it is clear that the optimum BARs for both heads should appear at lower ratio(<1) and higher ratio(>2), respectively, due to the arrangements of the heads along different directions.

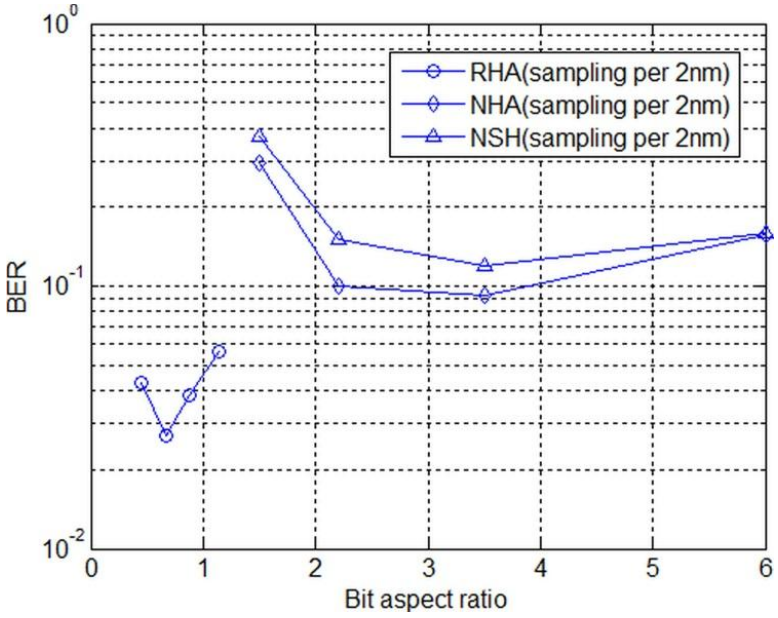

Figure 3.7 BER for various reader designs.

The channel capacities for various systems can be calculated with the Shannon Capacity limit according to the BER obtained in the simulation by assuming the recording channel to be a Binary Symmetric Channel (BSC). The maximum capacities (user bits/Channel bits) for these cases correspond to 0.821, 0.554 and 0.471, or areal densities of 9.85T/in^2, 6.64T/in^2 and 5.65T/in^2, respectively, as shown in Fig.3.8.

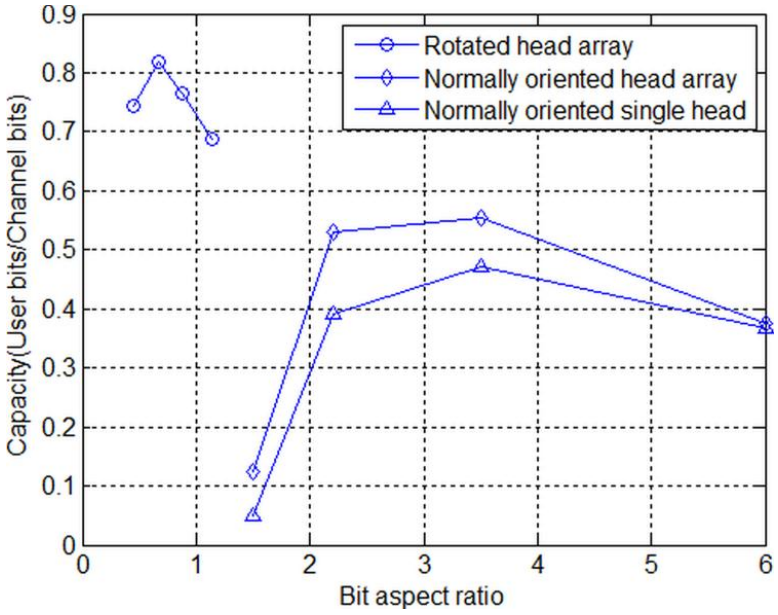

Figure 3.8 Capacity (user bits/channel bits) for various systems.

3.6.2 Performances for various coded systems

The conditional probability density functions (pdf) of equalized outputs for various systems can be obtained by simulation, as shown in Fig.3.9. In Fig.3.9, it is interesting to find that the overlap between conditional pdfs, which is usually reduced by using constrained codes with the penalty of reducing recording rates, is reduced by the RHA compared to the NHA. Correspondingly, we can derive that BER will be reduced by the RHA from the decreased overlap between conditional pdfs. Both curves have additional contributions that are caused by the unwritten bits (if no grain centroid falls within the bit) and residual interference. The unwritten bits will cause residual errors after the LMMSE equalization, because the mean of the equalizer output E[y*f^{LMMSE}] could be zero for the unwritten bits due to the independence of (y*f^{LMMSE}) from $x_{i,j}$. However, for written bits, E[y*f^{LMMSE}] = $x_{i,j}$ because the effect on the channel inputs, caused by the random placement of grains and additive noises, were cancelled out in the averaging.

Based on the conditional probability density, the log likelihood ratio (LLR) can be obtained for the equalized data, from Eq. (3.14)

$$L(z) = \ln(\frac{f_{-1}(z)}{f_1(z)}) \tag{3.14}$$

where z=(y*f^{LMMSE}) is the LMMSE equalizer output, $f_{-1}(z)$ and $f_1(z)$ are the conditional probabilities density of z given x= -1 and x=1.

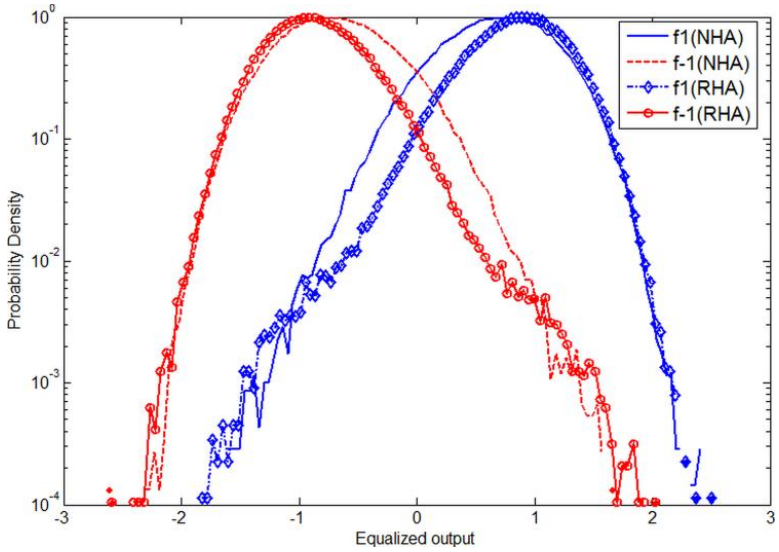

Figure 3.9 Conditional probability density function of equalized output for both rotated and normally oriented head array.

This LLR is then used as the soft input for quasi-cyclic LDPC (QC-LDPC) decoding, whose codeword length is 4096 bits. The reason for using QC-LDPC codes in this system is that its quasi-cyclic structure leads to simpler hardware design of decoders. After decoding, we observed the waterfall region with LDPC code of rate 0.8125 for the RHA, while such a code rate does not work for the NHA and NSH, shown in Fig. 3.10.When the code rate for the NHA is reduced to 0.55, its performance is still about 8.5dB worse than the RHA with code rate of 0.81, shown as Fig.3.10. This demonstrates the feasibility of user bit density near 10 Tbits/in^2 for the rotated head array. Notice that the layered algorithm [3.20] with maximum number of iterations equals 30 is adopted as the decoding approach in the above simulations. It is important to note that the simulations for both Fig.3.10 and Fig.3.11 are carried on with Voronoi model, and the SNR labeled in both figures are only head and system noises relative to the long wavelength signal. Correspondingly the simulation has included both media noise (already included in Voronoi model), head and system noise for Fig.3.10 and Fig.3.11.

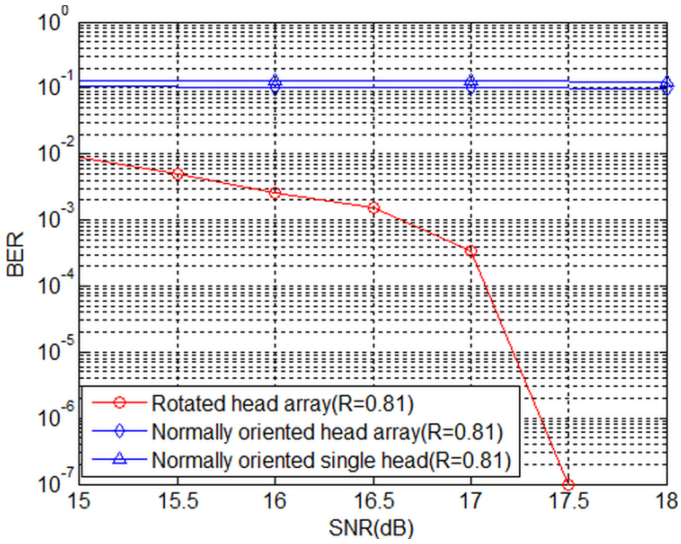

Figure 3.10 BER for various quasi-cyclic LDPC coded systems with code rate 0.8125 as a function of head and system SNR.

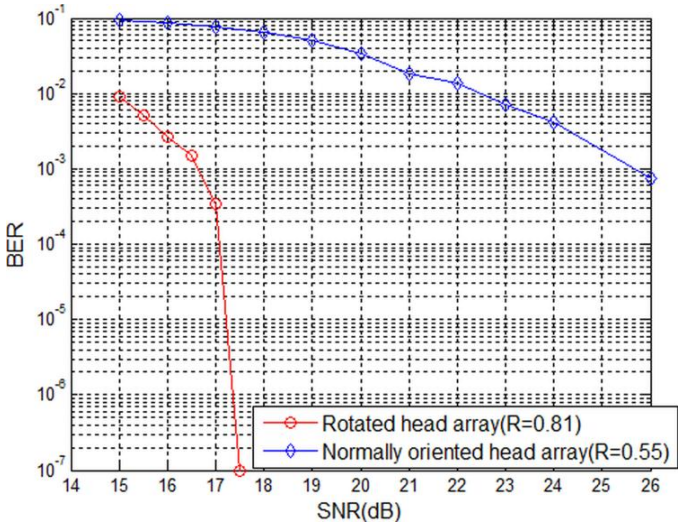

Figure 3.11 BER for various quasi-cyclic LDPC coded systems with different code rates as a function of head and system SNR.

3.7 Conclusion

In this chapter, a novel system design for sensing very high density magnetic recording data is investigated. The rotated single head with oversampled signals, MMSE equalizers and PDNPD has been proposed, and the BER can be decreased compared with a normally positioned head array, increasing density to 10 Tbits/inch^2. Additionally, the

performance of rotated and normally oriented heads are presented from a signal processing perspective, and the performance of various coded designs are examined with the quasi-cyclic low-density parity-check (QC-LDPC) code in a two-dimensional magnetic recording (TDMR) system. The study indicates that the significant improvement of performance of the rotated head compared to the normally oriented head can be attributed to the larger amplitude of its dibit response and the reduced overlap between conditional probability density functions (pdfs). With an oversampled signal, 2D LMMSE equalizer and LDPC codes, a user bit density near 10 Tbit/in^2 is feasible for a rotated head array.

Chapter 4 System Design for Readback above 1 Terabit/Inch^2 from Granular Media

4.1 Introduction

To overcome the superparamagnetic limit faced in conventional recording media, several novel system architectures have been proposed, such as bit patterned media recording (BPMR), heat-assisted magnetic recording (HAMR) and two-dimensional magnetic recording (TDMR) [4.1]. TDMR attempts to store approximately one channel bit per grain on conventional media, causing the raw error rate to be very high. It is supposed to be implemented with shingled writing (SW) and two-dimensional readback. In a TDMR system, the irregular grain boundaries, random distribution of grains and very few grains per bit produce extremely low signal-to-noise ratio (SNR). Furthermore, the severe inter symbol interference (ISI) and inter track interference (ITI) generate significant challenges for readback.

In a TDMR system, various 1-D and 2-D sub-optimal detectors have been used. An inversion detector has been studied [4.2], and reasonable error rate performance was reported. The 2-D and 1-D maximum a posteriori (MAP) detectors have been studied and compared in [4.3]. Huang and Kumar [4.4] used a linear minimum mean squared error equalizer and a low density parity check code to study the detection in a TDMR system.

Previously, we have proposed a novel system design for readback at 10 Tbits/in^2 user areal densities on conventional media [4.5]. The key idea is a rotated sense head, so that the shields are aligned down-track, combined with oversampled signal processing to regain the lost down-track resolution. Based on a random Voronoi grain model, simulation indicates that for bits with dimension of 8nm×6nm, 5.5nm grains, and a reader

with 4nm x 18nm x18nm free layer and 11 nm shield-shield spacing, the bit error rate (BER) is a factor 5 smaller for a single rotated head than for a normally oriented head array. The user density computed using the Shannon capacity limit, is greatly increased to 10.1 Tbits/in^2, that, however, allows very long code word length and assumes a binary symmetric channel.

In this paper, we vary the parameters of the proposed head design systematically for various channel densities. Then the performance of the rotated single head (RSH) and rotated head array (RHA) are compared with that of a normally oriented single head (NSH) at optimized bit aspect ratio (BAR). We also test the effect of head noises, magnetic fly height (MFH) and shield to shield spacing (SSS) on the performance of several designs.

4.2 Reader design

4.2.1 Principle and structure of reader

The premise of the rotated head design (Fig.4.1) is that ITI is a worse problem than ISI because 1) the geometry of a normally oriented head makes the ITI much worse than ISI for low bit aspect ratio case, which is inevitable for high channel density and 2) ITI and ISI are treated differently in the channel owing to the inability to adequately sample in the cross-track direction. It is known that a 2-D detector shows advantage over a 1-D detector because the former treats ITI as useful information while the latter one treats it as noise. However the 2-D detector is more computationally expensive, especially for large sector size and will cause latency owing to the need for information from several adjacent tracks [4.3]. By minimizing the unwanted effect of ITI, the rotated head design

can avoid the necessity of complex 2-D detectors, and reach similar or even better performance.

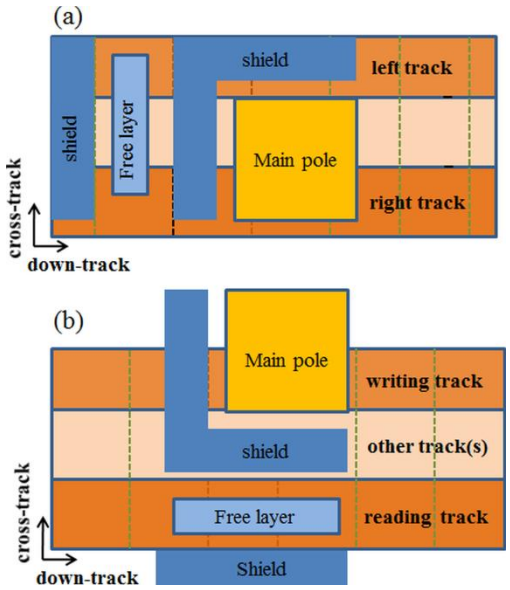

Figure 4.1(a) Normal single head design. (b) Rotated single head (RSH) design.

4.2.2 Parameters for simulation

Much of this study assumes that the size of a reader decreases when the channel bit density is increased in order to obtain reasonable resolution. Here a conventional giant magnetoresistance (GMR) based head is used, and the free layer (FL) dimension, shield to shield spacing (SSS), and magnetic fly height (MFH) have been varied for various channel densities, as shown in Table 4.1. This shrinking appears feasible over the next 5-10 years although the reduction of the shield to shield spacing may require novel approaches such as a scissor structure [4.6]. The same parameters are applied to both rotated and normal head when the channel density is the same.

Channel bit density (Tbit/in^2)	1	2	3	4	5	7
FL Width/Height (nm)	30	27.5	24.5	22	21.5	20
FL Thickness (nm)	5	5	5	4	4	4
MFH (nm)	7	6.5	5.5	5	4.5	4
SSS (nm)	16	15	14	13	12.5	12

Table 4.1 Geometric parameters of read head for various channel bit densities

Besides the head parameters mentioned above, the recording layer thickness is 10nm and the seed layer thickness between the soft under layer (SUL) and recording layer is 2nm. In the simulation, average grain pitch of 8nm with standard deviation of 20% is used; hence, the corresponding relation between the grains per channel bit and channel bit density is shown as Table 4.2. In this model, the media noise is controlled by varying the number of grains per bit in the Voronoi model, and the reader noise is taken to be flat band-limited noise with SNR dependent on data rate and free layer volume, according to accepted physical models [4.7],[4.8]. The magnetization noise and Johnson noise are both included in the head noise. Correspondingly, the reader noises for the various free layer dimensions and sampling periods are calculated in Table 4.3, where reader type (labeled from 1 to 7) corresponds to the reader described in Table 4.1 for channel densities ranging from 1 Tbit/in^2 to 7 Tbits/in^2. It is found in Table 4.3 that the decrease of free layer volume and sampling period both decrease the reader SNR, where SNR in dB is shown for reader noise relative to long wavelength signal.

Grains per channel bit	12.8	6.4	4.2	3.2	2.5	1.8
Channel bit density (Tbit/in^2)	1	2	3	4	5	7

Table 4.2 Relation between grains per channel bit and channel bit density

Reader Type	1	2	3	4	5	7
Sampling per 10 nm (SNR/dB)	31.0	29.2	27.8	27.1	26.5	26.1
Sampling per 2nm (SNR/ dB)	24.0	22.3	20.9	20.2	19.5	19.2

Table 4.3 Noises for various readers and sampling periods.

4.2.3 Detection with designed head

During the writing process, a perfect writer has been used based on a Voronoi grain model [4.9]. For reading back, the reciprocity principle [4.10] is used by convolving a

head potential from a finite difference code [4.9] with the divergence of media magnetization to obtain the playback signals for the GMR head.

The playback signals calculated using the reciprocity principle are considered to be channel output signals, which have been processed with a moving average filter before going through the equalizer. For both rotated and normal single heads, the 1D MMSE equalizer is used, and its size is 1×15 or 1× [15× bit length/2nm]for a sampling period of 1 bit or 2nm, respectively. The size of the 1D target is 1×3, and the monic constraint is adopted whose first coefficient is 1.

For a head array, the 2D general partial response (GPR) target that forces ITI to zero and keeps only the controlled ISI is adopted; with size is 3×3. We choose a 2D equalizer of size 3×15 or 3× [15× bit length/2nm] for the rotated head array when the sampling period is 1 bit or 2nm.

After both 1D and 2D equalizers, a conventional Viterbi detector is implemented. In principle, such a detector is sub-optimal since the media noise is nonstationary, correlated and data-dependent, and the performance could be improved with a more sophisticated noise prediction algorithm. However, it will entail a significant increase in complexity and thus computational time owing to the extensive amount of data presented in this paper. Furthermore, our previous work shows that a Pattern Dependent Noise Prediction Detector only enhances BER by a small factor [4.5].

4.3 Numerical evaluation

4.3.1 Optimum bit aspect ratio for various readers

For both the rotated and normally oriented head, the same head parameters are adopted, and the bit aspect ratio (BAR) is varied for each channel density to obtain the

optimum results for each. As the bit aspect ratio is not limited by the fabrication process, it can be alternated by varying the timing of writing current. In simulation, the BAR varies within the range of 5:1 to 1:3 depending on the channel density. We examined BER as a function of BAR for channel density ranging from 2 to 7 Tbits/in^2 as shown in Figure 4.2 to 4.6. Owing to the relatively small target and the large inter-symbol interference, each plot also displays the benefits of oversampling.

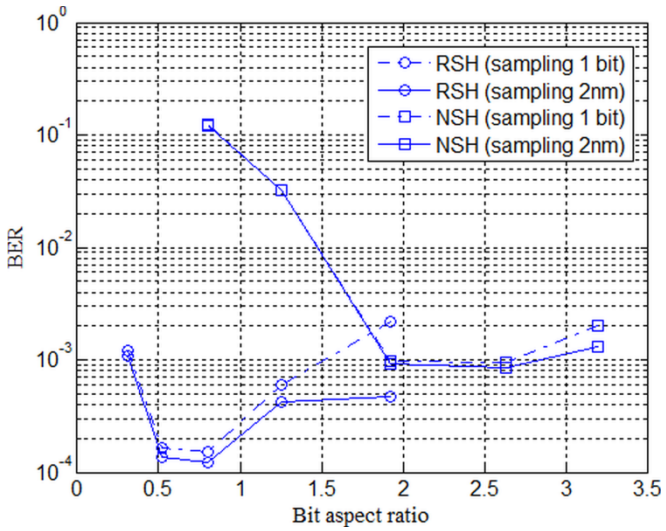

Figure 4.2 BER vs. BAR for various heads and sampling periods at 2 Tbits/in^2 channel bit density.

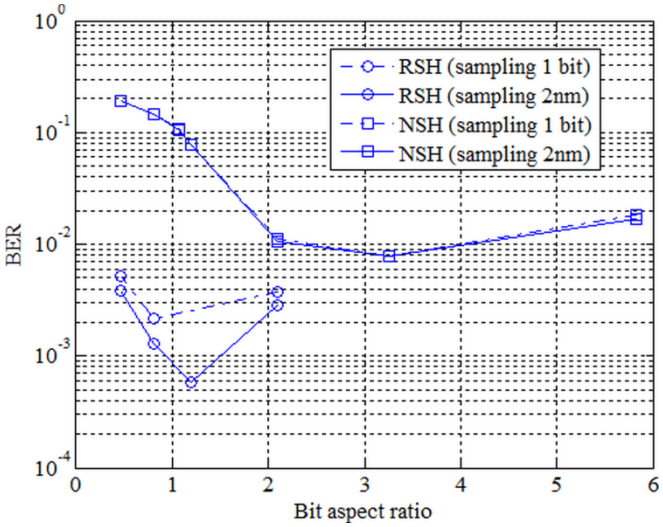

Figure 4.3 BER vs. BAR for various heads and sampling periods at 3 Tbits/in^2 channel bit density.

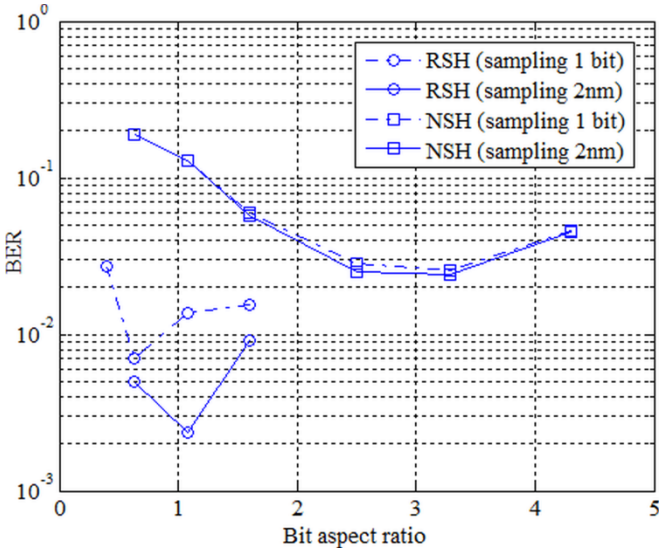

Figure 4.4 BER vs. BAR for various heads and sampling periods at 4 Tbits/in^2 channel bit density.

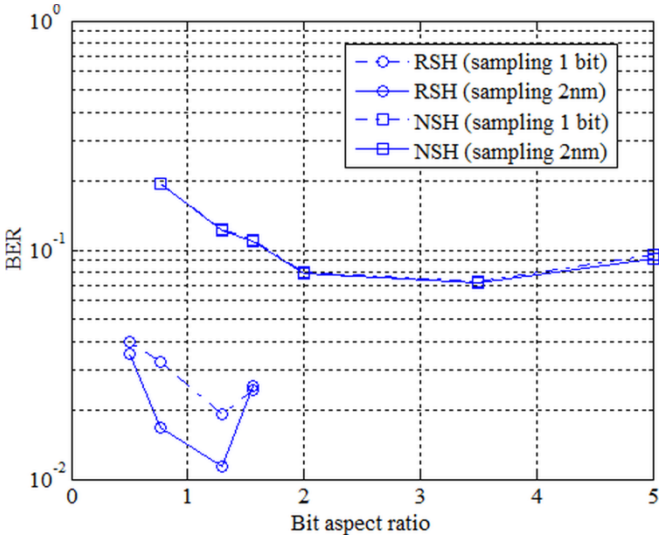

Figure 4.5 BER vs. BAR for various heads and sampling periods at 5 Tbits/in^2 channel bit density.

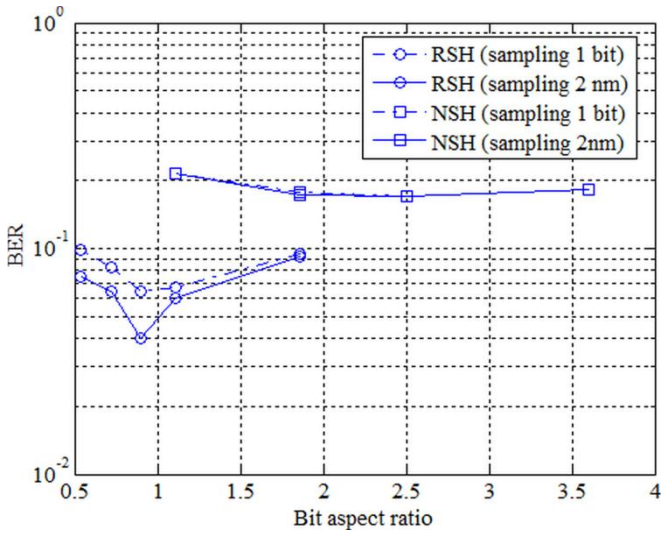

Figure 4.6 BER vs. BAR for various heads and sampling period at 7 Tbits/in^2 channel bit density.

According to Figure 4.2 to 4.6, it is found that the rotated single head outperforms the normally oriented head at all densities other than 2 Tbits/in^2 channel bit density at bit sampling with high BAR; the lowest BER reached by the former one is decreased about an order of magnitude compared to the latter case. Oversampling shows no obvious improvement for the NSH at any channel bit density, while the benefits of oversampling seems more obvious for the RSH when channel bit density is increased.

We also find that the optimized BAR for the NSH is large, i.e. above 2, while the optimized BAR for the RSH is around 1. The reason for this is that varying BAR means varying the amount of interference introduced by the reader in both downtrack and cross track directions. For the normally oriented single head, avoiding the effect of ITI is a major concern; correspondingly a high BAR is preferred. In contrast, the rotated single head addresses the two types of interference with approximately the same effectiveness; hence a nearly square bit becomes optimal. Figure 4.7 also shows the optimized BAR for

a rotated head array. Owing to the enhanced treatment of the ITI using 2D equalization, the optimized BAR becomes less than 1.

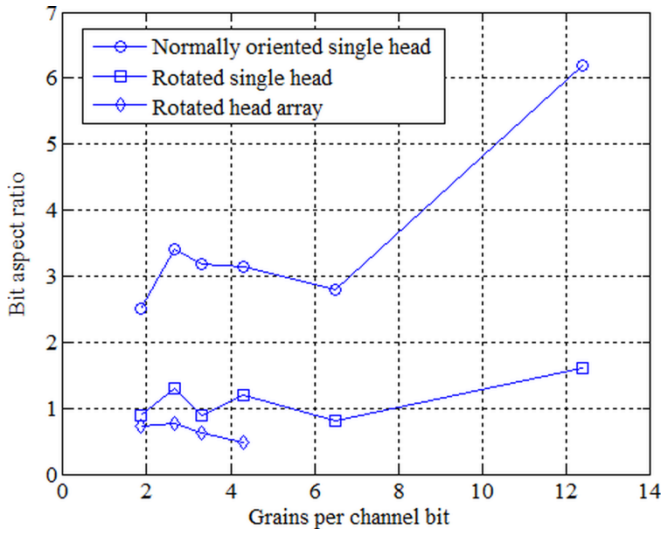

Figure 4.7 Optimum bit aspect ratio for various heads.

4.3.2 BER VS grains per channel bit

After we obtain the optimum performance for the NSH, RSH and RHA cases, it is easy to obtain the optimum BER as function of grains per channel bit, shown as Figure 4.8 and Figure 4. 9.

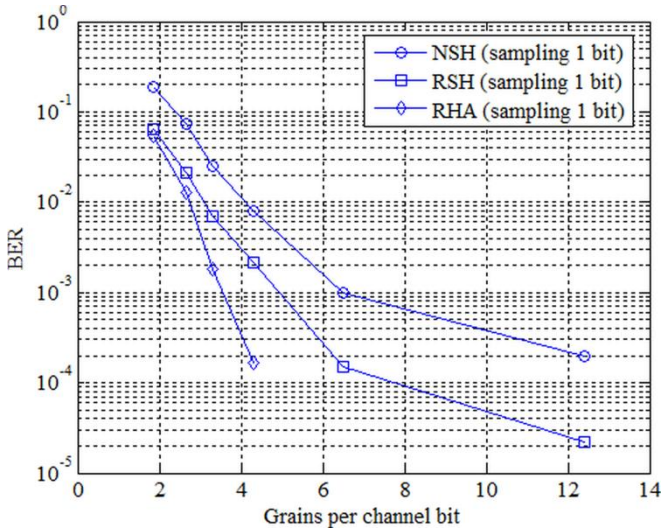

Figure 4.8 BER vs. grains per channel bits for various heads with sampling per bit.

Figure 4.8 and 4.9 indicate that the RSH always outperforms the NSH for various channel densities independent of whether sampling per bit or per 2nm is used. Furthermore, oversampling can greatly decrease BER for the RSH compared to sampling per bit, while it shows little improvement for the NSH. When sampling per bit, the RSH and the RHA can provide 1.3X and 1.9X density gain compared to the NSH for target BER of 10^{-3}. It is also found that the RSH and the RHA with a sampling period of 2nm can provide 1.7X and 2.1X density gain compared to the NSH, respectively. The choice of RHA with sampling per bit or RSH with sampling per 2nm will apparently depend on the feasibility of array fabrication versus high frequency detection.

We also find that the rotated head design can decrease BER greatly compared to a NSH at quite high density, such as fewer than two grains per channel bit. Such performance has not been obtained with a 2-D MAP detector at these densities: it shows little improvement over a 1-D detector and maintains BER around 20% [4.3]. With our new design, the rotated head array can decrease BER from 17% for a NSH to around 3% for 1.84 grains per bits; correspondingly the user density calculated with Shannon Capacity is greatly increased from 2.5Tbits/in^2 to 5.8Tbits/in^2.

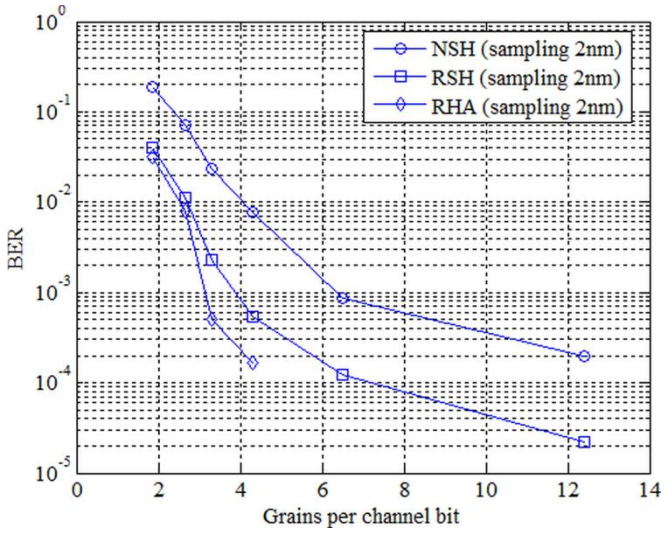

Figure 4.9 BER vs. grains per channel bits for various heads with sampling 2nm.

4.3.3 The effect of head noise on performance

To examine the effect of head noise, we have included the physically realistic head noise listed in table II and twice that value in the readback signal. After simulation, BER as function of grains per channel bit is shown as Fig.4.10.

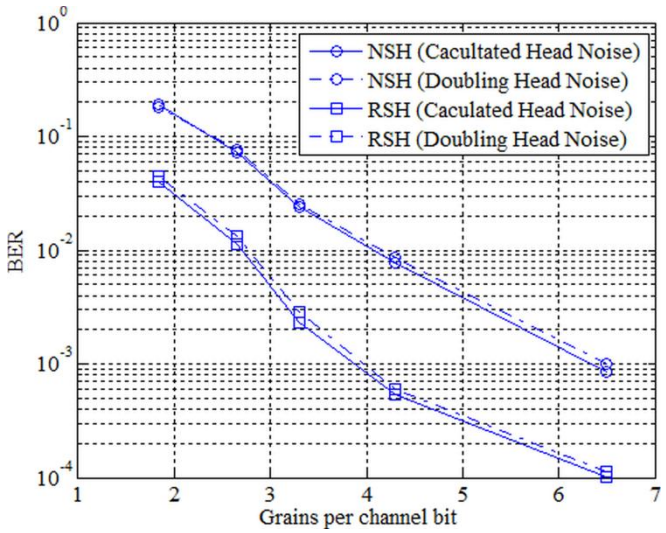

Figure 4.10 BER vs. grains per channel bit for various head noise.

It is found that doubling head noise has little influence on the BER curve for both heads. Instead, we find that head noise power must increase by 9 dB, i.e., a factor 8, before the BER doubles. This reflects the terrible media SNR, below a few dB in most cases, dominating the much smaller head noise.

4.3.4 Effect of magnetic fly height on performance

We have also examined the effect of magnetic fly height on BER. Besides adopting the assumed MFH for various densities in TABLE I, we also tried the case with fixed MFH of 7nm for all channel densities. This would be relevant if fly height improvement ends. The simulation results are shown as Fig.4.11.

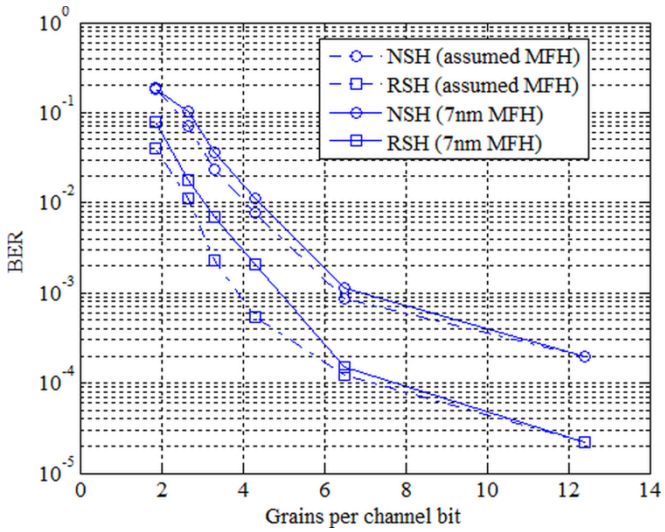

Figure 4.11 BER curve for various MFHs with both heads.

Figure.4.11 indicates that keeping a large magnetic fly height has increased the BER for both a normally oriented single head and rotated single head. The performance discrepancy between the two fly heights increases with decreased grains per bit, especially for the rotated single head down to 3 grains per bit. The reason is that the increased difference between fixed 7nm MFH and the previous assumed MFHs in Table 4.1 causes a wider readback waveform. The decreased bit size also brings more severe ITI. The problem can be solved with a rotated head array that addresses the ITI by detecting information from adjacent tracks with the side heads and 2D equalization, as shown in Figure 4.12.

It can be seen in Fig.4.12 that a rotated head array with 7nm MFH can reach almost the same performance as the rotated single head with the smaller MFH listed in TABLE I. Correspondingly, the rotated head array shows an advantage over a single rotated head when the constraint on MFH is loosened. Therefore, its greater difficulty of fabrication may be worthwhile if magnetic fly heights do not decline in the future.

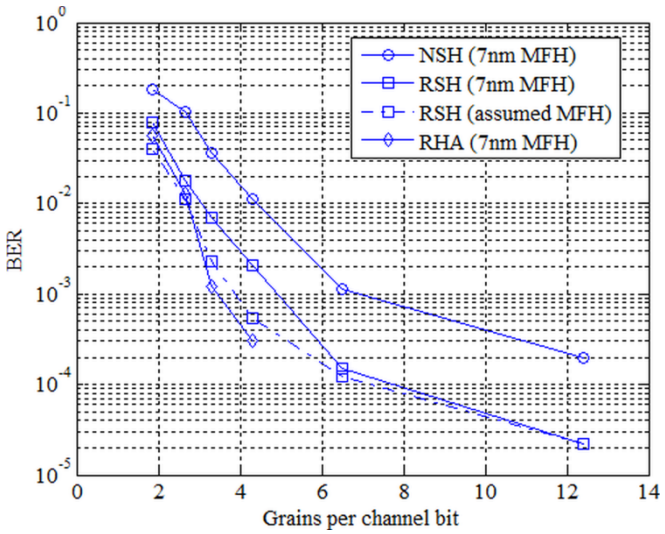

Figure 4.12 Comparison of performance of three heads at 7nm MFH with RSH at MFH in Table 4.1.

4.3.5 Effect of shield-to-shield spacing on performance

Similarly, we have also examined the effect of shield to shield spacing (SSS) on BER. Besides adopting the assumed SSS for various densities in TABLE I, we also tried the case with fixed SSS of 20nm for all channel densities. This would be relevant if no further improvement in shield-shield spacing can be achieved. The simulation results are shown as Fig.4.13.

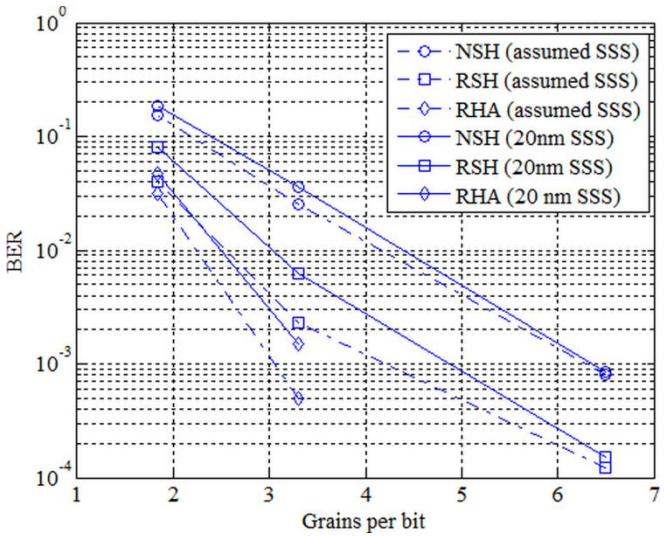

Figure 4.13 BER curve for various SSS with three heads.

It is found that the performance of the rotated single head (RSH) and the rotated head array (RHA) still outperform that of a normal single head (NSH) at larger shield to shield spacing. However, larger shield to shield spacing (SSS) has degraded the performance of the rotated single head slightly more than that of the normal single head. The reason is that the RSH relies on narrow SSS to obtain resolution in the crosstrack direction, and the larger SSS introduces additional ITI which is treated as noise by the RSH, but additional ISI introduced by the larger SSS for the NSH along the downtrack direction can be handled with the Viterbi detector. This issue can be addressed with a rotated head array that forces the additional ITI to zero with information detected from the adjacent tracks and 2D equalization. It is found that the performance of the RHA with 20nm SSS is quite close to the RSH with narrow SSS.

4.4 Conclusion

In this chapter, a novel system design for readback above 1 Tbit/in^2 density of conventional media is investigated. Simulation indicates that a rotated head achieves a density gain of 1.7x (single head) or 2.1x (array) over a normally oriented single head at a target BER of 10^{-3} with sampling period of 2nm, minimum mean square error equalizer and a Viterbi detector. It is found that the new design performs best for low bit aspect ratio, which differs from the normally oriented head. Head noise is predicted to have only a minor impact unless an order of magnitude increase is observed relative to accepted physical models. The rotated head array shows increased advantage over the single rotated head for larger magnetic fly heights and shield to shield spacing. The rotated head combined with oversampled signal processing shows great advantage at all densities over the normally oriented single head with a 1D detector and avoids the implementation of a

complex 2D detector and head array. It means established 1D detector schemes can still be applied to very high density systems with the proposed head design, thus limiting the change in detection technologies.

Chapter 5 Reader design for bit patterned media recording at 10 Tbits/in^2 densities

5.1 Introduction

Bit patterned media recording (BPMR) is a promising technology that has been proposed to extend area density beyond 1 Tbit/in^2 because thermal stability is based on the volume of the whole bit, not individual constituent grains [5.1]. The density can be greatly increased to 10 Tbits/in^2 when shingled writing [5.2, 5.3] is used to record on the bit patterned media. At such a high recording density, inter-symbol interference (ISI) and inter-track-interference (ITI) will be a major impairment that seriously degrades the system performance.

Several detection and equalization methods have been proposed for BPMR. The modified Viterbi algorithm to mitigate ITI has been studied [5.4]. It is found that joint-track equalization and detection [5.5] can enhance performance when the ITI is more severe. Two-dimensional (2D) equalization technology using a 2D equalizer with a one-dimensional (1D) generalized partial response (GPR) target has been considered in Ref. [5.6]. Additionally, a 2D GPR target combined with maximum a posterior (MAP) detector and low-density parity-check (LDPC) has been used to reach 4 Tb/in^2 [5.7]. However, little research has been performed to design a reader to effectively combat the ISI and ITI better than the various existing detection schemes.

In this chapter, a novel reader is proposed for BPMR systems at extremely high density. This concept is also useful for other very high density media such as the media in two-dimensional magnetic recording (TDMR) systems. The simulation shows that the proposed reader has more than a 20 dB gain compared to a normal arranged head array

for reading back bit patterned media at 10 Tbit/in^2**.** Additionally, the performance of the new design is examined for various bit patterns, island jitters, and head noises.

5.2 Reader design

5.2.1 Normal read head array

Use of a shingled writer to write 10 Tbits/in^2 bit patterned media has been studied in reference [5.2, 5.3]. However, read back at such high density for a realistic reader with satisfactory detection performance has not been reported yet.

The severe ITI and ISI make reading back using a single head without multiple passes impossible. Thus, we first employed an array of read heads as shown in Fig.5.1 to detect the bit patterned media at 10 Tbits/in^2, where the island size D is 4×4nm, and the center to center island distance on the down-track direction B_x and the cross-track direction B_z are both 8nm, respectively. The central head A is used to primarily pick up the information on the main track, and the side heads primarily read back the adjacent tracks' information. Here the conventional giant magnetoresistance (GMR) based read head has a shield to shield spacing (SSS) of 11nm and magnetic fly height (MFH) is 4nm. The free layer thickness is 4nm. The head width (along the cross track direction) is 18nm, which facilitates fabrication. However, this means that the head extends over multiple tracks. A 1D Viterbi algorithm (VA) was adopted with a 2D equalizer. For the equalizer design, a 1D target was used here to force ITI to zero and keep the ISI controllable along the down track direction, thus avoiding the more complex 2D Viterbi algorithm [5.6].

The results of simulation are not satisfactory, as shown in Session IV, and are poor compared to the lower density results reported in Ref.[5.4, 5.5, 5.6, 5.7]. In order to

compare the results with previous papers, the first part of the study assumes the noise is additive white Gaussian noise (AWGN), and the SNR is defined as follows:

$$SNR = 10log_{10}(\frac{V_P^2}{\sigma^2}) \quad (5.1)$$

Where V_P is the peak value of the readback signal of an isolated land and σ^2 is the variance of the noise. Here, V_p =1.

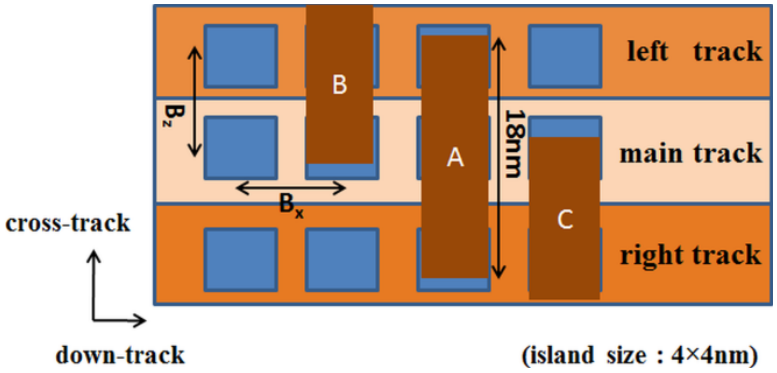

Figure 5.1 Schematic of head array on the bit patterned media.

After analysis, we found that the ITI becomes much more severe as the density is increased, especially when the density approaches 10 Tbits/in^2. This differs from previous studies of detection in BPMR systems, where density is around 4Tbits/in^2 or even smaller. This result is also related to the geometry and arrangement of the reader compared to the island size and island center to center distance in the cross track direction. Here, the head almost spans three tracks, as the head length is 18nm, which is close to the length of three islands (20nm) along the cross-track direction. Hence, ITI correction is limited to 3 poorly resolved input signals, although the down-track ISI can be corrected quite well with a Viterbi algorithm. This means that addressing the ITI in a better way needs to be studied; it may be that rearrangement of our system is a possible solution.

5.2.2 Rotated head design

The above analysis and unsatisfactory results for the usually oriented head array suggests that rotation of the read head together with oversampling in the down-track direction will greatly improve performance. Previously, we [5.8] proposed a similar structure for use in a TDMR system, and it worked quite well compared to a normally oriented head. The idea for this design is that the tightly placed shields are used to guarantee the resolution (for sufficient ratio of track pitch to head media spacing) in the cross-track direction, and oversampled signal processing is used to obtain the down track resolution. In this study, we tried the new head design with both a single head, shown in Fig.5.2 (b), and a head array.

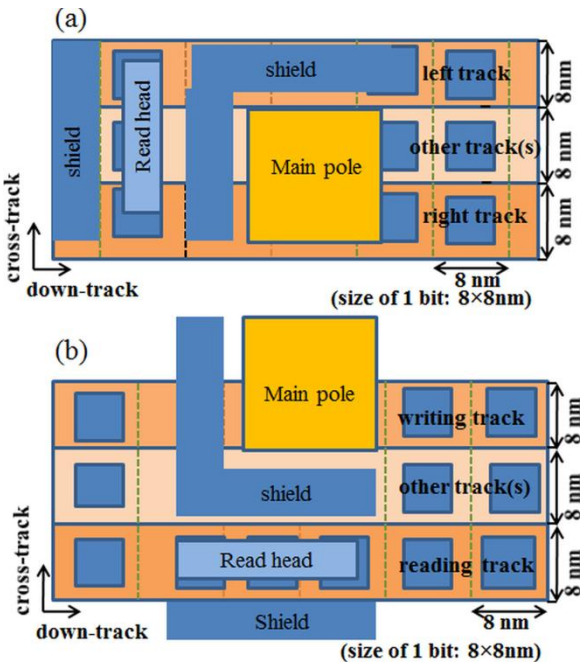

Figure 5.2 (a) Normal single head design for BPMR; (b) Rotated single head design for BPMR.

In the new design, the dimensions remain the same, i.e, the free layer is still 4nm x 18nm, the SSS is 11nm, the magnetic fly height is 4nm, the recording layer thickness is 14nm and the seed layer thickness between the soft under layer (SUL) and recording layer is 2nm. Here, exchanged coupled (ECC) media is used. The first part of the paper assumes all the noises are white noise so as to make the results comparable to other researchers' paper: the second part of the paper introduces media jitter and reader noise based on proven physical models [5.9, 5.10] in order to obtain a more realistic system performance.

5.3 Detection schemes with various head design

5.3.1 Writing and reading process

In this paper, we assume no writing errors occurred. For reading back, the reciprocity principle [5.11] is used by convoluting a head potential from a finite difference code [5.12] with the divergence of media magnetization to obtain the playback signals for the GMR head.

5.3.2 Detection with various head designs

For the rotated single head design, the ISI is more severe than ITI. Along the down-track direction, a 1D equalizer and Viterbi detector are used to combat the ISI; in the cross-track direction, the shields are utilized to combat the ITI. As described in Ref.[5.8], the 1D MMSE equalizer [5.13] uses a target size of 1×3, namely the length of ISI is 3. Here the monic constraint (g_0=1) is adopted for its optimal target shape. This constraint can be shown as

$$g=[1,g_1,g_2] \tag{5.2}$$

The constraint can be expressed as eq.(5.3),where c=1 and $E=[1,0,0]^T$.

$$E^T g = c \tag{5.3}$$

Then the optimized target and equalizer coefficient vector can be obtained with Eq. (5.4), (5.5) and (5.6).

$$\lambda = (E^T (A - T^T R^{-1} T)^{-1} E)^{-1} c \tag{5.4}$$

$$g = (A - T^T R^{-1} T)^{-1} E \lambda \tag{5.5}$$

$$f = R^{-1} T g \tag{5.6}$$

In Eqn.(5.4), (5.5) and (5.6), λ is a vector containing the Lagrange multipliers, g and f are the optimized target and equalizer coefficient, E and c are obtained with Eqn.(5.3), R is the auto-correlation matrix of the channel output, T is the cross-correlation of the input data and the channel output data , A is the auto-correlation of the input data, namely $R=E\{y_k y_k^T\}$, $T=E\{y_k a_k^T\}$ and $A=E\{a_k a_k^T\}$, where E denotes the expectation. The playback signals calculated using the reciprocity principle are considered to be the channel output signals y, the channel input data is a. We choose an equalizer of size 1×15 or $1\times [15\times \text{bit length}/2\text{nm}]$ for a sampling period of 1 bit or 2nm, respectively.

In order to compare with our new head design, we also tried the normal oriented single head and head array. For the normally oriented single head, shown as Fig.5.2 (a), joint-track equalization detection [5.5] has been examined. In this scheme, the 2D GPR target G is designed as a 3×3 matrix, shown in Eqn.(5.7)

$$G = \begin{pmatrix} g_{0,-1} & g_{1,-1} & g_{2,-1} \\ g_{0,0} & g_{1,0} & g_{2,0} \\ g_{0,1} & g_{1,1} & g_{2,1} \end{pmatrix} \tag{5.7}$$

Here the constraint on the target G has been set to make the corner entries $g_{0,-1}$, $g_{0,1}$, $g_{2,-1}$ and $g_{2,1}$ equal to zero. A Viterbi algorithm with a modified branch metric has been adopted here similar to Ref [5.5].

For the normally oriented head array, shown as Fig.5.1, and the rotated head array, ISI and ITI can both be addressed using 2-D equalization and detection. By imposing a constraint on the 2D target that forces ITI to zero and keeps only the controlled ISI, the conventional VA can handle ISI well. If we make a target of size 3 ×3, namely the length of ISI and ITI are 3, these constraints are similar to Eq. (15) to (19) in Reference [6]. Then the optimized target and equalizer coefficient vectors can still be obtained with Eq. (5.5), (5.6) and (5.7). Here we choose a target of size 3×3 for the rotated head array and an equalizer of size 3×15 or $3\times[15\times \text{bit length}/2\text{nm}]$ for the rotated head array when the sampling period is 1 bit or 2nm, respectively. An equalizer of size 7×15 or $7\times[15\times \text{bit length}/2\text{nm}]$ is chosen for the normally oriented head array in an effort to make its performance acceptable.

5.4 Numerical evaluation of the new design with white noise

5.4.1 Further study on the read back in TDMR system

First we have performed some further studies on the performance of the rotated single head in granular TDMR systems based on our previous study [5.8]. In the simulation, a head similar to the structure shown as Fig.5.2.(b) reads back the media with an average grain pitch of 5.5nm and bit size of 8nm×6nm. Previously the lost information in the down-track direction, caused by a large head size compared to the bit size, was recovered with oversampling. However, increasing the target length is also an option. The readback performance with larger target length and sampling once per bit is compared with the case of shorter target length and oversampling in Table 5.1.

Target length	BER(Sampling 2nm)	BER(Sampling 3nm)	BER(Sampling 1 bit)
L=3	4.7%	5.7%	8.4%
L=5	4.5%	5.2%	7.6%
L=7	4.4%	5.0%	7.4%

Table 5.1 BER for various target length and sampling periods in TDMR system.

Table 5.1 indicates that oversampling and increased target length both decrease the BER, as the former method can discretize the observation with no loss of information and the latter method equalizes the impulse response of the reader more precisely with longer target length. It is also found that the performance of the design with oversampling and L=3 is still better than the case with sampling per bit and longer target length L=7. Oversampling can lessen the loss of signal, which is a major concern in the extremely low SNR environment of TDMR system, although the longer target length can provide better equalized impulse response of the head and decrease the edge effect. Overall, considering the complexity of the Viterbi algorithm with longer target length and correspondingly greater detector cost, the method with oversampling and shorter target length is preferred.

5.4.2 New head design in the BPMR system

For a recording density of 10 Tbits/in^2 in a BPMR system, the rotated single head (RSH), rotated head array (RHA), normal single head (NSH) and normal head array (NHA) have been utilized with the various equalization technologies described in Session III. Here the sampling periods of 1 bit and 2nm have been both tried for our new design, as shown in Fig. 5.3 and Fig. 5.4, respectively.

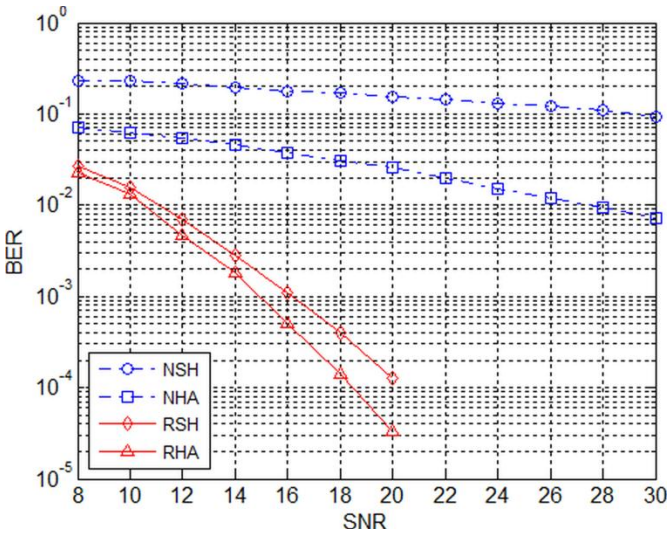

Figure 5.3 BER curves for various head designs with sampling period of one bit.

Fig.5.3 indicates that the rotated single head and rotated head array greatly outperform the normal oriented single head and normal oriented head array when the sampling period is one bit. Note that the normal head array cannot reach the target BER of 10^{-3} for any reasonable SNR. Reducing the target BER to 10^{-2} means that the new design offers more than 15 dB gain compared to the normal head array. The rotated head array performs slightly better than the single head, providing around 2 dB gain for the target BER of 10^{-3}, because the head array can combat the inter-track interference more effectively owing to the additional information detected by the side heads and the 2D equalization. However, like any head array, this will probably complicate treatment of head skew.

It is shown in Fig. 5.4 that oversampling can further improve the performance for the new design. Oversampling provides around 4 to 6 dB gain compared to sampling per bit for both the rotated single head and the head array. Another interesting observation is that, if the signal of our new head is oversampled, BER can still reach around 10^{-3} when the SNR is as low as 10dB. Such a good performance at low SNR has been seldom found in previous reports [5.4, 5.5, 5.6, 5.7]. This is caused by two factors as follows. On one hand,

the oversampling discretizes the signal with as few losses as possible. On the other hand, the rotated head picks up much less noise from adjacent tracks compared to the normal oriented head owing to the arrangement of the shields.

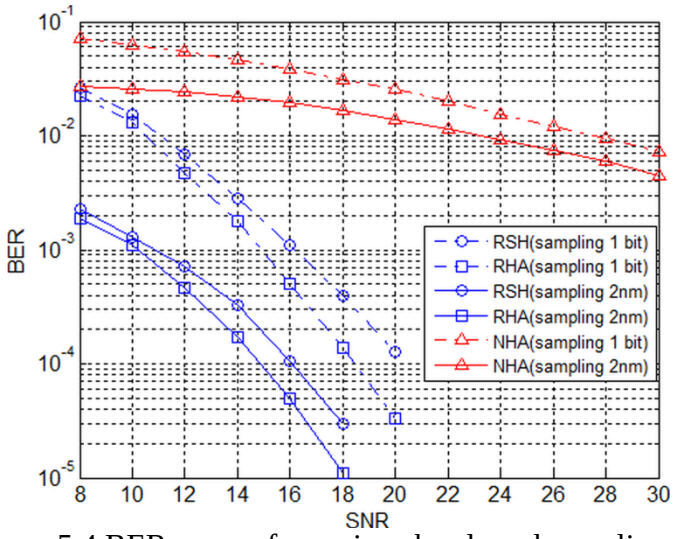

Figure 5.4 BER curves for various heads and sampling periods.

We also compared the performance of the rotated single head with the head array at various magnetic fly heights (MFH), assuming the sampling period is 1 bit, shown as Fig.5.5.

The performance discrepancies between rotated single head and head array increase with increased magnetic fly height, as shown in Fig.5.5, because the pulse width of the readback waveform in the cross track increases with increasing MFH; correspondingly, the inter-track interference becomes more severe. The head array can combat ITI more effectively than the single head with a single pass. The noise floor formed for the rotated single head with MFH=5nm is dominated by the residual ITI along the cross-track direction caused by this increased pulse width: it is better addressed by the head array. Figure 5.5 shows that the performance of the rotated single head and head array are

almost the same for 3nm MFH, However, the latter one outperforms the former one when the MFH approaches 5nm.

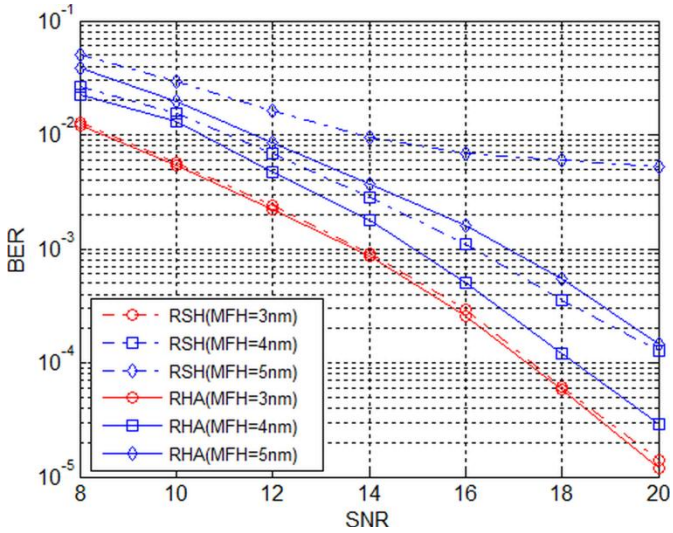

Figure 5.5 BER curve for new designs with various MFH.

Compared to the regularly rectangular arrays of islands (Fig. 5.6.a), hexagonal arrays (Fig.5.6.b) can be formed spontaneously by directed block copolymer self-assembly and other self-assembly techniques that are considered to be a promising cost-effective approach to achieving higher density and dimensional uniformity. Hence we also examined the new head design for the hexagonal islands case, shown as Fig.5.7.

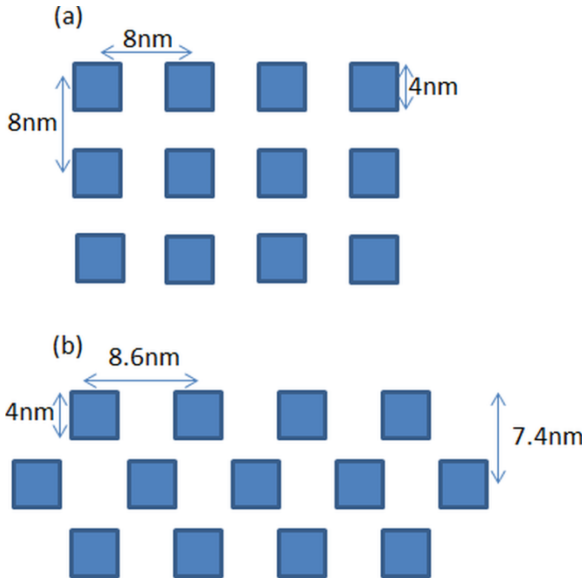

Figure 5.6 (a) Rectangular array for 10 Tbits/in^2; (b) Hexagonal array for 10 Tbits/in^2.

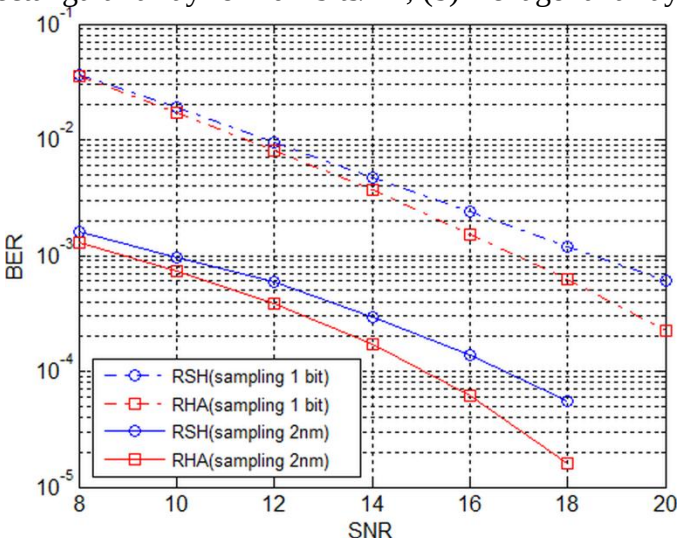

Figure 5.7 BER curves for Hexagonal array of bits with various sampling periods.

We find that the rotated single head has lower performance when detecting a hexagonal array of bits than when detecting a rectangular array because the center to center island distance in the crosstrack is decreased in the former case, and the ITI becomes more severe.

5.5 Numerical evaluation with more realistic parameters

In this section, we evaluate the performance of our new head design with more accurate simulation. The dominant contribution to the media noise is the randomness of island locations, namely jitter, which is nonstationary and data dependent. Reader noise is known to be flat band-limited noise with SNR dependent on data rate and free layer volume, according to accepted physical models [5.9, 5.10]. Due to the difference of real noise and AWGN noise, the jitter noises are simulated with both Taylor expansion and more accurate techniques, and the head noises are calculated with a physical model. This will provide more valuable and accurate results compared to the method of section IV where all noises were treated as additive AWGN noise.

5.5.1 Simulation methods

The media jitter in both down track and cross track directions are modeled as two independent, zero-mean Gaussian random variables Δx and Δz, with variances $\sigma_{\Delta x}^2$ and $\sigma_{\Delta z}^2$. Then the readback signal obtained by the head centered at (x, z) with an island centered at (x+Δx, z+Δz) can be expressed in a Taylor series expansion [5.11], shown as Eq.(5.9).

$$
\begin{aligned}
V(x+\Delta x, z+\Delta x) &= V(x,z) + \Delta x V_x(x,z) + \Delta z V_x(x,z) \\
&+ \frac{1}{2}\left[(\Delta x)^2 V_{xx}(x,z) + 2\Delta x \Delta z V_{xz}(x,z) + (\Delta z)^2 V_{zz}(x,z)\right] \\
&+ \frac{1}{6}\left[(\Delta x)^3 V_{xxx}(x,z) + 3(\Delta x)^2 \Delta z V_{xxz}(x,z) + 3(\Delta z)^2 \Delta x V_{xzz}(x,z)\right. \\
&+ \left.(\Delta z)^3 V_{zzz}(x,z)\right] + \varepsilon(x,z) \qquad (5.9)
\end{aligned}
$$

The jitter induced voltage is shown in Eq.(5.10).

$$V_e = V(x+\Delta x, z+\Delta z) - V(x,z) \qquad (5.10)$$

Here $\varepsilon(x,z)$ is the residual error if the first three orders are included. V_e is the jitter induced voltage. For the Taylor expansion method, the entire first, second and third order derivative terms are included when the jitter noise is >5% in order to make the residual error small.

We have also modeled the island jitter noises with a more realistic model. In this model, the system is discretized with a 0.1nm grid to simulate the randomness of small bits' location. The jitters along both down-track and cross-track directions are randomly and independently generated for each island: the position of each island varies in both directions. We compare the read back signal for the case without jitter to that with jitter. This method is very computationally intensive.

Head noise consisting of Johnson noise and magnetization noise based on accepted physical models is also included. The magnetization noise of the GMR can be calculated with eq.(7) in [5.9], shown as Eqn.(5.11)

$$SNR_{mag} \approx \frac{P\left(\frac{\Delta R}{R}\right)^2\left(\frac{H_{sig}}{H_{stiff}}\right)^2/(16K_BTB)}{1+P\left(\frac{\Delta R}{R}\right)^2\alpha/[4\gamma(H_{stiff})^2M_{sf}V_{free}]} \quad (5.11)$$

Where we assume $P=I_b^2R$, MR ratio $\Delta R/R$ = 15%, free layer stiffness H_{stiff}=10Oe, damping constant α =0.01, gyromagnetic ratio γ = 17.6 Mrad/(sOe), free layer magnetization M_{sf} =1600 emu/cm^3, resistivity ρ equals 20 uΩ·cm, and biasing current I_b=5mA. The band width is B; V_{free} is the volume of the free layer. Johnson noise can be estimated as Eq.(1) in [5.10]. The head media velocity is assumed to be 20m/s. The results are shown as Table 5.2.

Sampling period	6 nm	3nm	2nm
Bandwidth of Signal (GHZ)	3.33	6.67	10
Magnetization noise (SNR/dB)	30.7	27.7	26.0
Johnson noise(SNR/dB)	23.1	20.1	18.3
Total noise(SNR/dB)	22.4	19.4	17.6

Table 5.2 Noises for various sampling periods.

5.5.2 Study on island jitter noises

In order to study the media noise characteristics more precisely, we have modeled the island jitters with both methods mentioned previously; the jitter variance is 10%. Here, we consider around 10^5 bits, and the readback voltage is obtained with a small head with 4nm×4nm×4nm free layer as we want to decrease the effect of the ISI. The point here is to observe the jitter noises more precisely, and it is not to discuss whether the head can be fabricated or not. The histograms of the jitter induced readback voltages with both simulation methods have been illustrated as Fig.5.8 and Fig.5.9, where the readback voltage and counts have been both normalized.

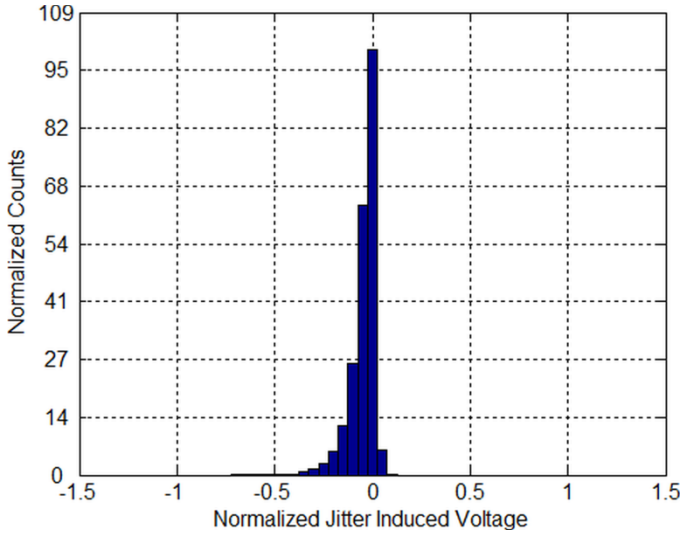

Figure 5.8 Histogram for normalized jitter induced voltage using the Taylor expansion technique.

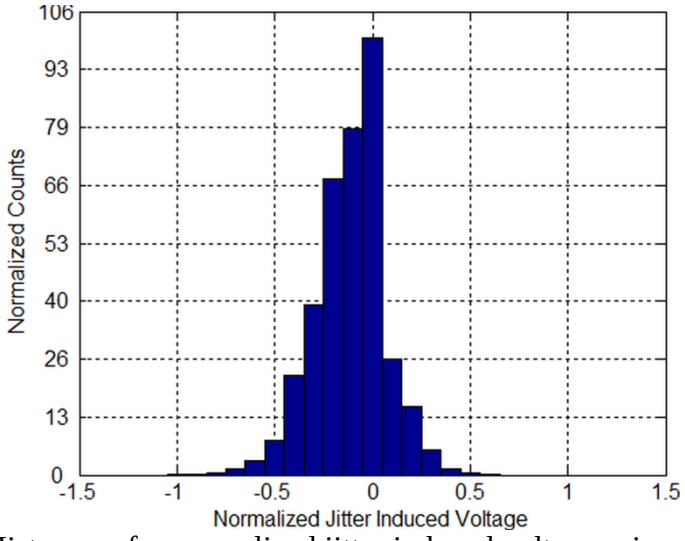

Figure 5.9 Histogram for normalized jitter induced voltage using exact signal.

Fig.5.8 and Fig.5.9 show that jitter induced readback voltage follows non-Gaussian distribution with most of the readback voltages negative. The two methods seem to agree with each other qualitatively, but the significantly broader histogram of the method using the exact signal indicates the high order effect of Taylor expansion. This illustrates that the third order approximation to the island jitter can be inadequate. The positive voltages are produced by the interference from neighboring bits.

We also calculated the jitter –induced readback voltages with more realistic free layer dimensions of 9nm×9nm×4nm and 18nm×18nm×4nm as shown in Fig.5.10 and Fig.5.11, respectively.

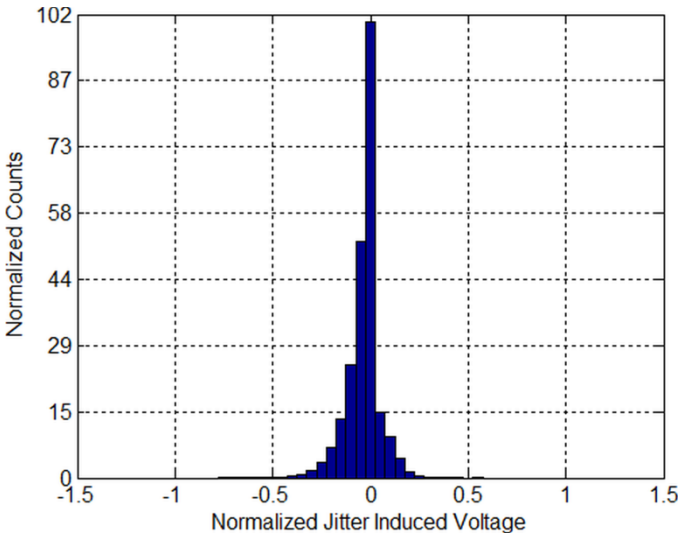

Figure 5.10 Histogram for normalized jitter induced voltage with 9nm head.

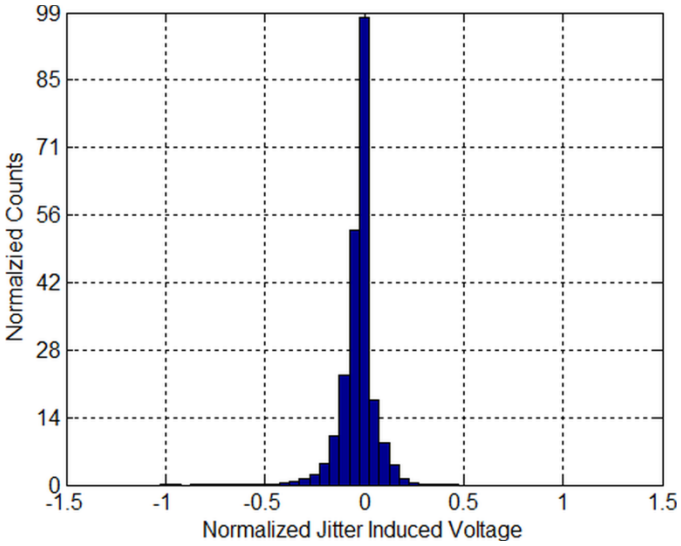

Figure 5.11 Histogram for normalized jitter induced voltage with 18nm head.

Fig.5.10 and Fig.5.11 show that the proportion of positive jitter induced voltage has increased when the head size is increased. This is due to the increased ISI caused by the increased head sizes. As the bits are written in a pseudorandom sequence, the interferences from the neighboring bits will be randomly distributed. Those interferences

combined with the jitter noises make jitter-induced readback voltages behave like parts of Gaussian distribution. However the statistics indicate that the proportion of negative voltage is still around 2 times larger than the positive ones even when the head is as large as 18nm.

We also study the performance of the new design (18nm×18nm×4nm free layer) when media and head noise are present. In this study, the media jitter ranges from 3% to 11%, the head noise is approximately 23.7 dB and 17.6 dB when the sampling periods are 1 bit and 2nm, respectively. The results are shown as Fig.5.12, where the linear y axis is adopted instead of the log y axis.

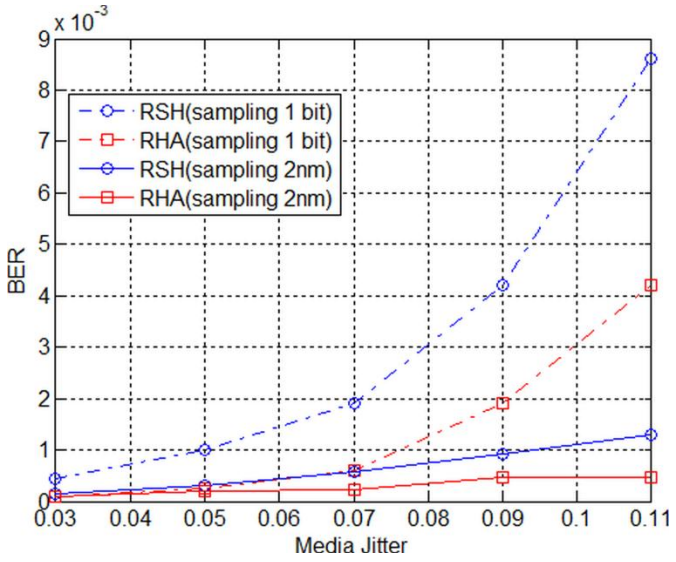

Figure 5.12 BER VS Media jitter and head noises for various schemes.

The head array can mitigate the jitter along the crosstrack direction better than the single head, thus producing the improved performance seen in Fig.5.12. Oversampling mitigates the jitter along the downtrack direction, also producing improved performance. Consequently, the rotated head array and oversampling provide the best resistance to severe jitter as shown in Fig.5.12.

5.6 Conclusion

In this chapter, a novel system design for readback at 10 Tb/in^{2}density is investigated, primarily for use in BPMR. The premise of the rotated head design is that ITI is a worse problem than ISI, because they are treated differently in the channel owing to the inability to adequately sample in the cross-track direction. The rotated head combined with oversampled signals, MMSE equalizer, and Viterbi detector can offer more than 20 dB gain over the conventionally oriented head array. Jitter noise is studied and found to be non-Gaussian. The rotated head array outperforms rotated single head when the MFH is larger than 3nm. The rotated head array combined with oversampling provides the best resistance to severe jitter.

Chapter 6 Study of Two-dimensional Magnetic Recording System including Micromagnetic Writer

6.1 Introduction

Two-dimensional magnetic recording (TDMR) has been proposed as a promising approach for ultra-high densities towards 10 Tbits/in^2 [6.1]. Shingled writing, which makes extensive use of track overlap, can be used for writing data in TDMR. During each pass, the head writes a wide (multiple tracks) signal, but then trims the signal to a single track width with the next pass. Readback can be implemented with various detection schemes, such as an inversion detector, 2D MAP detectors, etc. [6.2]. Previously, various writing and reading models have been proposed for TDMR systems. K.S.Chan [6.2] has proposed the grain-flipping probability model to study the performance of various detectors in TDMR with 6nm grain size. Reference [6.3] used a simplified writing process to study the TDMR specifications and compare various equalizer designs for 4.6nm grains.

However, few studies have been done for the design and optimization of the whole writer, reader and detector using a more accurate micromagnetic model to write realistic 8nm Voronoi grains. Previously, we proposed a rotated reader design for readback at ultra-high density from granular media [6.4] with perfect writing; the user density was greatly increased to 10.1 Tbits/in^2 with the new design. In this study, realistic writing with both conventional and optimized writers and reading with various readers have been studied using a micromagnetic model. First, a micromagnetic conventional writer was utilized to write data on exchanged coupled composite (ECC) media at 2 Tbits/in^2 channel bit density. Readback was implemented with both a single rotated sense head

(RSH) and a normally oriented single head (NSH) with sampling period of 2nm, minimum mean squared error equalizer and Viterbi detectors. Additionally the effect of skew was investigated. Also, an optimized shingled writer has been proposed to reach higher user density that approach the predicted maximum user areal density (4.66 Tbits/in^2) [6.5] for 8nm grains size with ideal writer and perfect reader resolution.

6.2 Shingled recording-conventional writer

6.2.1 Conventional writer design

First, a conventional writer consisting of a main pole and a trailing shield has been employed to study the achievable user density with shingled writing, shown in Fig.6.1. The dimension of the main pole and the trailing shield were 40 nm×60 nm and 80nm × 120nm in the cross-track and down-track directions, respectively. The trailing shield to main pole spacing was 40nm. The pole tip in the write head model was simulated micromagnetically. The main pole had an anisotropy field of 10 Oe oriented in the cross-track direction and saturation magnetization of 1910 emu/cm^3. The saturation magnetization of the trailing shield was 480 emu/cm^3. The magnetic fly height between recording media surface and air-bearing surface was considered to be 7nm. Simulation indicated the writer could generate a maximum perpendicular field of 11500 Oe with maximum gradients of 320 Oe/nm at the trailing edge.

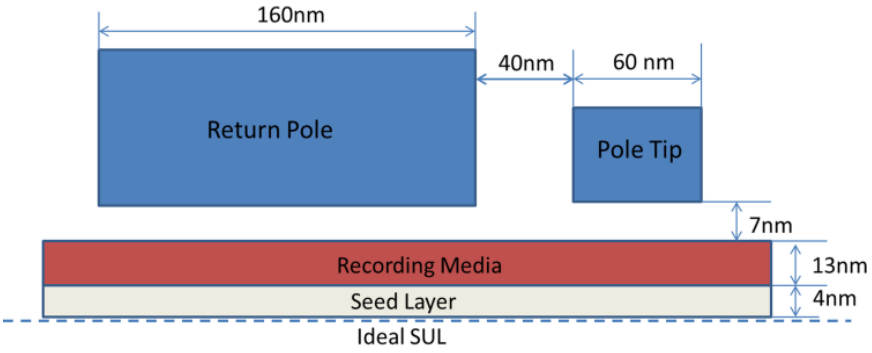

Figure 6.1 Down-track view of the conventional writer.

6.2.2 ECC media design

An ECC media structure was used for the micromagnetic simulations with soft under layer (SUL) replaced by an ideal imaging scheme assuming an infinite SUL with a permeability of 100. The recording layer was ferromagnetic ECC media with a top relatively soft layer and a bottom hard layer, whose thicknesses were both 6.5nm. The seed layer between recording layer and SUL was 4nm thick. Voronoi grain with average diameter of 8nm, non-magnetic grain boundaries of 1nm and a standard deviation of 20% were used in the simulation. The easy axis dispersion of the grains followed a Gaussian distribution with a standard deviation of 2°. The bottom layer had anisotropy field H_k=19.5 kOe and M_s=600 emu/cm^3. The top layer had H_k=6.5KOe and M_s=600 emu/cm^3. The intergranular exchange constant J_{ex} was 0.3 and the interlayer exchange coupling, J_{ex}/V was 9×10^6 erg/cm^3, where V was the volume of the grain [6.6].

Also we have employed an optimized ECC media with the same switching field, but thinner thickness of 10nm. The object was to maximize the ratio of the stabilizing energy barrier ΔE to the switching field H_s, $\xi \equiv 2\Delta E/(H_s * M_s * V)$, where M_s was the saturation magnetization and V was the volume of the grain. The thicknesses of the top soft layer and bottom hard layer were 6.7nm and 3.3nm, respectively. The bottom layer was the hard layer with H_k=167 KOe and M_s=150 emu/cm^3. The top layer had H_k=64 Oe and M_s=750 emu/cm^3. J_{ex} remained 0.3 and the interlayer exchange coupling, J_{ex}/V became 5.76×10^6 erg/cm^3 [6.6].

6.2.3 Reader design and detection scheme

Previously, a rotated reader design combined with oversampling signal processing was proposed for readback at ultra-high density from both granular media [6.4] and bit patterned media [6.7] with perfect writing. A schematic drawing of a rotated head array (RHA) is shown in Fig.6.2, where head labeled “A” detected the data in the current main track, while side heads labeled “B” and “C” were used to detect the adjacent tracks. The distance between the centers of central head and side heads was varied to obtain the lowest bit error rates. Here a conventional giant magnetoresistance (GMR)-based head was used, and the dimension of the free layer was 28nm × 28nm ×5nm, shield to shield spacing was 19nm and magnetic fly height was 7nm. For read back, the physically accurate reciprocity principle was used by convolving a head potential [6.5] with the divergence of media magnetization to obtain the playback signals.

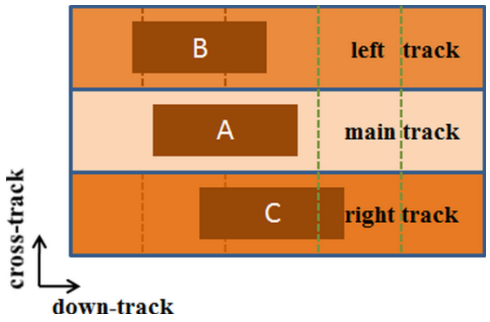

Figure 6.2 Schematic of rotated head array design.

The playback signals calculated with the reciprocity principle were considered as channel output signals, which were processed with a moving average filter before the equalization. For both rotated and normally oriented single head, the 1D MMSE equalizers was adopted, whose size was 1× [15 × bit length/2nm] for a sampling period of 2nm. The size of the 1-D target was 1×3 bits, and the monic constraint was used whose first coefficient was 1. For a rotated singled head with multiple scans and a head array, a 2-D MMSE equalizer of size 3× [15 × bit length/2nm] was used when the sampling

period was 2nm. Here, during the design of the 2-D general partial response (GPR) equalizer, a 1-D target with size of 1×3 bits (using the monic constraint) was used instead of a 2-D target; this design reached the same performance as the 2-D GPR equalizer with a 2-D zero forcing ITI target, but with a decreased computational complexity [6.8]. It's important to note that the multi-track output was still used to 2-D equalize the main track into an ITI free and controllable ISI 1-D target, hence there was no residual ITI. After both 1- and-2-D equalizers, a conventional Viterbi detector was implemented.

6.2.4 Simulation results for the conventional shingled writer

A conventional writer was utilized to write a pseudo-random binary sequence on ECC media. Both rotated and normally oriented readers were utilized. The reader noise was taken to be flat-band-limited noise with SNR dependent on the data rate and free layer volume, according to accepted physical models [6.9], [6.10]. The head noise consisted of both magnetization noise and Johnson noise. The reader SNR for sampling per 2nm was about 24 dB relative to a long wavelength signal. During the simulation, the BAR was varied during the writing process to obtain the optimum performance for each system. Then the corresponding user areal density (Fig. 6.3) can be calculated with the Shannon Capacity limit [6.11] according to the bit error rates obtained in the simulation.

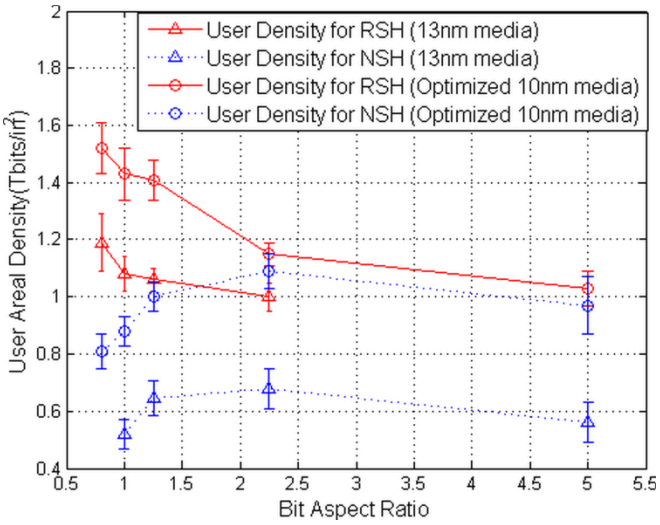

Figure 6.3 User Areal Density for various heads and media thicknesses.

Simulation indicated that user areal densities of 1.19Tbits/inch^2 and 0.68Tbits/inch^2 could be obtained by the RSH and the NSH with sampling period of 2nm for 13nm ECC media: this performance was not very satisfying due to the un-optimized writer and media design. It was also found that the optimum BAR for NSH was about 2.25, while the RSH performed better for lower BAR (<1) case. The reason for this was that varying BAR meant varying the amount of interference introduced by the reader in both down and cross track directions. For the normally oriented single head, avoiding the detriment of inter track interference (ITI) was a major concern; hence a higher BAR was wanted. In contrast, the rotated single head addressed the inter symbol interference (ISI) and ITI equally effectively; correspondingly a lower BAR approaching 1 became preferable. If optimized 10nm media was utilized in the simulation, user densities of 1.52Tbits/in^2 and 1.09Tbits/in^2 could be achieved with the RSH and the NSH due to the larger writing field and gradient allowed by the reduced media thickness, while the optimum BARs for both readers remained the same as those of the 13nm media case.

6.2.5 Effect of skew

The effect of skew is detrimental to the performance of shingled writing because it widens the erase band and broadens transitions. In this study, we compared the performances of rotated single head and normally oriented head for both the no skew and skewed cases for the 10nm medium, shown as Fig.6.4. It indicated that the skew angle (15°) degraded both the RSH and the NSH due to additional ISI and ITI introduced by the skew, The RSH with multiple scans (with the reader always centered over its track) could provide better resistance to the effect of skew angle because the additional information about adjacent tracks detected by multiple scans and 2-D equalization meant that the system could tolerate the additional ITI and ISI brought by the skewed reader more robustly.

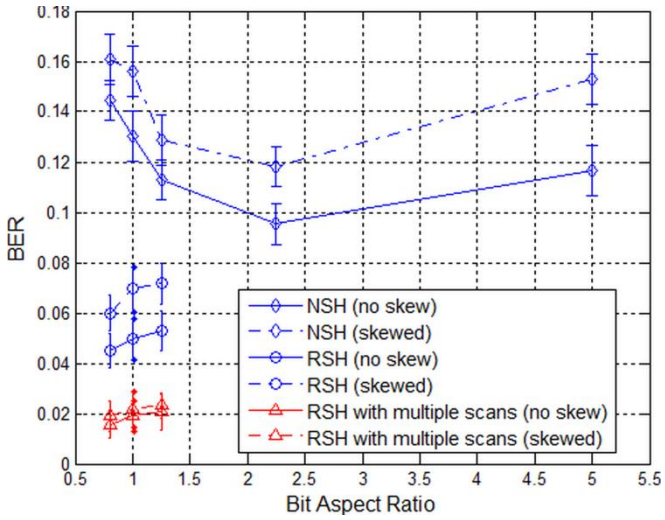

Figure 6.4 The BER for various heads with both skewed and no skew cases for the 10nm medium.

6.3 Optimized writer design

6.3.1 Specification of optimized writer

It is obvious that the conventional writer design above is not optimum for shingled writing due to the low head field gradient and lack of side shield, which will cause poor

transitions, and even severe erasure for adjacent tracks and bits. Correspondingly an optimized writer is needed to achieve higher user areal density. We proposed a shingled recording head, shown in Fig.6.4. Considering that the corner of the head was utilized to write data for shingled writing, maximizing the gradients at the writing corner and avoiding adjacent track erasure was the key to optimization. Fig.6.5 (a) is the down-track view of the proposed writer, and Fig.6.5 (b) illustrates the writer structure with a top down view. Our writer consisted of a main pole, side shield, a trailing shield, and a soft underlayer assumed to offer perfect imaging. A saturation flux of 2.4 Tesla was applied uniformly at the top surface of the main pole. The flux was completed by applying an equal but negative flux on the top surfaces of trailing and side pole. Both the bases of the main pole and return pole had widths of 20nm and shield to head spacing was assumed to be 10nm. It was found that a larger main pole (40nm) will cause more adjacent track erasure (ATE), while a smaller one (10nm) cannot provide large enough field. Both the trailing and side shields were utilized to control the field on both down and cross track direction. The slopes of the shield and main pole were optimized to be 45° and 30° to maximize the amount of flux into the writing pole tip and shield pole tip, thus maximizing the writing field and minimizing ATE.

In the optimized design, the saturation magnetization of the parts labeled in 1 and 2 in Fig.6.5 (a) were 2000 and 200 emu/cm^3, respectively. The low Ms (200 emu/cm^3) of both shields allows for efficient removal of flux from previously written bits and tracks without producing an ATE field. Simulation indicated that the field under the shield stayed below 1kOe, which was far smaller than the expected recording layer switching field (7000Oe). The parts of the head below the white dotted line in Fig.6.5 (a) had larger

anisotropies than the parts above the dotted line, which provided improved field strength and field gradients at the corner of the writing pole. The value of uniaxial anisotropy field (H_k) for parts below the dotted line labeled 1 and 2 were 4000 Oe and 2000 Oe, respectively. Above the dotted line, the anisotropies of the main pole and shields were much smaller, 10 Oe and 400 Oe, respectively.

6.3.2 Field profile

The recording field produced by the proposed writer could be obtained with micromagnetic simulation as Fig.6.6, where the field was evaluated 6nm below the air bearing surface. The maximum field of about 10 kOe was produced at the corner of the main pole, while the fields under the shield were below 1 kOe. The perpendicular writing field gradient of about 800 Oe/nm in both down track and cross track directions occurred at write fields of about 7 kOe, as shown in Fig.6.7. Correspondingly the switching field of the optimized 10nm ECC media was set to be 7 kOe. A sample magnetization pattern of random sequence was shingle written on the granular medium at about 4.5 Tbits/in^2 channel bit density, shown as Fig.6.8, where bits with the bit length of 12nm and the track pitch of 12nm were written.

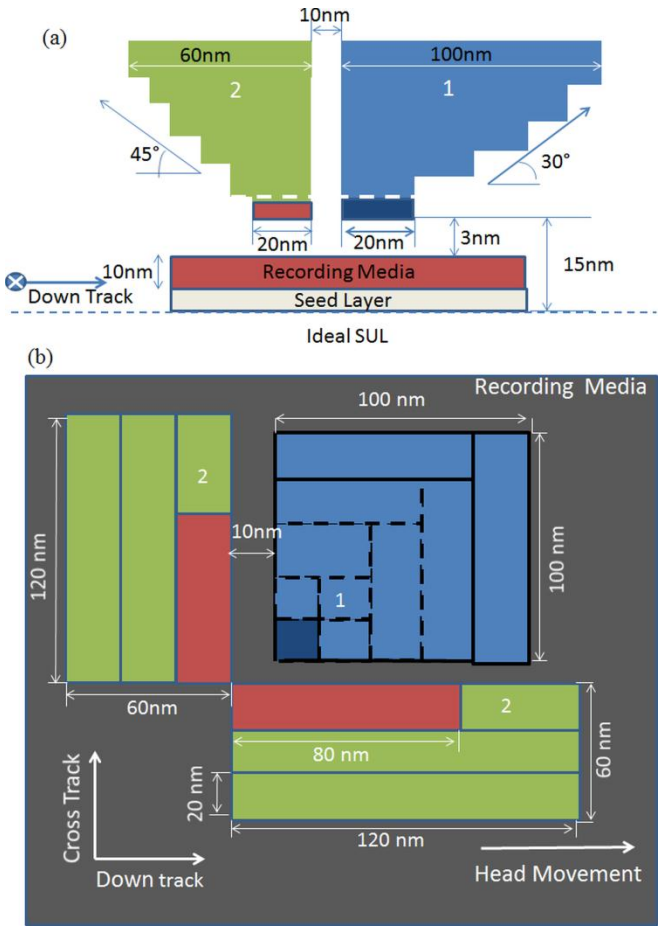

Figure 6.5 Optimized shingled recording head (a) the down-track view; (b) the air bearing surface view.

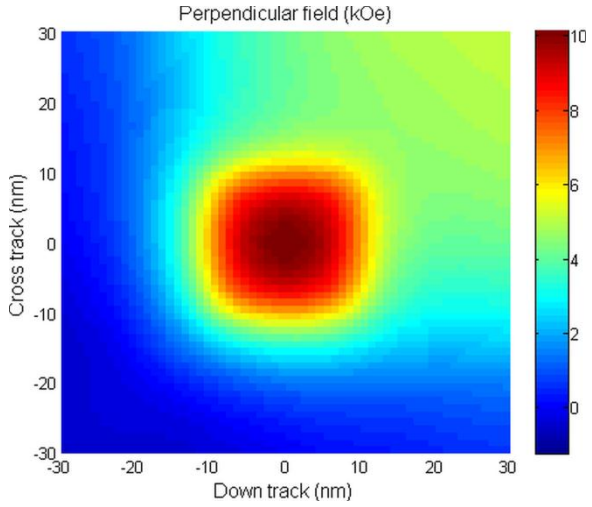

Figure 6.6 Shingled head perpendicular field profiles resulting from micromagnetic simulations.

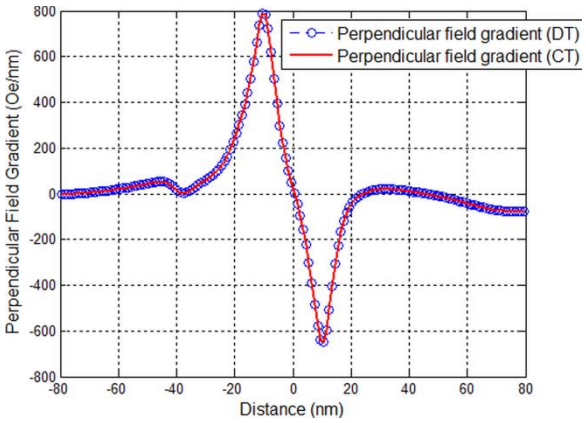

Figure 6.7 Perpendicular field gradients along both down and cross track directions.

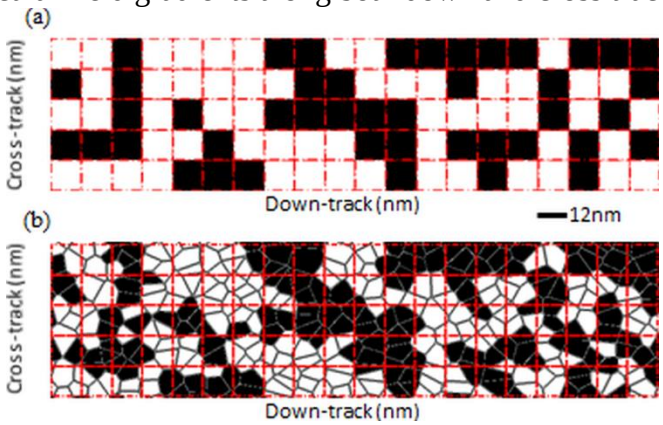

Figure 6.8 (a) Random magnetization pattern to be written on the granular medium. (b) The final written pattern using the proposed optimized writer.

6.3.3 Densities reached by the designed head

The proposed optimized writer was used to write a pseudo-random-bit sequence (PRBS) on the optimized 10nm ECC media. Both rotated single head and head array were utilized for readback. The dimension of the free layer was 18nm ×18nm ×4nm, and shield to shield spacing was 11nm. The reader SNR for sampling per 2nm was about 18 dB. In the simulation, the number of grains per bit and BARs were both varied during the writing process in order to obtain optimal results.

The possible capacities achieved by both readers were shown in Fig.6.8. It was found that our proposed system could obtain better results at lower bit-aspect ratio (≤1), which

was different from the usual high bit aspect ratio(≥2) adopted in the other reports [6.2], [6.3]. The reason for this was the field and field gradient produced by the proposed writer were symmetric in both down and cross track directions, which meant the writing performance was approximately the same along both directions. Besides the rotated reader design worked best for low BAR, especially for the RHA with the enhanced treatment of ITI [6.12]. Fig.6.9 indicated that the maximum user areal density achieved by the RSH and the RHA was about 3.60 Tbits/in^2 (with a track pitch of 12nm) and 4.03 Tbits/in^2 (with a track pitch of 10nm) for 2.88 grains/channel bits, respectively. For 2 grains/channel bits, the maximum user areal density achieved by the RSH and the RHA was about 3.76 Tbits/in^2 (with a track pitch of 7nm) and 4.52 Tbits/in^2 (with a track pitch of 7nm), which was close to the predicted maximum user areal density (4.66 Tbits/in^2) for 8nm grains with ideal writer and perfect reader resolution combined with a threshold detector [6.5]. For the RHA, optimization indicated that side heads should be moved closer to the main head instead of being at the center of adjacent tracks to obtain the lowest BER, and the optimum offset for side heads was about 2nm away from the center of adjacent tracks. We also observed that the RHA showed performance improvement compared to the RSH. Especially large improvements were found for few grains per bit because the information detected on the adjacent track and the 2-D equalization adopted by the RHA could better combat the severe ITI and ATE brought by the larger reader size and imperfect writer gradient when the bit size was decreased. The simulation also indicated that if the proposed writer was used to write a PRBS on granular media with 6nm grains, the BER was about 2% for a channel bit density of 6.7 Tbits/in^2; correspondingly, a user areal density of 5.8Tbits/in^2 could be reached.

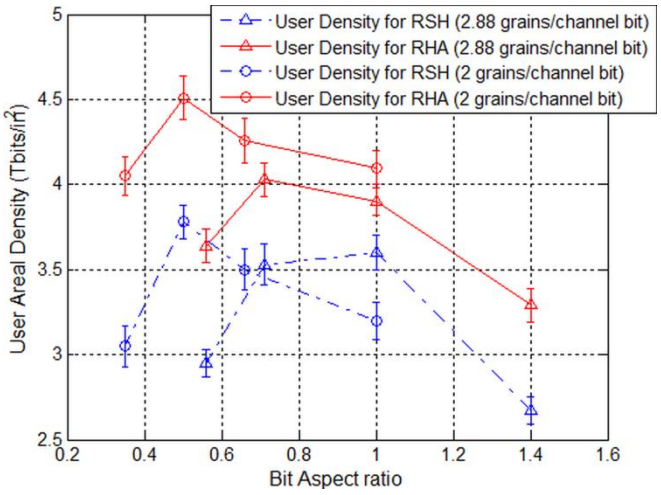

Fig.6.9 User Areal Density for the RSH and the RHA at 2.88 and 2 grains/channel bits for the optimized writer.

6.4 Conclusion

In this chapter, the performances of rotated and normally oriented single head were investigated when a conventional writer was used to shingle write data in a TDMR system. Simulation indicated that the user densities of 1.52Tbits/in^2 and 1.09Tbits/in^2 could be achieved with a rotated single read head and a normally oriented single read head with sampling period of 2nm, minimum mean squared error equalizer and Viterbi detectors, respectively. It was also found that the RSH with multiple scans and 2D equalization provided better resistance to skew. All user areal densities were calculated with the Shannon Capacity limit [11] by assuming a very long code word and treating the recording channel as a binary symmetric channel. With an optimized writer, for 2 grains/channel bits, the maximum user areal density achieved by the RSH and the RHA were about 3.76 Tbits/in^2 and 4.52 Tbits/in^2, which was close to the predicted maximum user areal density (4.66 Tbits/in^2) for 8nm grains with ideal writer and reader.

Summary

In this thesis, a novel reader design is proposed to readback user areal densities from 1-10 Tbits/in^2 recorded on granular media. The reader is also extended to readback bit patterned media with 10 Tbits/in^2 densities. A shingled micromagnetic writer is proposed and combined with the new reader design to reach user areal density above 4 Tbits/in^2 and near 6 Tbits/in^2 for 8nm and 6nm Voronoi grains, respectively.

Readback at ultra-high density from a granular media with a realistic reader, such as that envisioned for two-dimensional magnetic recording, is quite challenging due to the increased inter-track interference, inter-symbol interference, increasing writing errors and an extremely low signal-to-noise ratio (SNR) environment. The key idea of the novel reader design is a rotated sense head, so that the shields are aligned downtrack, combined with oversampled signal processing to regain the lost down-track resolution. Based on a random Voronoi grain model, simulation indicates that for near squared bits with 5.5 nm grains, and a rotated single reader, the bit error rate can drop from 20.9% for a normally positioned head array to 4.2% for a single-rotated single head with sampling period of 2 nm, a minimum mean squared error equalizer, and pattern-dependent noise prediction detector. The user density computed using the Shannon capacity limit is greatly increased to 10.1 Tb/in^2.

The reason for the superior performance of this reader is analyzed. The study indicates that the significant improvement in performance in the rotated head compared to the normally oriented head can be attributed to the larger amplitude of its dibit response and the reduced overlap between conditional probability density functions. An LDPC code is introduced for the system design with different bit aspect ratios. Simulation indicates that

maximum areal densities of 9.85T/in^2 and 6.64T/in^2 can be reached by the rotated head array (RHA) and normally oriented head array (NHA) at optimum bit aspect ratios of 0.67 and 3.5 for 5.5nm Voronoi grains, respectively. After decoding, the performance of the NHA is about 8.5dB worse than the RHA. With an oversampled signal, 2D linear minimum mean-squared error (LMMSE) equalizer and LDPC codes, a user bit density near 10 Tbits/in^2 is feasible for a rotated head array.

The performance of a rotated sense head is examined for densities of 2–7 Tbits/in^2 recorded on granular media, such as that envisioned for 2-D magnetic recording. Simulation shows that the new design achieves a density gain of 1.7X (single head) and 2.1X (head array) over a normally oriented single head at a target bit error rate (BER) of 10^{-3} with sampling period of 2 nm, minimum mean square error equalizer, and Viterbi detector. The new design shows greatly reduced BER relative to a normally oriented single head for all densities, including a very few grains per channel bit (<2).

If such a reader design is implemented for readback of bit patterned media at 10 Tbits/in^2. Simulation results show that the proposed reader has more than 20 dB gain compared with a normally oriented head array for reading back at 10 Tbits/in^2 for rectangular bits. We also examined the tradeoff between oversampling and increased target length. Island jitters are proved to be non-Gaussian distributed. The performance of the new design is investigated for both rectangular and hexangular bits combined with realistic island jitters.

A shingled micromagnetic writer is proposed for a TDMR system and readback with various readers. First, the performance of rotated and normally oriented single heads was investigated when a conventional writer was used to shingle write data in a TDMR

system. Simulation indicated that the user densities of 1.52Tbits/in^2 and 1.09Tbits/in^2 could be achieved with a rotated single read head and a normally oriented single read head with sampling period of 2nm, minimum mean squared error equalizer and Viterbi detectors, respectively. It was also found that the RSH with multiple scans and 2D equalization provided better resistance to skew. With an optimized writer, for 2 grains/channel bits, the maximum user areal densities achieved by the RSH and the RHA were about 3.76 Tbits/in^2 and 4.52 Tbits/in^2, which was close to the predicted maximum user areal density (4.66 Tbits/in^2) for 8nm grains with ideal writer and reader.

Reference

[1.1] Source: http://rondennison.com/services.htm.

[1.2] IBM 350 disk storage unit. [Online].Available: http://www.03.ibm.com/ibm /history/exhibits /storage/storage_350.html.

[1.3] H. J. Richter, "Recent advances in the recording physics of thin-film media," *Journal of Physics D - Applied Physics*, vol. 32, pp. R147-R168, Nov 7 1999.

[1.4] H. J. Richter, "The transition from longitudinal to perpendicular recording," *Journal of Physics D - Applied Physics*, vol. 40, pp. R149-R177, May 7 2007.

[1.5] H, J. Richter, A.Y. Dobin, O. Heinonen et al., "Recording on Bit-patterned media at densities of 1 Tb/in^2 and beyond", *IEEE Trans. Magn.*, vol.42,no.10, pp.2255-2260, Oct. 2006.

[1.6] Jian-Gang Zhu, X. Zhu and Y. Tang, "Microwave assisted magnetic recording", *IEEE Trans. Magn*., vol.44, no.1, pp.125-131, Jan. 2008.

[1.7] Roger Wood, "The feasibility of magnetic recording at 1 Terabit per square inch", *IEEE Trans. Magn*., vol.36, no.1, pp.36-42, Jan.2000.

[1.8] M. H. Kryder and R. W. Gustafson, "High-density perpendicular recording-advances, issues and extensibility," *J. Magn. Magn. Mat.*, vol. 287, pp. 449-458, Feb. 2005.

[1.9] M. H. Kryder, E. C. Gage, T. W. McDaniel, W. A. Challener, R. E. Rottmayer, G. Ju,Y.-T. Hsia, and M. F. Erden, "Heat assisted magnetic recording," *Proceedings of the IEEE*, vol. 96, no. 11, pp. 1810-1835, Nov. 2008.

[1.10] M. A. Seigler, W. A. Challener, E. Gage et al., "Integrated head assisted magnetic recording head: design and recording demonstration", *IEEE Trans. Magn*., vol.44, no.1, 119-124, Jan. 2008.

[1.11] S. Greaves, Y. Kanai, H. Muraoka, "Shingled recording for 2-3 Tbit/in^2", *IEEE Trans. Magn*., vol.45, no.10, pp.3823-3829, Oct. 2009.

[1.12] Source:http://www.seagate.com/about/newsroom/press-releases/terabit-milestone-storage-seagate-master-pr/.

[1.13] Y. Shiroishi, K. Fukuda, I. Tagawa, H. Iwasaki, S. Takenoiri, H. Tanaka, H. Mutoh, and N. Yoshikawa, "Future options for HDD storage," *IEEE Trans. Magn.*, vol. 45, no. 10, pp. 3816–3822, Oct.2009.

[1.14] Source : http://forensic-proof.com/archives/3160.

[1.15] Source:http://lookup.computerlanguage.com/host_app/search?cid=C999999&term= longitudinal+ recording&lookup.x=13&lookup.y=6.

[1.16] Source:http://lookup.computerlanguage.com/host_app/search?cid=C999999&term=perpendicular+recording&lookup=Go

[1.17] Felipe Garcia Sànchez and D. Weller. *Magnetic recording crisis and challenges.* N.d. Graphic. Thesis Web. 14 Nov. 2011.

[1.18] D. Z. Bai and J. G. Zhu, "Micromagnetics of perpendicular write heads with extremely small pole tip dimensions," *Journal of Applied Physics*, vol. 91, pp. 6833-6835, May 15 2002.

[1.19] Wood, R. ,"Shingled Magnetic Recording and Two-Dimensional Magnetic Recording," *IEEE Magnetics Society Meeting*, Santa Clara, CA, Oct. 19 2010.

[1.20] R.H.Victora and X.Shen, "Composite media for perpendicular magnetic recording" *IEEE Trans. Magn.*, vol. 41, no. 2, pp. 537–542, Feb.2005.

[1.21] D. Suess, "Multilayer exchange spring media for magnetic recording,"*Appl. Phys. Lett.*, vol. 89, p. 113105, 2006.
[1.22] M. N. Baibich, J. M. Broto, A. Fert et al., "Giant magnetoresistance of (001) Fe/(001) Cr magnetic superlattices", *Phys. Rev. Lett*. vol.61, pp. 2472-2475, 1988.
[1.23] Binasch, G., Grunberg, P., Saurenbach, F. & Zinn, W. "Enhanced magnetoresistance in layered magnetic structures with antiferromagnetic interlayer exchange", *Phys. Rev. B,* vol. 39**,** pp**.**4828–4830, Mar.1989.
[1.24] S. M. Thompson, "The discovery, development and future of GMR: The Nobel prize 2007," *J. Phys. D*, vol. 41, pp. 093001-1–093001-20, Mar. 2008.
[1.25] M. Takagishi *et al.*, "The applicability of CPP-GMR heads for magnetic recording," *IEEE Trans. Magn.*, vol. 38, no.5, pp. 2277-2282, Sep.2002.
[1.26] Childress J R and Fontana R E Jr, "Magnetic recording read head sensor technology," *Computers rendus Physique* vol. 6, issue 9, pp. 997-1012, 2005.
[1.27] H. Yuasa, M. Yoshikawa, Y. Kamiguchi, K. Koi, H. Iwasaki, M. Takagishi, and M. Sahashi, "Output enhancement of spin-valve giant magnetoresistance in current-perpendicular-to-plane geometry," *J.Appl. Phys.*, vol. 92, p. 2646, 2002.
[1.28] M. Saito *et al.*, "Narrow track width CPP spin-valve GMR heads utilizing half-metallicity materials," presented at the Intermag 2005 Conf., Nagoya, Japan, Paper FB-02.
[1.29] H. Oshima, K. Nagasaka, Y. Seyama, A. Jogo, Y. Shimizu, A. Tanaka, "Current-perpendicular spin valves with partially oxidized magnetic layers for ultrahigh-density magnetic recording," *IEEE Trans. Magn.,* vol.39, no.5, pp.2377-2380,Sep.2003.
[1.30] S. Yuasa and D. D. Djayaprawira, "Giant tunnel magnetoresistance in magnetic tunnel junctions with a crystalline MgO (001) barrier," *J.Phys. D.*, vol. 40, no. 21, pp. R337–R354, Nov. 2007.
[1.31] J. Mallinson, "On extremely high density magnetic recording," *IEEE Trans. Magn*, vol.10, no.2, pp.368-373, Jun. 1974.
[1.32] S. H. Charap, P. L. Lu, and Y. J. He, "Thermal stability of recorded information at high densities," *IEEE Trans. Magn*, vol. 33, no.1, pp. 978-983, Jan. 1997.
[1.33] Y. Dong and R. H. Victora, "Micromagnetic specification for bit patterned recording at 4 Tbit/in ," *IEEE Trans. Magn.*, vol. 47, no. 10,pp. 2652–2655, Oct. 2011.
[1.34] M. A. Siegler et al., "Integrated head assisted magnetic recording head: design and recording demonstration", *IEEE Trans. Magn*., vol.44, no.1, pp.119-124, Jan. 2008.
[1.35] K. S. Chan, R. Radhakrishnan, K. Eason, R. M. Elidrissi1, J. Miles,B. Vasic, and A. R. Krishnan, "Channel models and detectors for two dimensional magnetic recording (TDMR)," *IEEE Trans. Magn.*, vol.46, no. 3, pp.804-811, Mar. 2010.
[1.36] A.R.Krishman, R.Radhakrishnan, B.Vasic. eta., "2-D Magnetic recording: read channel modeling and detection", *IEEE Trans. Magn*. vol.45, no.10, pp.3830-3836, Oct.2009.
[1.37] Hwang E, Negi R, Kumar B V K V (2010),"Signal processing for near 10 Tbit/in^2 density in two-dimensional magnetic recording (TDMR)," *IEEE Trans. Magn.*, vol. 46, no. 6, pp. 1813–1816, Jun.2010.

[1.38] A. Fahrner, "On signal processing and coding for digital magnetic recording system," Ph.D. dissertation, Department of Telecommunications and Applied Information Theory, University of Ulm, Germany, 2004.
[1.39] S. Aviran, "Constrained coding and signal processing for data storage system," Ph.D. dissertation, Department of Electrical and Computer Engineering, University of California, San Diego, 2006.
[1.40] P. H. Siegel, "Recording codes for digital magnetic storage," *IEEE Trans. Magn.*, vo.21, no.5, pp. 1344–1349, Sept. 1985.
[1.41] J. G. Proakis, "Partial response equalization with application to high density magnetic recording channels," in *CRC Handbook for Coding and Signal Processing for Recording Systems*, B. Vasic and E. M. Kurtas, Eds. CRC Press, 2004.
[1.42] K. A. S. Immink, P. H. Siegel, and J. K. Wolf, "Codes for digital recorders," *IEEE Trans. Inf. Theory*, vol. 44, no. 6, pp. 2260 – 2299, Oct. 1998.
[1.43] J. Moon and W. Zeng, "Equalization for maximum likelihood detectors," *IEEE Trans. Magn.*, vol. 31, no. 2, pp. 1083-1088, Mar. 1995.
[1.44] P. Kovintavewat, I. Ozgunes, E. Kurtas, J. R. Barry, and S. W. McLaughlin, "Generalized partial-response targets for perpendicular recording with jitter noise," *IEEE Trans.Magn.*, vol. 38, no. 5, pp. 2340-2342, Sep. 2002.
[1.45] J. Coker, E. Eleftheriou, R. Galbraith, and W. Hirt, "Noise-predictive maximum likelihood (NPML) detection," *IEEE Trans. Magn.*, vol. 34, no. 1, pp. 110–117, Jan 1998.
[1.46] S. Karakulak, P. H. Siegel, J. K.Wolf, and H. N. Bertram, "A new read channel model for patterned media storage," *IEEE Trans. Magn.*, vol.44, no. 1, pp. 193–197, Jan. 2008.
[1.47] S. Nabavi, B. V. K. V. Kumar, and J.-G. Zhu, "Modifying Viterbi algorithm to mitigate inter-track interference in bit-patterned media," *IEEE Trans. Magn.*, vol. 43, no. 6, pp. 2274–2276, Jun. 2007.
[1.48] S.Karakulak, P. H. Siegel, andH.N. Bertram, "Joint-track equalization and detection for bit patterned media recording," *IEEE Trans. Magn.*, vol. 46, no. 10, pp. 3639–3647, Oct. 2006.
[1.49] S. Nabavi and B. V. K. V. Kumar, "Two-dimensional generalized partial response equalizer for bit-patterned media," in *Proc. IEEE Int. Conf. Commun.*, Glasgow, U.K., pp. 6249–6254, 2007.
[1.50] M. Keskinoz, "Two-dimensional equalization/detection for patterned media storage," *IEEE Trans. Magn.*, vol. 44, no. 4, pp. 533–539, Apr. 2008.
[1.51] W. Chang and J. R. Cruz, "Inter-track interference mitigation for bit-patterned media recording," *IEEE Trans. Magn.*, vol. 46, no. 11, pp. 3899-3908, Nov. 2010.
[1.52] Upamanyu *Madhow, Fundamentals of digital communication*. Cambridge, U.K.:Cambridge Univ. Press, 2008, pp. 311-324.
[1.53] Caroselli J, Altekar S A, McEwen P, Wolf J K (1997), "Improved detection for magnetic recording systems with media noise," *IEEE Trans. Magn.*, vol. 33, no. 5, pp. 2779–2781, Sep.1997.
[1.54] A. Kavcic and J. M. F. Moura, "The Viterbi algorithm and Markov noise memory,"*IEEE Trans. Inf. Theory*, vol. 46, no. 1, pp. 291-301, Jan. 2000.

[1.55] J. Moon and J. Park, "Pattern-dependent noise prediction in signal-dependent noise,"*IEEE J. Sel. Areas Commun.*, vol. 19, no. 4, pp. 730-743, Apr. 2001.
[1.56] Z. Wu, P. H. Siegel, J. K. Wolf, and H. N. Bertram, "Mean-adjusted pattern-dependent noise prediction for perpendicular recording channels with nonlinear transition shift," *IEEE Trans. Magn.*, vol. 44, no. 11, pp. 3761-3764, Nov. 2008.
[1.57] W. Tan and J. R. Cruz, "Signal processing for perpendicular recording channels with intertrack interference," *IEEE Trans. Magn.*, vol. 41, no. 2, pp. 730–735, Feb. 2005.
[1.58] K. S. Chan, R. Radhakrishnan, K. Eason, R. M. Elidrissi1, J. Miles,B. Vasic, and A. R. Krishnan, "Channel models and detectors for two dimensional magnetic recording (TDMR)," *IEEE Trans. Magn.*, vol.46, no. 3, pp.804-811, Mar. 2010.
[1.59] Y.Wu, J. A. O'Sullivan, N. Singla, and R. S. Indeck, "Iterative detection and decoding for separable two-dimensional intersymbol intereference," *IEEE Trans. Magn.*, vol. 39, no. 4, pp.2115-2120, Jul. 2003.
[1.60] R. W. D. Palmer, P. Ziperovich and T. Howell, "Identification of nonlinear write effects using pseudorandom sequences," *IEEE Trans. Magn.*, vol. 23, no.5, pp. 2377–2379, Sept. 1987.
[1.61] Y.Tang and C. Tsang, "A technique for measuring nonlinear bit shift," *IEEE Trans. on Magn.*, vol. 27, no.6, pp. 5316–5318, Nov. 1991.
[1.62] F.Lim and A. Kavcic, "Optimal precompensation for partial erasure and nonlinear transition shift in magnetic recording using dynamic programming," in *Proc. IEEE Global Telecommun. Conf., Globecom'05*, vol. 1, St. Louis, Missouri, USA, Nov. 28–Dec. 2, 2005, pp. 58–62.
[1.63] Z. Wu, H. N. Bertram, P. H. Siegel, and J. K. Wolf, "Nonlinear transition shift and write precompensation in perpendicular magnetic recording," in *Proc. IEEE Int. Conf. Commun. ICC'08*, Beijing, China, May 19–23, 2008, pp. 1972–1976.
[2.1] W. F. Brown, *Micromagnetics.* John Wiley & Sons, Inc.1963.
[2.2] E. Della Tore, "Magnetization Calculation of fine of fine particles", *IEEE Trans. Magn.*, vol.22, no.5, pp.484-489, Sep.1986.
[2.3] R. H. Victora, J. Xue, and M. Patwari, "Areal density limits for perpendicular magnetic recording," *IEEE. Trans. Magn.*, vol. 38, no. 5, pp.1886–1891, Sep. 2002.
[2.4] M. E. Schabes and A. Aharoni, "Magnetostatic interaction fields for three dimensional array of ferromagnetic cubes", *IEEE. Trans. Magn.*, vol. 23, no.6, pp.3882– 3889, Nov. 1987.
[2.5] G. A. Mohr, *Finite elements for solids, fluids and optimization*. Oxford University Press, New York, 1992.
[2.6] B. D. Cullity, *Introduction to magnetic materials*. Addison-Wesley Publishing Company, Inc. 1972.
[2.7] W. F. Brown, JR., "Thermal fluctuations of a single-domain particle", *Phys. Rev.* Vol. 130, No.5, 1677-1686, 1963.
[3.1] R. Wood, M. Williams, A. Kavcic, and J. Miles, "The feasibility of magnetic recording at 10 Tb/in^2 on conventional media", *IEEE Trans. Magn.*, vol. 45, no.2, pp.917-923, Feb. 2009.

[3.2] E. Hwang, R. Negi, and B.V.K.V. Kumar, "Signal processing for near 10 Tbit/in^2 density in two-dimensional magnetic recording (TDMR)," *IEEE Trans.Magn.*, vol. 46, no. 6, pp. 1813-1816, Jun. 2010.

[3.3] Y. Wang, S. Frohman, R. H. Victora, "Ideas for detection in two dimensional magnetic recording systems," *IEEE Trans. Magn.*, vol. 48, no. 11, pp. 4582–4585, Nov.2012.

[3.4] A. R. Krishnan, R. Radhakrishnan, B. Vasic, "LDPC decoding strategies for two-dimensional magnetic recording," in *Proc. IEEE Global Telecommun. Conf.*, Honolulu, HI, pp. 1–5, 2009.

[3.5] K. S. Chan, R. Radhakrishnan, K. Eason, M. R. Elidrissi, J. J. Miles, B. Vasic, A.R. Krishnan, "Channel models and detectors for two dimensional magnetic recording," *IEEE Trans. Magn.*, vol. 46, no. 3, pp. 804–811, Mar.2010.

[3.6] E. Hwang, R. Negi, B. V. K. V. Kumar, "Signal processing for near 10 Tbit/in^2 density in two-dimensional magnetic recording (TDMR)," *IEEE Trans. Magn.*, vol. 46, no. 6, pp. 1813–1816, Jun.2010.

[3.7] S. Nabavi, B. V. K. V. Kumar, "Two-dimensional generalized partial response equalizer for bit-patterned media," in *Proc. IEEE Int. Conf. Commun.*, Glasgow, U.K., pp. 6249–6254,2007.

[3.8] N. Smith, P. Arnett , "White-noise magnetization fluctuations in magnetoresistive heads," *Appl. Phys. Lett.*, vol. 78, no. 10, pp. 1448–1450,2001.

[3.9] R. Wood, J. Miles, T. Olsen, "Recording technologies for Terabit per square inch systems," *IEEE. Trans. Magn.*, vol. 38, no. 4, pp. 1711–1717, Jul. 2002.

[3.10] R. H. Victora, S. M. Morgan, K. Momsen, E. Cho, M. F. Erden, "Two-dimensional magnetic recording at 10 Tbits/in^2," *IEEE. Trans. Magn.*, vol. 48, no. 5, pp. 1697–1703, May. 2012.

[3.11] H. N. Bertram, *Theory of Magnetic Recording.* New York: Cambridge Univ. Press, pp. 112–119,1994.

[3.12] Y. Dong, Y. Wang, R.H. Victora, "Micromagnetic specification for recording self-assembled bit-patterned media," *J. Appl. Phys.*, vol. 111, p.07B904, 2012.

[3.13] J. Moon, W. Zeng, "Equalization for maximum likelihood detectors," *IEEE Trans. Magn.*, vol. 31, no. 2, pp. 1083–1088, Mar.1995.

[3.14] J. Caroselli, S.A. Altekar, P. McEwen, J.K. Wolf, "Improved detection for magnetic recording systems with media noise," *IEEE Trans. Magn.*, vol. 33, no. 5, pp. 2779–2781, Sep.1997.

[3.15] C. Shannon, "A mathematical theory of communications," *Bell Syst. Tech. J.*, vol. 27, pp. 379–423, 623–656, July, Oct. 1948.

[3.16] Y.Wang, M.F.Erden and R.H.Victora, "Novel system design for readback at 10 Terabits per square inch user areal density", *IEEE Magnetic Letters*, Vol.3, article #: 4500304, Dec.2012.

[3.17] M. P. C. Fossorier, "Quasi-cyclic low-density parity-check codes from circulant permutation matrices," *IEEE Trans. Inform. Theory*, vol. 50, no.8, pp. 1788-1793, Aug. 2004.

[3.18] I. Ozgunes and W. R. Eppler, "Synchronization-Free Dibit Response Extraction From PRBS waveforms", *IEEE Trans. Magn.*, vol. 39, no. 5, pp. 2225–2227, Sep. 2003.

[3.19] A.R. Krishnan, R. Radhakrishnan, B. Vasic, A. Kavcic, W. Ryan, and F. Erden, "2- D magnetic recording: Read channel modeling and detection," *IEEE Trans. Magn.*, vol. 45, no. 10, pp. 3830–3836, Oct. 2009.

[3.20] D. E. Hocevar, "A reduced complexity decoder architecture via layered decoding of LDPC codes," in *Proc. of IEEE Workshop Signal Process.Syst. (SIPS)*, pp. 107–112, Oct. 2004.

[4.1] R. Wood, M.Williams, A. Kavcic, and J.Miles, "The feasibility of magnetic recording at 10 Tb/in^2 on conventional media", *IEEE Trans. Magn*., vol. 45, no.2,pp.917-923, Feb. 2009.

[4.2] A. Krishnan, R. Radhakrishnan et al. "LDPC decoding strategies for two-dimensional magnetic recording," in *Proc. IEEE Global Telecommunications Conf.(GLOBECOM)*, Honolulu, HI,Dec.2009.

[4.3] K. S. Chan, E. M. Rachid, K. Eason et al. "Comparison of one-and two-dimensional detectors on simulated and spin-stand readback waveforms", *Journal of Magnetism and Magnetic Materials,* vol.324, no.3, pp.336-343, 2012.

[4.4] E. Hwang, R. Negi, and B. V. K. V. Kumar, "Signal processing for near 10 Tbit/in^2 density in two-dimensional magnetic recording (TDMR)" , *IEEE Trans.Magn*., vol.46,pp.1813-1816, Jun.2010.

[4.5] Y. Wang, M. F. Erden and R. H. Victora, "Novel system design for readback at 10 Terabits per square inch user areal density", *IEEE Magnetic Letters*, Vol.3, article #: 4500304, Dec.2012.

[4.6] R. Lamberton, M. Seigler, K. Pelhos et al. "Current-in-Plane GMR trilayer head design for hard disk drive: characterization and extendibility", *IEEE Trans. Magn.*, vol.43, no.2, pp.645-650, Feb.2007.

[4.7] N. Smith and P. Arnett, "White-noise magnetization fluctuations in magnetoresistive heads", *Appl. Phys. Lett*. vol. 78, no. 10, pp. 1448-1450, Mar. 2001.

[4.8] R. Wood, J. Miles, T. Olsen, "Recording technologies for Terabit per square inch systems", *IEEE. Trans. Magn*., vol.38, no.4, pp.1711-1717, Jul.2002.

[4.9] R. H. Victora, S. M. Morgan et al "Two-dimensional magnetic recording at 10 Tbits/in^2", *IEEE. Trans. Magn*., vol.48, no.5, pp1697-1703, May.2012

[4.10] H. N. Bertram, *Theory of Magnetic Recording.* Cambridge University Press, NY, 1994, pp.112-119.

[5.1] H. J. Richter *et al.*, "Recording on bit-patterned media at densities of 1Tb/in^2 and beyond," *IEEE Trans. Magn.*, vol. 42, pp. 2255–2260, Oct.2006.

[5.2] S. Wang, Y. Wang and R.H.Victora, "Shingled magnetic recording on Bit Patterned Media at 10 Tb/in^2", *IEEE Trans. Magn*., vol. 49, no.7, pp. 3644–3647, Jul. 2013.

[5.3] S. Xu, G. Zhou, J. Chen and B. Liu, "Shingled writer design for achieving 10 Tb/in^2 patterned media recording", Intermag, FH-03, 2012.

[5.4] S. Nabavi, B. V. K. Vijaya Kumar, and J. G. Zhu, "Modifying Viterbi algorithm to mitigate intertrack interference in bit-patterned media", *IEEE Trans. Magn.*, vol. 43, no.6, pp. 2274–2276, Oct.2006.

[5.5] S. Karakulak, P. H. Siegel, and H. N. Bertram, "Joint-track equalization and detection for bit patterned media recording", *IEEE Trans. Magn.*, vol. 46, pp. 3639–3647, Oct. 2006.

[5.6] S. Nabavi and B. V. K. Vijaya Kumar, "Two-dimensional generalized partial response equalizer for bit-patterned media," in *Proc. IEEE Int. Conf. Commun. (ICC)*, Jun. 2007, pp. 6249–6254.

[5.7] K. Cai, Z. Qin, S. Zhang et al, " Modeling, detection and LDPC codes for bit-patterned media recording", *IEEE Globecom 2010 workshop on application of communication theory to emerging memory technologies*, pp.1910-1914.

[5.8] Y. Wang, M. F. Erden and R. H. Victora, "Novel system design for readback at 10 Terabits per square inch user areal density", *IEEE Magnetic Letters*, Vol.3, article #: 4500304, Dec. 2012.

[5.9] N. Smith and P. Arnett, "White-noise magnetization fluctuations in magnetoresistive heads", *Appl.Phys.Lett.* vol.78, no.10, pp. 1448-1450, Mar. 2001

[5.10] R. Wood, J. Miles, T. Olsen, "Recording technologies for Terabit per square inch systems", *IEEE.Trans.Magn.*,vol.38,no.4,pp.1711-1717, Jul. 2002.

[5.11] H. N. Bertram, "Theory of Magnetic Recording", Cambridge University Press, NY, 1994, pp.112-119, pp.310-336.

[5.12] R. H. Victora, S. M. Morgan et al, "Two-dimensional magnetic recording at 10 Tbits/in^2", *IEEE.Trans.Magn.*,vol.48, no.5, pp.1697-1703, May 2012.

[5.13] J. Moon and W. Zeng et al "Equalization for maximum likelihood detectors", *IEEE Trans.Magn.*, vol.31, no.2, pp.1083-1088, Mar. 1995.

[6.1] R. Wood, M. Williams, A. Kavcic, et al, "The feasibility of magnetic recording at 10 Tb/in^2 on conventional media", *IEEE Trans. Magn.*, vol. 45, no.2, pp.917-923, Feb. 2009.

[6.2] K. S. Chan, R. Radhakrishnan, K. Eason, M.R. Elidrissi, J.J. Miles, B. Vasic, A.R. Krishnan, "Channel models and detectors for two dimensional magnetic recording," *IEEE Trans. Magn.*, vol. 46, no. 3, pp. 804–811, Mar. 2010.

[6.3] M. Yamashita, Y. Okamoto, Y. Nakamura, et al., "Modeling of writing process for two-dimensional magnetic recording and performance evaluation of two-dimensional neural network equalizer," *IEEE Trans. Magn.*, vol. 48, no. 11, pp. 4586–4589, Nov. 2012.

[6.4] Y. Wang, M. F. Erden and R. H. Victora, "Novel system design for readback at 10 Terabits per square inch user areal density", *IEEE Magnetic Letters*, vol. 3, article #: 4500304, Dec. 2012.

[6.5] R. H. Victora, S. M. Morgan et al, "Two-dimensional magnetic recording at 10 Tbits/in^2", *IEEE. Trans. Magn.*, vol.48, no.5, pp.1697-1703, May. 2012.

[6.6] R. H. Victora and X. Shen, "Exchange coupled composite media for perpendicular magnetic recording," *IEEE Trans. Magn.*, vol. 48, no. 11, pp. 2828–2833, Oct. 2005.

[6.7] Y. Wang and R. H. Victora, "Reader design for bit patterned media recording at 10 Tbits/in^2 density," *IEEE Trans. Magn.*, vol. 49, no. 10, pp. 5208–5214, Oct. 2013.

[6.8] M. Keskinoz, "Two-dimensional equalization/detection for patterned media storage," *IEEE Trans. Magn.*, vol. 44, no. 4, pp. 533–539, Apr. 2008.

[6.9] N. Smith and P. Arnett, "White-noise magnetization fluctuations in magnetoresistive heads", *Appl.Phys.Lett*. vol. 78, no.10, pp. 1448-1450, Mar. 2001.

[6.10] R. Wood, J. Miles, T. Olsen, "Recording technologies for Terabit per square inch systems", *IEEE.Trans.Magn.*,vol. 38,no. 4,pp. 1711-1717, Jul. 2002.
[6.11] C. E. Shannon, "A mathematical theory of communications," *Bell Syst. Tech J.*, vol. 27, pp. 379–423, 623–656, July, Oct. 1948.
[6.12] R. H. Victora and Y. Wang, "System design for readback above 1 Tbits/in^2 from granular media", *IEEE Trans. Magn.*, vol. 50,no. 3, article #: 3100606, Mar. 2014.